AD_____

Award Number: W81XWH-07-1-0GJÌ

TITLE: Ö^ç^\|[ ] { ^}oﬂ-æﬁ˘ |ãæ&^c^åÚçæ¦ãæ}ÁÔæ}&^¦Á¦æ}^˘câ8Áæ}åÁQ æ̊ã¦*ÁŒ̊^}c

PRINCIPAL INVESTIGATOR: Ølæ}&æÁÙﬂŒ̊æ\¦æ}åﬀÁÚ@ÖÈ

CONTRACTING ORGANIZATION: University of Ù[˘c@^¦}ÁÔæﬁã[¦}ãæ
                          Š[•ÁŒﬂ*^|^•ËﬁÔŒﬀÁﬁ€€ì J

REPORT DATE: O̊¦¦ãﬂ̊ÁG€FF

TYPE OF REPORT: Øã}æﬂ

PREPARED FOR: U.S. Army Medical Research and Materiel Command
               Fort Detrick, Maryland 21702-5012

DISTRIBUTION STATEMENT: Approved for public release; distribution unlimited

The views, opinions and/or findings contained in this report are those of the author(s) and should not be construed as an official Department of the Army position, policy or decision unless so designated by other documentation.

REPORT DOCUMENTATION PAGE

Form Approved
OMB No. 0704-0188

Public reporting burden for this collection of information is estimated to average 1 hour per response, including the time for reviewing instructions, searching existing data sources, gathering and maintaining the data needed, and completing and reviewing this collection of information. Send comments regarding this burden estimate or any other aspect of this collection of information, including suggestions for reducing this burden to Department of Defense, Washington Headquarters Services, Directorate for Information Operations and Reports (0704-0188), 1215 Jefferson Davis Highway, Suite 1204, Arlington, VA 22202-4302. Respondents should be aware that notwithstanding any other provision of law, no person shall be subject to any penalty for failing to comply with a collection of information if it does not display a currently valid OMB control number. **PLEASE DO NOT RETURN YOUR FORM TO THE ABOVE ADDRESS.**

1. REPORT DATE (DD-MM-YYYY)	2. REPORT TYPE	3. DATES COVERED (From - To)
01-04-2011	Final	1 APR 2007 - 31 MAR 2011

4. TITLE AND SUBTITLE		
Development of a Multifaceted Ovarian Cancer Therapeutic and Imaging Agent	**5a. CONTRACT NUMBER**	
	5b. GRANT NUMBER W81XWH-07-1-0298	
	5c. PROGRAM ELEMENT NUMBER	

6. AUTHOR(S)		
Francis S. Markland, Ph.D.	**5d. PROJECT NUMBER**	
	5e. TASK NUMBER	
E-Mail: markland@usc.edu	**5f. WORK UNIT NUMBER**	

7. PERFORMING ORGANIZATION NAME(S) AND ADDRESS(ES)	8. PERFORMING ORGANIZATION REPORT NUMBER
University of Southern California Los Angeles, CA 90089	

9. SPONSORING / MONITORING AGENCY NAME(S) AND ADDRESS(ES)	10. SPONSOR/MONITOR'S ACRONYM(S)
U.S. Army Medical Research and Materiel Command Fort Detrick, Maryland 21702-5012	
	11. SPONSOR/MONITOR'S REPORT NUMBER(S)

12. DISTRIBUTION / AVAILABILITY STATEMENT
Approved for Public Release; Distribution Unlimited

13. SUPPLEMENTARY NOTES

14. ABSTRACT Ovarian cancer (OC) is the deadliest of all gynecological cancers, with five year survival rates of <45%. One critical feature of the disease is that two-thirds of the women diagnosed have advanced disease, and the five year survival rate of this group is <30%. This project outlines the development of a recombinant version of a member of a class of proteins known as disintegrins as an innovative imaging and diagnostic agent for ovarian cancer (OC). Vicrostatin (VN) is a recombinant protein based on the venom disintegrin contortrostatin (CN), which has shown impressive antitumor and antiangiogenic activities in models of human ovarian cancer. OC cells have been shown to display integrins $\alpha v\beta 5$ and $\alpha 5\beta 1$, and the antitumor activity of CN, and demonstrated for VN, is based on the high affinity interaction between the disintegrin and these integrins. Thus far we have developed and shown that we have a robust and viable system for the production of VN and that the protein produced displays a high affinity for integrins displayed on ovarian cancer cells. In ongoing experiments we are evaluating the imaging potential for VN to be used for both evaluation of treatment and diagnosis of OC. The high affinity of VN for the integrins found on OC cells make for an excellent candidate for improvement of OC diagnosis and therapy.

15. SUBJECT TERMS
Ovarian Cancer, Imaging, Novel Agent, Disintegrin, Integrins

16. SECURITY CLASSIFICATION OF:			17. LIMITATION OF ABSTRACT	18. NUMBER OF PAGES	19a. NAME OF RESPONSIBLE PERSON USAMRMC
a. REPORT U	b. ABSTRACT U	c. THIS PAGE U	UU	90	19b. TELEPHONE NUMBER (include area code)

Standard Form 298 (Rev. 8-98)
Prescribed by ANSI Std. Z39.18

Table of Contents

Final Progress Report

<u>Introduction</u>
The project entitled "Development of a Multifaceted Ovarian Cancer Imaging Agent" covers the period from April 1 2007 - March 31, 2011 (no cost extension, original end date 03/31/2010). This final report covers the entire period of the project and summarizes our findings of the project from April 1, 2007 through March 31, 2011. The project focuses on the development of a production method for a recombinant disintegrin vicrostatin (VN), whose structure is based on the snake venom disintegrin contortrostatin (CN), and the use of this integrin-binding protein in imaging ovarian cancer. As a therapeutic agent the peptide is delivered via intra-peritoneal injection as a liposomal formulation. Additionally, PET imaging radiotracers can be covalently attached to VN and the peptide used as an imaging and diagnostic agent in ovarian cancer (OC). In the previous reporting periods we utilized our expression system, described in the first year's report, to produce VN for use as an imaging agent, we then further evaluated and quantitatively determined the integrin affinity of VN for a select group of integrins believed to be important in ovarian cancer, and evaluated the circulatory half-life of both VN and liposomal encapsulated VN (LVN). Recently, we have succeeded in developing VN as an OC PET imaging agent and have established methods for radionuclide attachment to VN and produced PET images of ovarian cancer at an early stage. Finally, we have shown that that the attachment of the PET tracer to VN does not alter its biological activity or ovarian cancer cell binding.

Summary of Progress on Specific Aims
During the period of this grant we have made significant progress toward successful completion of the goals and milestones of this project. Building on work from the previous years in this final year we were able to successfully develop ^{64}Cu-VN as a PET imaging agent. We were able to successfully label VN with ^{64}Cu and evaluate its ability to image and detect an ovarian tumor in vivo. Progress in these studies has lead to significant advances toward our final two milestones. Our Specific Aims and Milestones for this project are:
Specific Aim 1: Prepare VN, a recombinant disintegrin with proven *in vivo* antiangiogenic activity (**Milestone 1**, **completed Year 1**), and produce a liposomal formulation (LVN) with stability characteristics appropriate for clinical application (**Milestone 2**, **completed Year 1**).
Specific Aim 2: Demonstrate imaging potential and biological efficacy of a LVN formulation in a mouse model of ovarian cancer (**Milestone 3, completed**).
Specific Aim 3: Evaluate the use of VN as a novel tumor imaging agent both for diagnostic use and for evaluation of tumor suppression following treatment (**Milestone 4, completed/in progress**).

Annual Progress Reports
April 2008
Preparation of vicrostatin (VN)
        <u>Recombinant expression of a venom derived disintegrin:</u> For a number of years the Markland laboratory has worked with contortrostatin (CN), a disintegrin isolated from *Agkistrodon contortrix contortrix* venom. A major block in the pathway to clinical development of CN was the supply and availability of the protein: for purification, it exists as a very small fraction of the total venom protein (~0.01%), and for recombinant production, its peculiar structure stabilized by numerous disulfide bonds makes its expression in commonly-employed recombinant systems a very difficult task. Nonetheless, we have successfully employed a recombinant expression system for which we developed a proprietary production method capable of generating substantially more than 200mg of purified active recombinant disintegrin from one liter of bacterial culture in small-scale laboratory conditions. To generate recombinant disintegrins, we have successfully adapted a commercially-available *E. coli* expression system consisting of the Origami B (DE3) expression host in combination with the pET32a vector (Novagen) for our production needs. A sequence-engineered form of CN, called Vicrostatin (VN), has been directionally cloned into pET32a expression vector incorporating a unique TEV protease cleavage site, which facilitates the removal of the thioredoxin fusion partner from the expressed VN. Briefly for recombinant VN production, multiple colonies of transformed Origami B cells were used to establish primary cultures by inoculating 5ml LB broth batches containing carbenicillin (100µg/ml), tetracycline (12.5µg/ml), and kanamycin (15µg/ml). The primary cultures were grown overnight at 37°C and 250 rpm in a shaker-incubator and used to seed secondary cultures. Batches of fresh 500ml LB broth in the presence of the three antibiotics were then inoculated with the previously-established primary cultures and

grown at 37°C and 250 rpm to an OD600 of 0.6-1.0. At this point, the cells were induced with IPTG added to a final concentration of 1mM and cultured for another 4-5 hours at either 25°C or 37°C and 250 rpm. At the end of the induction period, the cultures were centrifuged at 4000xg and bacterial pellets lysed by utilizing a scalable homogenization method for breaking open the bacteria. The cells were homogenized in a microfluidizer (Microfluidics M-110L, Microfluidics, Newton, MA) at room temperature by resuspending the cell pellets in 5 volumes of water before commencing the process. The operating conditions of the homogenizer included applied pressures of 14,000–18,000 psi, bacterial slurry flow rates of 300–400ml per minute and multiple passes of the slurry through the processor. The insoluble cellular debris was then removed by centrifuging the bacterial lysates at 40,000xg and the soluble cell lysates collected and further analyzed by SDS-PAGE for recombinant protein expression. The expressed fusion protein (Trx-VN) was proteolysed by adding recombinant TEV to the soluble cell lysates according to the manufacturer's protocol (Invitrogen). The TEV treatment efficiently cleaved off VN from its TrxA fusion partner, the proteolysis status being monitored by SDS-PAGE. When proteolysis was complete, the proteolyzed lysates were passed through a 0.22µm filter, diluted 100-fold in water and ultrafiltered through a 50kDa molecular weight cut-off cartridge (Biomax50, Millipore, MA) in a tangential flow ultrafiltration device (Labscale TFF system, Millipore, MA) that removed most of the higher molecular weight bacterial proteins. The resulting ultrafiltrates were then re-concentrated against a 5kDa molecular weight cut-off cartridge (Biomax5, Millipore MA) using the same tangential flow ultrafiltration device. VN was further purified by reverse phase HPLC. The recombinant disintegrin we have produced through this system is recognized by polyclonal antisera raised against native CN and inhibits ADP induced platelet aggregation in a dose dependent manner with an IC_{50} almost identical to native CN (~60nM). Moreover, VN inhibits cell adhesion to vitronectin and fibronectin, inhibits endothelial cell and tumor cell invasion through a laminin-rich reconstituted basement membrane, and inhibits endothelial cell tube formation in a manner indistinguishable from native venom derived contortrostatin. In conclusion, due to its robustness and reproducibility, we believe that our recombinant production method will be easily translatable to bioreactors for scale up for clinical use.

Preparation of Liposomal Vicrostatin (LVN)

Liposomal encapsulation of VN using a homogenization method: To prepare liposomal vicrostatin (LVN), stock solutions of the phospholipids and cholesterol were prepared by dissolving each lipid in a chloroform/methanol solvent mixture. Thin lipid films were created by pipetting aliquots of the lipid solutions into round bottom glass tubes followed by solvent evaporation at 65°C under a stream of nitrogen gas. The dried lipids and cholesterol were further dried under vacuum for 48 hours. This process yielded lipid powder mixtures that were used to prepare LVN. For homogenization or sonication, VN was dissolved in a hydration buffer (10mM sodium phosphate and 262mM sucrose, pH 7.2) and added to the dried lipids. The lipid dispersion was incubated for five minutes at 50°C. The LVN was formed by either probe sonication at 10% power for 3 to 5 minutes in a Branson Probe Sonifier or homogenized by passing the material through a microfluidizer (M110L; Microfluidics, Newton, MA). The material was processed between 10,000 and 18,000 psi while maintaining an elevated temperature (45-65°C). Samples of the liposome batch were taken during the process and the size distribution of LVN was determined with an Ultrafine Particle Analyzer (UPA150) (Microtrac, North Largo, FL). After processing, unencapsulated VN was removed by ultrafiltration using an Amicon UF membrane of 100,000 MWCO and LVN sterilized by filtration through a 0.2µM PVDF filter. To determine the optimal processing conditions to formulate the LVN in large scale, we performed a series of processing studies using the Microfluidizer and compared these preparations with the sonication method that had been used to produce lab-scale LVN for all of the *in vitro* and *in vivo* studies performed previously. The homogenized LVN was evaluated for size distribution, ease of 0.2µM filtration and percent encapsulation of VN into the liposome to determine the best formulation **(Table 1)**. In the first experiment, 25ml of LVN (2mg/ml VN) was processed at 18,000 psi for three separate 1 minute intervals at 60-65°C and the temperature controlled using a heat exchanger set at 45°C. After each one minute homogenization cycle, a sample was evaluated for size distribution (**Figure 1**). After the third 1 minute homogenization cycle, the formation of LVN was complete based on size distribution and the relative translucence of the product. As compared to the sonicated material, the homogenized LVN was similar in range (55-85nm average range for sonicated LVN, **Table 1**) with an average diameter of 68nm and a standard deviation of 21.1nm. In a second study, 25ml of LVN (2mg/ml VN) was processed at 10,000 psi for five separate 30 second intervals at 50-55°C and the temperature controlled using a heat exchanger set at 45°C. The rationale for this processing condition was

two-fold. First, we reduced the time/temperature and pressure of the homogenization parameters in an attempt to reduce the possibility of VN degradation and second, to produce larger vesicles that might encapsulate a greater quantity of VN. After each 30 second homogenization cycle, a sample was evaluated for the size distribution (**Figure 2**); the average size of LVN was 83nm and liposome formation was considered complete based on the size distribution and the relative translucence. Despite the larger vesicles prepared, the percent encapsulation was in the same range as the previously formulated material (**Table 1**). Under the recirculation conditions used in the first two experiments, it is possible that not all of the LVN was processed for the same amount of time due to a mixing effect during this type of processing. In a third processing experiment, 25ml of LVN (2mg/ml VN) was processed at 18,000 psi for seven separate passes at 60-65°C and the temperature controlled using a heat exchanger set at 45°C. In this experiment, the size distribution of the sample never reached completion. The average size of the liposomes remained greater than 200nm and the standard deviation was greater than 500nm. Optically, this preparation appeared flocculent and was not translucent like the other batches and was not filterable through a 0.2µM filter (data not shown). In a final experiment, 60ml of LVN (2mg/ml VN) was processed at 13,000 psi for three separate 1 minute intervals at 60-65°C and the temperature controlled using a heat exchanger set at 45°C. The final processed material showed a size distribution of 68nm (+/- 20nm). This material filtered easily through a 0.2µM filter and was optically translucent. Taken together, these data indicate LVN can be processed by homogenization and that these liposomes appear equal in size, filterability and percent encapsulation to LVN previously formed by sonication. In addition, the homogenized material has been scaled to 60ml per batch, which is 12 times that of the sonicated batches. Since homogenization has been used by others in the industry for liposome preparations, we are encouraged that this product can be scaled to volumes necessary for commercialization.

In vitro activity

i. Binding to integrins on cell surfaces: We have shown that VN binds with different affinities to a panel of human ovarian cancer cell lines dependent on the integrin display status of the individual cell line (**Table 2**). Using a FACS based assay we evaluated the ability of fluorescently labeled VN to bind to Human Umbilical Vein Endothelial Cells (HUVEC) and the ovarian cancer cell lines OVCAR-3 and A2780 (**Figure 3**). This study revealed differential binding to the cells, and this appears to be dependent on their integrin profiles. The results of these studies supports our hypothesis that the promiscuous nature of integrin binding by VN allows for broad targeting toward ovarian cancer.

ii. Inhibition of cell adhesion to various ECM proteins: The effect of VN on cell adhesion was assayed using the OC cell lines OVCAR-3, A2780 and HUVEC incubated in serum-free DMEM (Dulbecco's Modified Eagle's Medium) with various concentrations (0-1000nM) of VN for 30 min and then seeded in wells pre-coated with 100 µl of Fibronectin (Fn) or Vitronectin (Vn) (15µg/ml) in a 96-well plate at 25,000 cells/well. The seeded cells were allowed to adhere to immobilized Fn or Vn for 1hr at 37C in the presence of 5% CO2. The non-adherent cells were then washed away and the number of adherent cells for each condition was estimated colorimetrically using the MTS cell viability assay. The results were calculated in % adhesion (**Figure 4**), where the untreated control was considered as 100% adhesion. With Fn there was a dose dependent inhibition of adhesion by VN with an IC_{50} of <100nM comparable to the value observed previously with native CN. Treatment of the cells with 1000nM VN allowed for less than 25% of the cells to adhere. Inhibition of adhesion to vitronectin by VN displayed a slightly higher IC_{50} somewhat greater than 100nM, but again comparable to that seen with CN. With cells plated on Vn, treatment with 1000nM VN shows that less than 40% of the cells remain adherent. VN produced by the recombinant system retains biological activity equal to that of the natural protein, CN.

iii. Inhibition of cellular invasion: To assess the ability VN to block the invasion of HUVEC, OVCAR-3 and A2780 cells through a reconstituted basement membrane, we used a cell invasion assay kit from Chemicon (Temecula, CA). This kit utilizes an invasion chamber, which consists of cell culture inserts that fit into a 24-well tissue culture plate. The inserts contain an 8 µm-pore size polycarbonate membrane, over which a thin layer of ECMatrix™ was applied. The ECMatrix™ serves as an in vitro reconstituted basement membrane and is a solid gel of ECM proteins prepared from the Engelbreth Holm-Swarm (EHS) mouse tumor. The ECM layer occludes the membranes pores, blocking non-invasive cells from migrating through. The HUVEC, OVCAR-3 and A2780 cells were starved overnight in DMEM containing 0.1% FBS and harvested and resuspended in serum free DMEM (at $1x10^6$ cell/ml). The cells were incubated in the presence of various concentrations (10, 100, 1000nM) of VN for 30 min at 25C. Then 300µl of cell aliquots from each condition

were added to each invasion insert, whereas the bottom well of the chamber received 500µl of chemoattractant (conditioned medium from human HT1080 fibrosarcoma cells). The invasion chamber was then incubated for 8hr at 37C in the presence of 5% CO_2 and the cells were allowed to invade through the ECM toward the chemoattractant. After 8hr, the cells that invaded through the pores into the lower chamber were detached, collected and lysed. The total DNA content from each cell lysate was determined after labeling with a DNA-binding fluorescent dye according to the manufacture's protocol. The numbers of invaded cells for each condition were approximated by further quantitating the labeled DNA using a SPECTRAmax GeminiEM fluorescent plate reader. The results were calculated in % invasion (**Figure 5**), where the untreated control was considered as 100% invasion. VN inhibits the invasion of all of the cell lines tested. The IC_{50} for OVCAR-3 and A2780 were <20nM, while the IC_{50} for HUVEC approaches 1nM (data not shown).

iv. Inhibition of HUVEC tube formation: To assess the ability of VN to interfere with tube formation, HUVEC cells were maintained in EGM-2 complete media and grown to confluency. The HUVEC cells were then harvested by brief trypsinization, washed in the presence of soybean trypsin inhibitor (1mg/ml), and resuspended in basal media. After being maintained in suspension for 15-30 min, cells were seeded on to Endothelial Cell Tube Formation plates (BD BioCoat™ Angiogenesis System), an *in vitro* endothelial tubulogenesis system, at a concentration of 25,000 cells per well and immediately treated with various concentrations of VN, CN (control), or Suramin salt (supplier provided positive control) and incubated for 18 hours at 37C. At the end of the incubation period, cells were washed twice with PBS and then stained with 8 µg/ml Calcein AM in PBS at 37C. After 30 min the cells were washed again two times with PBS and then imaged (**Figure 6**) using confocal microscopy at 2.5X and 10X magnifications. On the captured images, the total length of tubes was quantitated with Zeiss LSM image software and data plotted (**Figure 7**) against the total length of tubes (in µm) generated by untreated cells. Representative tubes from 6 different wells were measured by 3 separate individuals and averaged to form each data point (**Figure 7**). VN inhibits tube formation as effectively as CN (data not shown).

Key Research Accomplishments
- Produced recombinant form of disulfide rich disintegrin
- Encapsulated in liposomes as potential therapeutic
- Evaluated the ability of recombinant protein to inhibit adhesion, migration and invasion as well as assayed for ability of the protein to bind to tumor cells
- Evaluated the ability to inhibit endothelial cell tube formation

Conclusion
LVN is a novel liposomal formulation of a disintegrin engineered using standard recombinant techniques. The results from the studies clearly show that LVN prepared by a commercially viable technique retains integrin binding and antiangiogenic activity equivalent to the laboratory prepared material. Based on this integrin affinity in the next phase of the studies we will evaluate the *in vivo* OC cell binding and subsequent use of VN as a pet imaging agent.

Progress Report 2009
Binding to integrins on cell surfaces: In the previous year's progress report we have shown that the recombinant VN binds with different affinities to a panel of human ovarian cancer cell lines dependent on the integrin display status of the individual cell line. To quantitatively assess the binding affinities of VN with soluble functional integrins, two approaches were evaluated. First the disintegrins were immobilized on the surface of a BiaCore surface Plasmon resonance chip. The soluble integrin was then allowed to interact with the immobilized disintegrin. This approach was unsuccessful with VN, presumably because the integrins had limited access to VN. This was confirmed by flowing an anti-VN antibody across the surface and this also displayed limited binding. It is believed that the disintegrin interaction with the carboxymethyl cellulose surface causes VN to be buried and unavailable for binding. In an attempt to solve this issue fluorescence polarization (FP) was used to determine binding kinetics. In this method, differing concentrations of functional integrin were incubated with a constant amount of FITC labeled VN. As VN is a small molecule it rapidly depolarizes the excitation light. Upon binding to the large integrin, the fluorescent tag on VN tumbles in solution at a slower rate resulting in increased levels of polarization. The measured FP value is a weighted average of FP values of the bound and free fluorescent VN and is therefore a direct measure of the fraction bound. Data generated

in these experiments can be analyzed like standard radioligand binding, and kinetics of binding can be determined as with Scatchard analysis using a non-linear curve fit. From this set of experiments we determined the dissociation constants for VN and CN with integrins αvβ3, α5β1 and αvβ5 (**Table 3**). Recombinant VN was purposely designed with a carboxy terminal extension, which was expected to enhance affinity for α5β1. This was confirmed as CN and VN exhibit nearly identical affinities for αvβ3 and similar affinity for αvβ5, while there is an order of magnitude difference in the Kd values for binding to α5β1 when comparing VN (higher affinity binding) to CN. In the evaluation of the dissociation constants of VN for integrins αvβ3, αvβ5 and α5β1 (integrins that are over expressed on ovarian cancer cell lines) we found that the carboxy terminal modification in VN does impart a higher affinity for α5β1, as designed. The results of these studies support our hypothesis that the promiscuous nature of integrin binding by VN allows for broad targeting toward ovarian cancer.

Determination of circulatory half-life of LVN: Previously we had determined the circulatory half-life of CN and liposomal CN. We repeated these studies for VN and liposomal VN (LVN). To carry out this study blood samples were taken 0.5, 1, 3, 6, 18, 24, 48 and 72 hours following i.v. administration of ^{125}I-VN or L-^{125}I-VN. Gamma counting of collected blood samples revealed that there was a rapid decrease to <0.1% of the administered counts in the blood at 6 hours after i.v. injection of ^{125}I-VN. However, in animals given L-^{125}I-VN, the percentage of total injected counts in the blood drops to a level of 63% of the injected counts 6 hours postinjection and gradually decreases over the following 66 hours. By plotting the decrease in radioactivity in blood over time following i.v. administration in tumor-free mice, we observed a circulatory half-life of 0.4 h for ^{125}I-VN and 20.4 h for L-^{125}I-VN. Thus, encapsulation of VN in liposomes not only protects the protein but also maintains it in the circulation for a much longer period of time than native unencapsulated VN, enabling more effective access to the tumor.

Labeling VN for use as a PET imaging agent: For use as a PET imaging agent in ovarian cancer VN needs to be adducted to an appropriate PET radionuclide. In this instance the radionuclide utilized was ^{64}Cu, selected due to its relatively long (for a PET agent) half life, 12.7hrs, which makes it more suitable for larger peptide or protein based PET imaging, and enhances the efficacy of conjugation to the macrocylic chelator 1,4,7,10-tetraazacyclododecane-*N,N',N'',N'''*-tetraacetic acid (DOTA), a heterobifunctional crosslinker that can be attached to Lys residues in proteins. To create a VN-DOTA conjugate DOTA is first activated by 1-ethyl-3-[3-(dimethylamino)propyl]carbodiimide (EDC) and N-hydroxysulfonosuccinimide (SNHS) at pH 5.5 for 30 min with a molar ratio of DOTA:EDC:SNHS = 10:5:4. The DOTA-succinimide reaction mixture (15 μmol, calculated on the basis of SNHS) was cooled to 4°C and added to VN (3:1 molar ratio) dissolved in 500 μL of water. The reaction mixture was adjusted to pH 8.5 with 0.1N NaOH and allowed to incubate overnight at 4°C. The DOTA-coupled VN was purified by semipreparative HPLC. The peak containing the conjugate was collected, lyophilized, and dissolved in water (2 mg/mL) for use in radiolabeling reactions. For ^{64}Cu labeling of the VN-DOTA conjugate 20 μL of [64]CuCl$_2$ (74 MBq in 0.1N HCl) was diluted in 400 μL of 0.1 mol/L sodium acetate buffer (pH 6.5) and added to the DOTA-VN solution (a 1 mg/mL solution of peptide was made and separated into aliquots; 80 μg of DOTA-VN and 37 MBq of ^{64}Cu were used for labeling). The reaction mixture was incubated for 1 h at 40C. ^{64}Cu-DOTA-VN was then purified by semipreparative HPLC, and the radioactive peak containing the desired product was collected. After removal of the solvent by rotary evaporation, the residue was reconstituted in phosphate-buffered saline for in vivo animal experiments. The labeling yield of ^{64}Cu-DOTA-VN is 74% based on HPLC profile. Current studies are ongoing to evaluate the retention of bioactivity of the labeled VN.

Binding of an integrin targeted peptide to an orthotopic xenograft ovarian tumor: In these studies we established an orthotopic xenograft ovarian tumor through surgical exposure of the ovary and direct injection of the ovarian cancer cells (1x10^6 cells in 50μl) into the stroma of the ovary. The tumors were allowed to grow untreated for 28 days. At this time an integrin-targeted disintegrin-like peptide ligand was injected systemically by intravenous injection. The FITC labeled cyclic peptide contains the sequence CTRKKHDNAQC, cyclized through the Cys sidechains, and is based on the putative integrin binding loop of the disintegrin domain of Jararhagin, a metalloproteinase with a disintegrin domain isolated from *Bothrops jararaca*, a venomous pit viper found in Brazil, Paraguay and northern Argentina.   After the peptide is injected systemically (10μg/mouse), the ovary is surgically exposed and imaged (Fluorescence Mode, Xenogen IVIS100 System).

Figure 8 shows that the tumor has a high level of fluorescence associated with the tumor tissue surrounding the ovary. Conversely the tissue surrounding the control non-tumor bearing ovary shows little fluorescence indicating specific binding to the tumor cells by the fluorescently labeled integrin ligand. Ongoing studies are in progress to repeat this experiment in an orthotopic model with FITC-VN.

Key Research Accomplishments
- Determined the enhanced affinity of the recombinant disintegrin for an integrin overexpressed on ovarian tumors
- Evaluated the circulatory half-life of VN versus LVN
- Determined a method to radiolabel VN (and CN) with PET radionuclides
- Evaluated the ability and specificity of an integrin targeted peptide ligand to bind to an orthotopic xenograft ovarian tumor

Conclusion
LVN is a novel liposomal formulation of a disintegrin engineered using standard recombinant techniques. The results from the Year I studies clearly show that LVN prepared by a commercially viable technique retains integrin binding and antiangiogenic activity equivalent to the laboratory prepared material. In the second year of this project we have been successful in determining the Kd of VN for integrins important to OC. We have shown that an integrins can be specifically labeled *in vivo* and finally we have begun development of the methods necessary for use of VN as PET imaging agent.

Progress Report 2010
Body
Labeling VN for use as a PET imaging agent: For use as a PET imaging agent in ovarian cancer VN needs to be complexed with an appropriate PET radionuclide. In this instance the radionuclide utilized was ^{64}Cu, as described above (Progress Report 2009). For in vitro bioactivity studies cold $CuCl_2$ was substituted for $^{64}CuCl_2$; all other procedures were carried out as with the radioactive material.

Retention of biological activity of Cu labeled disintegrin: To assess the biological activity of Cu-DOTA-VN we measured its ability to block processes critical to tumor survival and progression: adhesion, migration and invasion. We measured the inhibitory effect on different tumor cell lines, as well as endothelial cells. Inhibition of adhesion is evaluated through the ability of Cu-DOTA-VN to block cell attachment to a number of different extracellular matrix proteins. We observed a dose dependence in the inhibition of adhesion of OVCAR-5 and A2780 ovarian cancer cell lines as well as human umbilical vein endothelial cells (HUVEC), to both vitronectin and fibronectin, extra-cellular matrix (ECM) proteins that are ligands for integrins targeted by VN (data not shown). Cellular migration is also inhibited by VN in a dose dependent manner. To evaluate tumor and endothelial cell migration a phagokinetic tracking assay is employed. In this assay cells are plated on a collagen coated cover-slip with an overlay of colloidal gold. As the cells move they displace or ingest the colloidal gold leaving tracks on the surface of the cover-slip. Then, using dark-field microscopy the tracks can be visualized and photographed. Using image analysis software the area of the tracks in a photographed field can be determined and a "migration index" can be calculated as a percentage of the field lacking gold. Following treatment by increasing concentrations of VN and Cu-DOTA-VN the migration of both cancer and endothelial cells is significantly limited. Finally, the ability of cells to invade through the ECM was evaluated using modified Boyden chambers. These chambers contain a Matrigel coated porous membrane (pore size 8μm). A chemoattractant is placed in the lower chamber and untreated cells invade through the membrane toward the attractant. Both Cu-DOTA-VN and VN block the invasion of endothelial (HUVEC) and OVCAR-5 cells in a dose dependent manner with IC_{50} at low nM concentrations. These results show that Cu-DOTA-VN has essentially identical activity to VN in inhibiting invasion of endothelial and ovarian cancer (OVCAR-5) cells. The results also convincingly demonstrate one of the important attributes of VN, that it inhibits endothelial cell as well as tumor cell invasion in the low nM range.

Binding of Cu labeled VN to integrins found on ovarian cancer cell surfaces: In the previous year's progress report we showed that recombinant VN binds with different affinities to a panel of human ovarian cancer cell lines dependent on the integrin display status of the individual cell line. In the present studies fluorescence polarization (FP) was used to determine binding kinetics to the identified subset of integrins. In

6

this method, differing concentrations of functional integrin were incubated with a constant amount of Cu-DOTA-labeled FITC-VN, non radioactive Cu was used in these experiments but the process for labeling was carried out identically to that used with the PET tracer agent. As Cu-DOTA-FITC-VN is a small molecule it rapidly depolarizes the excitation light. Upon binding to the large integrin, the fluorescent tag on VN tumbles in solution at a slower rate resulting in increased levels of polarization. The measured FP value is a weighted average of FP values of the bound and free fluorescent VN and is therefore a direct measure of the fraction bound. Data generated in these experiments can be analyzed like standard radioligand binding, and kinetics of binding can be determined as with Scatchard analysis using a non-linear curve fit. From this set of experiments we determined the dissociation constants for FITC-VN and Cu-DOTA-FITC-VN with integrins αvβ3, α5β1 and αvβ5. Cu-DOTA-FITC-VN and VN exhibit nearly identical affinities for αvβ3 (9.3nM and 7.4nM), α5β1 (16.7nM and 15.2nM) and αvβ5 (43.6nM and 41.2nM), respectively. In the evaluation of the dissociation constants of Cu labeled VN for integrins αvβ3, αvβ5 and α5β1 (integrins that are over expressed on ovarian cancer cell lines) we found that the addition of the crosslinker and Cu atom to VN does not affect the affinities for the targeted receptors. The results of these studies support our hypothesis that the promiscuous nature of integrin binding by VN allows for broad targeting toward ovarian cancer, and that derivatization with Cu-DOTA will not adversely affect integrin binding by VN.

Preferential tumor binding by a recombinant disintegrin: In order to determine if there was preferential tumor binding by a recombinant disintegrin, VN the recombinant form of the venom derived disintegrin contortrostatin, was compared to a cyclic peptide, cyclo(-RGDfV-), similar to Cilengitide, which binds to integrins αvβ3 and αvβ5, and is currently in clinical trials for therapy of glioma. We evaluated VN as a PET imaging agent. This experiment was designed to show tumor specific binding of VN utilizing an existing bone metastasis model. In this case, androgen dependent prostate cancer cells were injected into the tibia of nude mice and were allowed to grow untreated for ~5 weeks until the tumors were 10-14mm in diameter. Animals were then injected with ^{64}Cu labeled VN or ^{64}Cu labeled peptide cyclo(-RGDfV), and imaged using a Concorde Systems micro-PET imaging system. As can be seen in **Figure 9**, injected ^{64}Cu-DOTA-VN localizes to the tumor with much higher specificity and binding affinity than the cyclic RGD peptide. This indicates that the recombinant disintegrin, VN, binds to the tumor and could serve as an effective imaging or therapeutic agent. While there is a high level of background from the reticuloendothelial system (RES), this can be overcome through two methods: first, masking to observe only the tumor under study, and second through serial images at longer time points than we attempted in this preliminary study. With masking, the tumor being treated can be identified and the region of interest evaluated would only be that of the tumor. In allowing more time for the labeled material to be removed from the body before imaging, the high affinity long-lived disintegrin bound to integrins on the tumor cells would remain, whereas the disintegrin associated with the RES would disappear.

Key Research Accomplishments
- Successfully labeled VN with both radioactive and non-radioactive copper
- Evaluated the retention of biological activity of VN following labeling
- Determined the binding affinities of copper labeled VN for soluble integrins important in ovarian cancer
- Performed comparative experiments of the potential for PET tumor imaging with copper labeled VN and a cyclic RGD peptide

Conclusion
LVN is a novel liposomal formulation of a disintegrin engineered using standard recombinant techniques. The results from the Year I-III studies clearly show that LVN prepared by a commercially viable technique retains integrin binding and antiangiogenic activity equivalent to the laboratory prepared material. In the third year of this project we have been successful in determining the Kd of copper labeled VN for integrins important to OC. We have shown that integrins can be specifically labeled *in vivo*, and finally we have begun development of the methods necessary for use of VN as PET imaging agent.

Progress Report 2011
Body

(Note: the molecule we formerly identified as VN in this report has been renamed VCN to distinguish it from the common abbreviation used for vitronectin (Vn) and to more correctly give credit to the source of the protein)

PET Imaging of Early Ovarian Tumors: In the evaluation of the ability to image and successfully detect ovarian tumors we repeated studies that we had done previously. However, in the present studies we utilized an animal model model employing the cell line OVCAR-3^{luc}. This cell line is stably transfected with the gene for luciferase. This modified protocol will allow us to observe both the tumor itself in a living animal, and also co-register the PET image with the optical image and identify the ability to detect tumors in the intraperitoneal (IP) space of living animals. For these experiments we injected 2.5×10^5 OVCAR-3^{luc} cells IP and allowed the tumors to age for 28 days. At this point with no obvious sign of disease we imaged the tumors using the optical imaging system to detect the presence of luciferase. Since luciferase will only be found in the tumor, this enables us to specifically image the tumor. Following these images ^{64}Cu-DOTA-VCN (200µCi) is injected into the tail vein of the study animals and allowed to circulate for 90 minutes. At this time the animal is placed onto the mounting tray of the PET imaging instrument and introduced into the detector. As can be seen in **Figure 10C** there is a specific accumulation of ^{64}Cu-DOTA-VCN in an area in the lower abdomen that correlates with a location of luciferase activity as seen in the optical image (**Figure 10D**). Both of these positions were confirmed by dissection and exposure of the tumor in the sacrificed animal (**Figure 10A&B**). The images shown are representative of experiments performed under similar conditions (number of cells, amount of ^{64}Cu-DOTA-VCN injected). Experiments in which a larger number of cells are injected IP produce unusable images, as the tumors have grown large and coat many of the surfaces in the IP space and yield bright and indistinguishable structures in the mouse abdomen.

One problem of note is the high level of uptake by the kidneys at the 90 minute time point. As can be seen in F**igure 11A** the kidneys shield the ability to view an ovarian tumor via a dorsal or ventral total slice view. When viewed transversely (**Figure 11B)** there is clear separation between the kidneys and the tumor mass which binds the ^{64}Cu-DOTA-VCN. Three dimensional reconstruction yields a three dimensional model that can be rotated and rendered to observe the position of the tumor in relationship to the kidneys in space. This three dimensional model is available in our laboratory, but we are unable to append to this progress report.

Key Research Accomplishments

- Successfully applied PET imaging to ovarian cancer at a relatively small size using ^{64}Cu-VCN
- Definitively identified the tumor imaged with PET and optical imaging to be the identified ovarian tumor
- Identified a method to separate tumor signal from other structures that retain counts in the peritoneal cavity.

Conclusions

^{64}Cu-DOTA-VCN proves to be a useful imaging agent for detection of small earlier stage ovarian cancer. If the cancer is allowed to spread to cover the peritoneum the images obtained show wide dissemination of disease and do not allow for regional observation of tumors. Future studies will evaluate the usefulness of ^{64}Cu-DOTA-VCN in imaging tumors post debulking to evaluate reoccurrence and or success in tumor removal. As illustrated throughout this report a number of hurdles needed to be overcome to get to the point we are presently in the development of a novel integrin targeted ovarian cancer imaging agent. Future success will build on the developments and goals achieved through this project sponsored by the CDMRP/DOD Ovarian Cancer Research Program. *In future research we will use a targeted approach to more specifically localize the imaging agent to the tumor to avoid binding by the kidney and other elements of the RES.*

Reportable Outcomes

1.   Swenson, S., Minea, R. and Markland F.S. Development of an integrin targeted antiangiogenic agent. In: Tumor Angiogenesis: From Molecular Mechanisms to Targeted Therapy (F.S. Markland S. Swenson and R. Minea, Eds) Wiley-Blackwell, Weinheim Germany. Pg 181-206, 2010
2.   Minea, R., Helchowski, C., Rubino, B., Brodmann, K., Swenson, S., and Markland, F., Jr. (2011). Development of a chimeric recombinant disintegrin as a cost-effective anti-cancer agent with promising translational potential. Toxicon.(2011, in Press)

3.   Swenson, S., Minea, R., Zidovetzki, S., Helchowski, C., Costa, F. and Markland, F.S.: Anti-angiogenesis and disintegrins. In: Toxins and Hemostasis: From Bench to Bedside (R.M. Kini, M.A. McLane, K. Clemetson, F.S. Markland, Eds.), Springer: Pg 301-329, 2010

4.   Minea, R.O., Helchowski, C.M., Zidovetzki, S.J., Costa, F.K., Swenson, S.D., and Markland, F.S., Jr. (2010). Vicrostatin - an anti-invasive multi-integrin targeting chimeric disintegrin with tumor anti-angiogenic and pro-apoptotic activities. PLoS One *5*, e1092

5.   Helchowski, C.M., Minea, R.O., Swenson, S.D., and Markland, F.S., Jr. (2009). The use of pepsin in receptor internalization assays. Biochem Biophys Res Commun *388*, 240-246.

References

None

Appendices

1.   Tables 1-2
2.   Figures 1-11
3.   PDFs of reportable outcome publications

Table 1 Properties of Homogenized Liposomes

Condition	Size Distribution +/- StDev	Filterablity	Percent Encapsulation
Sonicated LVN	62nm +/- 12.3nm	Good	74
Homogenized LVN 1	68nm +/- 21.1nm	Good	72
Homogenized LVN 2	83nm +/- 47.1nm	Good	75
Homogenized LVN 3	225nm +/- 750nm	Poor	Not Determined
Homogenized LVN 4	68nm +/- 12.6nm	Good	78

LVN1-4 were prepared under slightly different homogenization conditions

Table 2 Integrin Profiles of Selected Ovarian Cancer Cell Lines

Ovarian Cancer Cell Lines	Relative Integrin Surface Expression				
	αv	αvβ3	α5β1	β1	α2β1
OVCAR-3	+	-	+++	+++	+++
A2780	++	-	++	+++	+++
Reference Cell Line					
MDA-MB-435	+++	+++	++	++	+

Table 3 Dissociation constants for interactions of VN and CN with Soluble Integrins

Disintegrin	Integrin Kd		
	αvβ3	α5β1	αvβ5
CN	6.6nM	191.3nM	19.5nM
VN	7.4nM	15.2nM	41.2nM

Values calculated through fluorescence polarization measurements following steady state binding
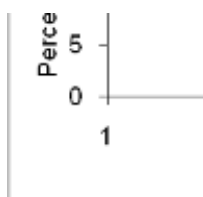
Figure 1 Size distribution of LVN processed by homogenization at 18,000psi for 3 minutes. Samples collected after 1 minute intervals.
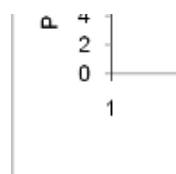
Figure 2. Size distribution of LVN processed by homogenization at 10,000psi and sampled at 1 .5 (sample 1), 2 (sample 2) and 2.5 (sample 3) minutes of processing.
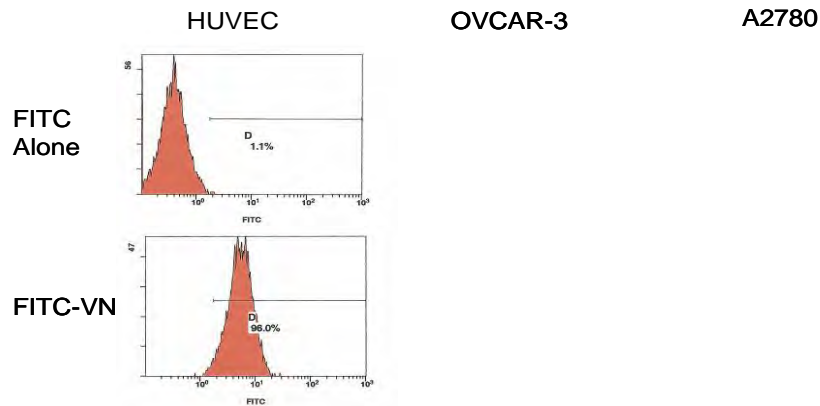
Figure 3: Binding analysis of FITC-VN by FACS. HUVEC OVCAR-3 and A2780 were incubated with FITC alone and FITC-VN The direct binding of labeled protein was assessed by flow cytometry. As shown in the above representative flow-cytometric plots, FITC labeled VN binds avidly to both cell lines as well as the primary vascular endothelial cells.
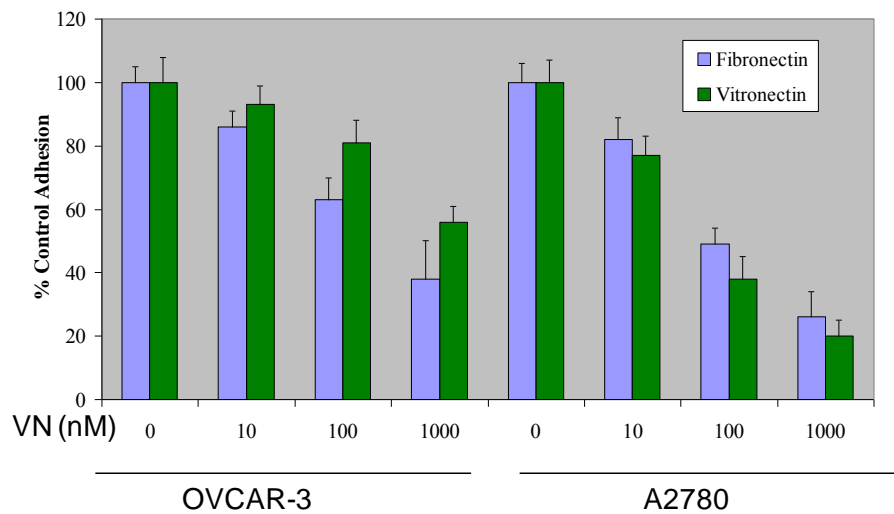
Figure 4: Inhibition of human ovarian carcinoma cells adhesion to extracellular matrices. OVCAR-3 and A2780 cells were pre-incubated with various concentrations of VN (0-1000nM) and then allowed to adhere onto either purified human fibronectin (blue bars) or vitronectin (green bars). The number of adherent cells for each condition was quantitated using an MTS-based assay. The adhesion of both cell lines was inhibited by VN in a dose dependent manner.
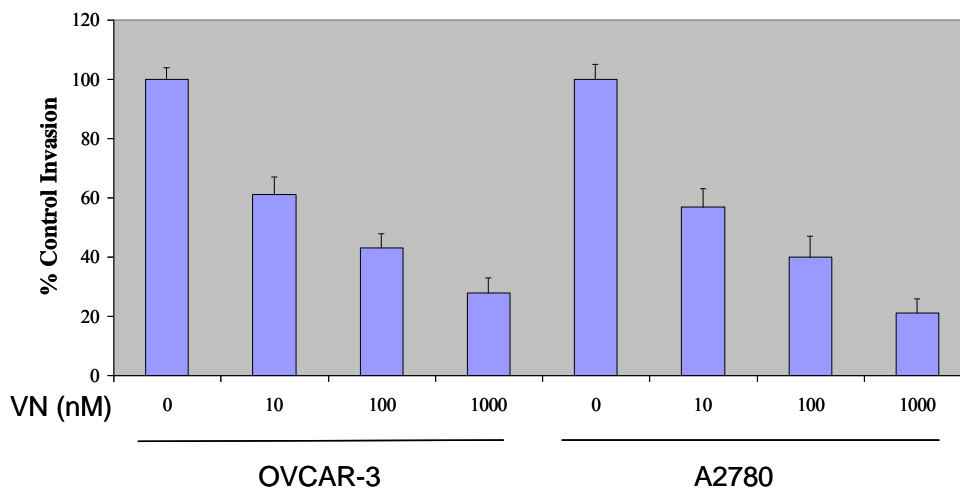
Figure 5: Inhibition of tumor cell invasion through a reconstituted basement membrane. OVCAR-3 and A2780 were preincubated with various concentrations of VN (0-1000nM) for 10 minutes before being seeded on porous inserts coated with ECMatrix and allowed to migrate against a chemoattractant gradient for 18hrs. The invaded cells were detached, lysed, stained with CyQuant, a DNA-binding fluorescent dye, and quantitated in a fluorescent plate reader. The invasion of both the OVCAR-3 and A2780 was inhibited in a dose dependent manner by VN. The IC_{50} in both cell lines is <20nM, comparable to that observed with venom purified CN.

A   B

C   D   E
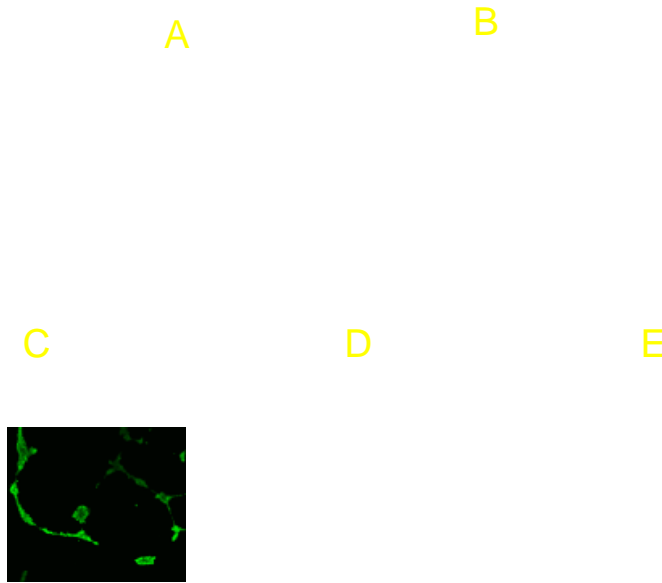
Figure 6: Inhibition of HUVEC tube formation by VN (representative images from multiple experiments). HUVEC cells were plated on 'Endothelial Cell Tube Formation' plates (BD Biosciences) in the presence of various concentrations of VN (0-1000nM), or a known tube formation inhibitor Suramin (used as a positive control). Representative figures from independent experiments were shown above: panel A - untreated control; panel B– 100uM suramin; panel C - 1nM VN; panel D -10nm VN; and panel E 1000nm VN. Cells were stained with Calcein AM and imaged using confocal microscopy. VN is an effective inhibitor of tube formation.
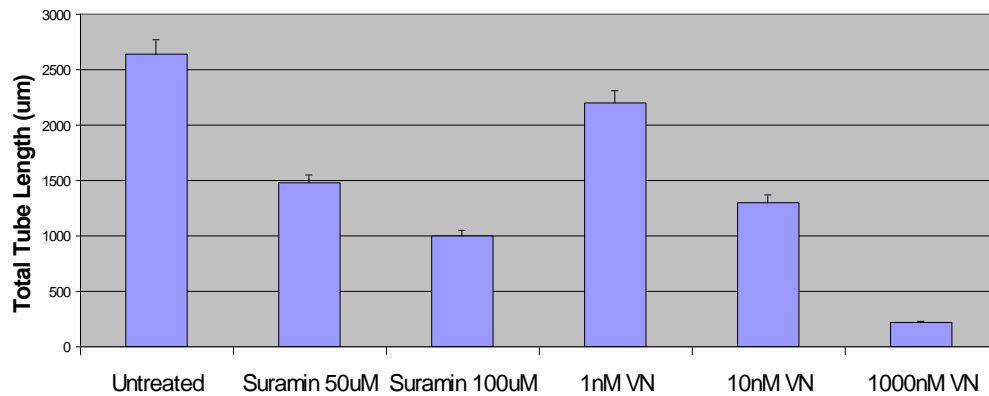
Figure 7: Quantitation of tube formation inhibition by varying concentrations of VN. The tubes formed by HUVECs were quantitated in multiple fields collected from three repeated experiments by computing the total tube length with Zeiss LSM image software and averaged to form each data point. The data shown above was assembled from multiple independent experiments.
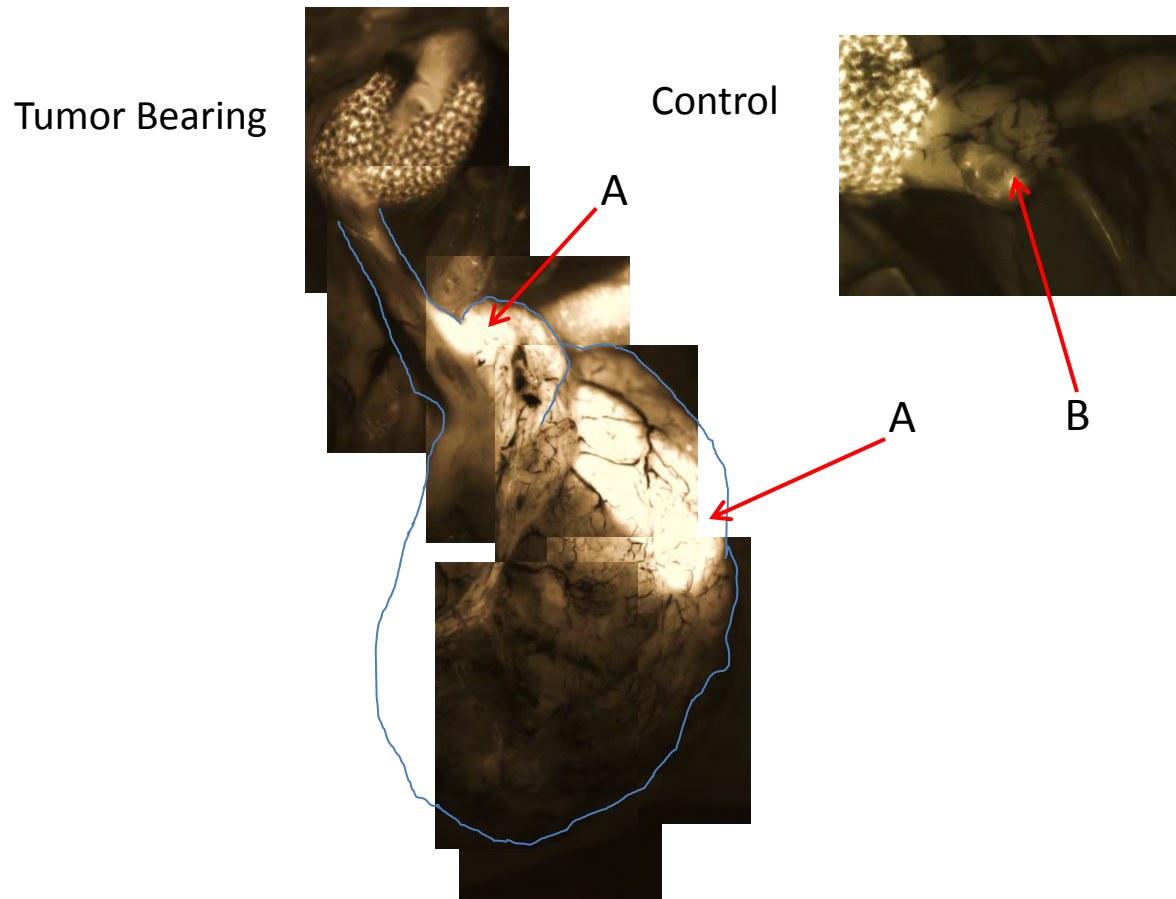
Figure 8 FITC labeled integrin-binding peptide specifically binds to an orthotopic, xenograft ovarian tumor. OVCAR-3 cells were implanted orthotopically into the ovary following its surgical exposure in a balb/c/nu/nu mouse. The tumor was allowed to grow untreated for 28 days. At this time a disintegrin-like, FITC-labeled peptide, CTRKKHDNAQC cyclized through the cysteine side chains, was delivered IV (10 μg). Thirty minutes post peptide injection the ovary was again surgically exposed and fluorescent and optical images of the ovary and surrounding tissue, normal and tumor, were obtained. A high level of fluorescence is observed in the tumor implanted ovary (red arrows A), while little fluorescence is observed in the tissue surrounding the control ovary (red arrow B). The blue line represents the margins of the tumor (there is a dramatic difference in the size of the tumor implanted ovary as compared to the control ovary) and the stitched image in the tumor sample enables the large tumor to be visualized (there is a limited area in the photographic field of the Xenogen instrument).

^{64}Cu Cyclic RGD ^{64}Cu VCN
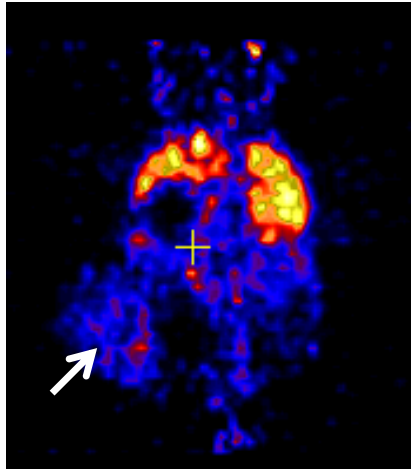
Figure 9: ^{64}Cu-VCN binds to implanted bone tumor. Comparison of binding efficacy of ^{64}Cu-labeled VCN and a cyclic RGD peptide to an existing tumor implanted in the tibia of a nude mouse (white arrow points to tumor. As can be seen VCN binds with much higher affinity than the RGD peptide to the existing tumor, following intravenous administration of the ^{64}Cu-labelled imaging agents. These findings plus other results indicate that VCN can be used as both a therapeutic or a PET imaging agent for ovarian cancer, and most likely for other solid tumors as well.
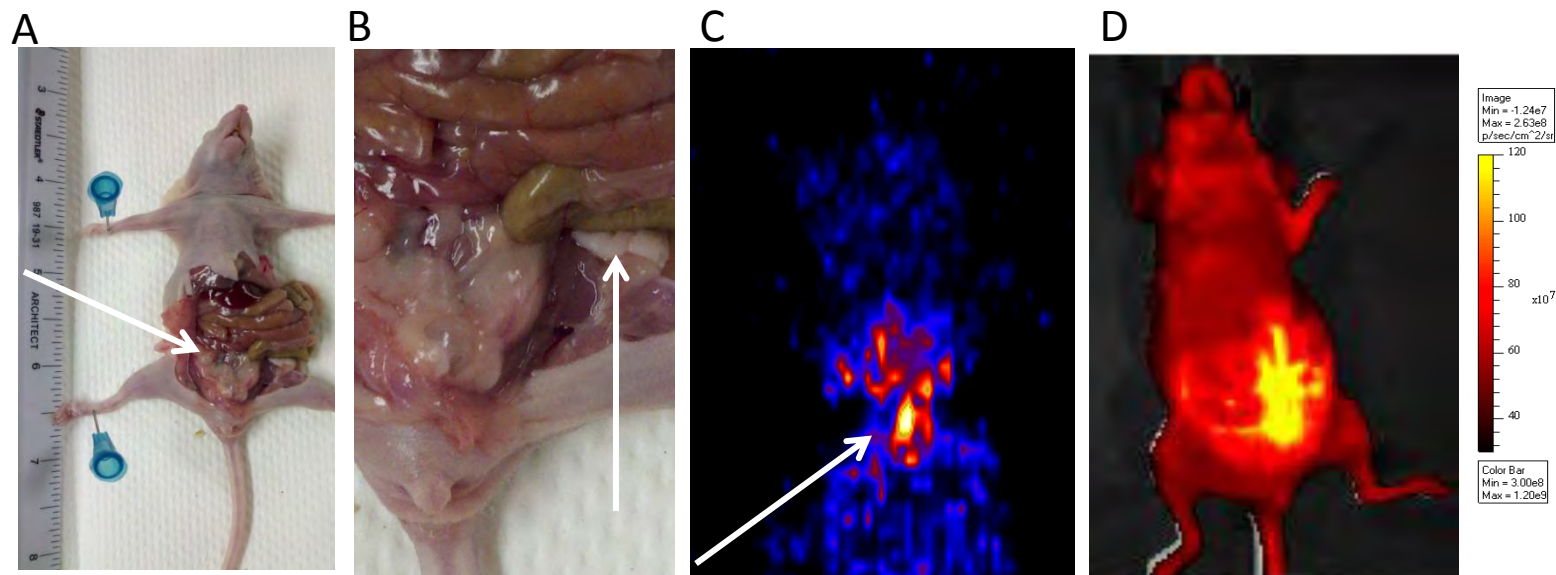
Figure 10: Dissection, PET and Luciferase Imaging of ovarian cancer. Athymic female mice had 2.5 x 10^5 OVCAR-3[luc] cells implanted into the intraperitoneal space via direct injection. The cells stably express luciferase. Panel **A** shows a representative image of a dissected mouse; the arrow indicates the location of the tumor. Panel **B** shows a close-up of the tumor (the tumor appears as the white mass identified by the arrow). Panel **C** is a PET image of the tumor prior to sacrifice of the mouse (200μCi, 100μg VCN injected). This ventral slice shows ^{64}Cu-VCN bound to the tumor (identified by the arrow). Panel **D** is a Xenogen image of the luciferase transfected tumor; luciferase is secreted from the tumor cells the area of the tumor appears diffuse but correlates with both the PET image and the dissected animal (the tumor is on the right side of the upright animal).
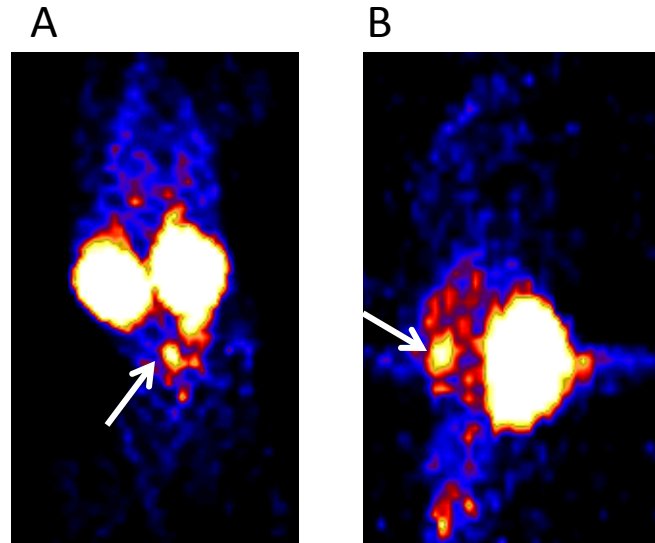
Figure 11: The kidneys retain a large amount of ^{64}Cu-VCN. After dissection the tumor is clearly differentiated from the kidney using alternate views. Panel **A:** In a straight dorsal or ventral (shown) reconstruction encompassing all slices from the PET image, the kidneys clearly accumulate ^{64}Cu-VCN and it is difficult to differentiate the tumor from the high background. Panel **B:** In viewing a transverse section, the kidneys appear as a single bright element, but the tumor is clearly distinct from the kidney. Three dimensional reconstruction and rotation of this image make it evident that the ovarian tumor is clearly and specifically binding ^{64}Cu-VCN (arrows points to the tumor in both views).

Development of a chimeric recombinant disintegrin as a cost-effective anti-cancer agent with promising translational potential

Radu Minea [a,b], Corey Helchowski [a,b], Barbara Rubino [a,b], Kyle Brodmann [a,b], Stephen Swenson [a,b], Francis Markland, Jr. [a,b,*]

[a] Department of Biochemistry and Molecular Biology, University of Southern California, Keck School of Medicine, 1303 N Mission Road, CRL-106, Los Angeles, CA 90033, USA
[b] Norris Comprehensive Cancer Center, University of Southern California, Keck School of Medicine, 1303 N Mission Road, CRL-106, Los Angeles, CA 90033, USA

ARTICLE INFO

ABSTRACT

Vicrostatin (VCN) is a chimeric recombinant disintegrin generated in Origami B (DE3) *Escherichia coli* as a genetic fusion between the C-terminal tail of a viperid disintegrin echistatin and crotalid disintegrin contortrostatin (CN). The therapeutic modulation of multiple integrin pathways via soluble disintegrins was previously shown by us and others to elicit potent anti-angiogenic and anti-metastatic effects in several animal cancer models. Despite these favorable attributes, these polypeptides are notoriously difficult to produce recombinantly in significant quantity due to their structure which requires the correct pairing of multiple disulfide bonds for biological activity. In this report, we show that VCN can be reliably produced in large amounts (yields in excess of 200 mg of active purified disintegrin per liter of bacterial culture) in Origami B (DE3), an *E. coli* expression strain engineered to support the folding of disulfide-rich heterologous proteins directly in its oxidative cytoplasmic compartment. VCN retains the integrin binding specificity of both parental molecules it was derived from, but with a different binding affinity profile. While competing for the same integrin receptors that are preferentially upregulated in the tumor microenvironment, VCN exerts a potent inhibitory effect on endothelial cell (EC) migration and tube formation in a dose-dependent manner, by forcing these cells to undergo significant actin cytoskeleton reorganization when exposed to this agent *in vitro*. Moreover, VCN has a direct effect on breast cancer cells inhibiting their *in vitro* motility. In an effort to address our main goal of developing a clinically relevant delivery method for recombinant disintegrins, VCN was efficiently packaged in liposomes (LVCN) and evaluated *in vivo* in an animal breast cancer model. Our data demonstrate that LVCN is well tolerated, its intravenous administration inducing a significant delay in tumor growth and an increase in animal survival, results that can be partially explained by potent tumor apoptotic effects.

1. Introduction

The ability of transformed cells to evade the restrictive environmental control exerted by the normal tissue architecture and grow in an anchorage-independent fashion is one of cancer's hallmarks (Hanahan and Weinberg, 2000). One class of cell surface receptors known to play a critical role in the process leading to the acquisition of an anchorage-independent phenotype is represented by the integrins (Hood and Cheresh, 2002).

Integrins are heterodimeric receptors that evolved to mediate the complex cell-ECM interactions that regulate the ability of cells to mechanically sense their microenvironment. In the ecology of multicellular organisms, integrins are major contributors to the homeostasis of tissue architecture by keeping epithelial cells in a differentiated, specialized state (Bissell et al., 2003). Conversely, as epithelia transition to malignancy they evade the microenvironmental constraints by both altering their integrin affinity and avidity for ECM proteins (inside-out signaling) and/or shifting their integrin expression (Hood and Cheresh, 2002; Mizejewski, 1999). The precise roles, however, played by different integrin subunits in various aspects of tumor progression and why some integrins appear to be especially supportive of tumor progression (Desgrosellier et al., 2009) are still poorly understood. Despite these limitations, due to their pivotal roles in cancer biology, integrins represent attractive therapeutic targets. For instance, although it doesn't seem to be essential for the formation of vasculature during development (Reynolds et al., 2002), nor during physiological angiogenesis associated with wound healing or tissue repair (Hamano et al., 2003; Serini et al., 2006), the $\beta 3$ integrin appears to be critically involved in the regulation of pathological angiogenesis (Mahabeleshwar et al., 2008). Similarly, $\alpha v\beta 5$ and $\alpha 5\beta 1$ as well as a number of other integrins (notably $\alpha 2\beta 1$, $\alpha 4\beta 1$, and $\alpha 6\beta 4$) have also been shown to play important roles in tumor angiogenesis (Serini et al., 2006; Silva et al., 2008). These observations prompted the exploration of pharmacological blockade of integrins which was eventually demonstrated to significantly reduce tumor angiogenesis in numerous cancer models and led to the development of several drug candidates that are currently in clinical trials (Folkman, 2007; Nemeth et al., 2007).

Disintegrins are among the most potent soluble ligands of integrins representing a class of cysteine-rich polypeptides historically isolated from the venoms of snakes belonging to the Viperidae family (Gould et al., 1990). These natural polypeptides (4–16 kDa), first discovered in 1983 (Ouyang and Huang, 1983) and named in 1990 (Gould et al., 1990), hold a significant translational potential as anticancer agents based on their anti-angiogenic and anti-metastatic effects demonstrated in various experimental settings (Huang et al., 2001; McLane et al., 2008; Swenson et al., 2004). In the time that has passed since the first disintegrin was identified almost three decades ago (Ouyang and Huang, 1983), over 100 additional disintegrins have been named and studied (McLane et al., 2008). Despite their enormous therapeutic potential, to the best of our knowledge none of these natural products or their recombinant variants has made it yet into human clinical trials.

Nonetheless, many of these natural polypeptides continue to be intensely investigated preclinically in various animal models of human disease while they are evaluated for imagistic and therapeutic applications for pathologies as diverse as cancer, cardiovascular thrombotic events, chronic inflammation, asthma, osteopenia etc. (McLane et al., 2008). From earlier attempts to investigate the anti-thrombotic applications of disintegrins, such as echistatin (Shebuski et al., 1990) and kistrin (Barker et al., 1992; Gold et al., 1991), most subsequent preclinical efforts have focused on the anti-angiogenic and anti-metastatic properties of these compounds for anti-cancer applications (Kang et al., 2000; Kim et al., 2003; Marcinkiewicz et al., 2003; Ramos et al., 2008; Swenson et al., 2004). Another promising clinical application of disintegrins is represented by the tumor imagistic potential of these integrin-targeted molecules. To explore this particular application of disintegrins, McQuade et al. investigated the tumor specificity of radiolabeled bitistatin (which binds to $\beta 3$ integrins) in a breast carcinoma animal model (McQuade et al., 2004). In this model, bitistatin was radiolabeled with either ^{125}I or a beta-emitting radionuclide, ^{64}Cu, which is an effective positron emission tomography (PET) tracer. Although preliminary, the results from this imagistic study showed that the tumor specificity of radiolabeled bitistatin was similar or better to that of much smaller RGD-containing peptides and the fact that radiolabeled bitistatin accumulated in tumors that do not themselves express the $\beta 3$ integrin.

The integrin-binding activity of disintegrins depends on the appropriate pairing of several cysteine residues responsible for the disintegrin fold, a mobile 11-amino acid loop protruding from the polypeptide core displaying a tripeptide recognition motif, usually RGD (Arg–Gly–Asp), that is conserved in many disintegrins (Moiseeva et al., 2008; Saudek et al., 1991). Although these molecules naturally evolved to efficiently bind to the activated platelet-specific integrin $\alpha IIb\beta 3$, thus disrupting the process of platelet aggregation (the final step in blood clotting), most purified snake venom disintegrins are rather promiscuous in that they bind to several $\beta 1$, $\beta 3$ or $\beta 5$ integrin members, albeit with different affinities and selectivity (McLane et al., 1998). Two of the most studied native disintegrins are the homodimer contortrostatin (CN) (Trikha et al., 1994b) and the monomer echistatin (McLane et al., 2008). Similar to echistatin, the anti-tumor activity of CN is based on its high affinity interaction with integrins $\alpha v\beta 3$, $\alpha v\beta 5$, and $\alpha 5\beta 1$ on both cancer and angiogenic endothelial cells (Trikha et al., 1994a; Zhou et al., 1999, 2000). We have previously shown (Swenson et al., 2004) that a liposomal formulation of CN can delay tumor growth by significantly reducing the microvascular density in an orthotopic animal cancer model. We provided evidence that disintegrins can be safely and effectively administered intravenously by a clinically acceptable delivery method (i.e., liposomal delivery), and that they passively accumulate at the tumor site. Furthermore, when packaged in liposomes, disintegrins did not interact with the components of blood coagulation system (platelets) nor elicit a neutralizing immune response. Here, we provide further evidence that a chimeric disintegrin, vicrostatin (VCN) can be efficiently made recombinantly in Origami B (DE3) *Escherichia coli*. VCN retains the integrin

specificity of CN but it engages these receptors with a unique binding affinity. Unlike cyclic RGD peptides, VCN appears to inappropriately elicit a cascade of signaling events rapidly leading to actin stress fibers disassembly in HUVEC plated on complete Matrigel, an effect that may explain the *in vitro* anti-migratory effects of VCN against endothelial and cancer cells. Finally, we demonstrate here that liposomal formulations of VCN are efficacious *in vivo*, exerting a potent tumor apoptotic effect in a breast carcinoma animal model and significantly prolonging the survival of these animals.

2. Materials and methods

2.1. Controtrostatin purification

Venom of *Agkistrodon contortrix contortrix* was purchased from Miami Serpentarium (Punta Gorda, FL) and CN was purified as previously described (Trikha et al., 1994b).

2.2. Cells and reagents

The MDA-MB-435 cells were obtained from Dr. Janet Price (MD Anderson Cancer Center, Houston, TX) and the MDA-MB-231 cells from Dr. Toshiyuki Yoneda (Osaka University, Osaka, Japan). HUVEC were purchased from PromoCell (Heidelberg, Germany) and maintained according to the manufacturer's protocol. The Origami B (DE3) *E. coli* strain and pET32a expression vector carrying the bacterial thioredoxin A gene (trxA) were purchased from Novagen (San Diego, CA). The oligonucleotide primers used for rCN and VCN cloning were synthesized by Operon Biotechnologies, Inc. (Huntsville, AL). The 'Endothelial Cell Tube Formation' plates were purchased from BD Biosciences (San Jose, CA). The tube formation inhibitor Suramin, the actin modifier Cytochalasin D, and the cyclo(Arg–Gly–Asp–DPhe–Val) peptide were purchased from Calbiochem (San Diego, CA). The complete Matrigel was from BD Biosciences (Bedford, MA). The recombinant TEV protease, Calcein AM, and Rhodamine-Phalloidin were purchased from Invitrogen (Carlsbad, CA). A column-based FITC-labeling kit (EZ-Label) and an endotoxin removal kit were purchased from Pierce (Rockford, IL). The DeadEnd™ Fluorometric TUNEL assay kit was from Promega (Madison, WI). The mouse $\beta3$ integrin 7E3 antibody was a gift from Dr. Marian Nakata (Centocor, Horsham, PA). Purified soluble $\alpha v\beta3$ and $\alpha v\beta5$ integrins were purchased from Millipore and soluble recombinant $\alpha5\beta1$ integrin from R&D Systems (Minneapolis, MN). All other reagents were purchased from Sigma Chemical Co. (St. Louis, MO). Avastin (bevacizumab) was a gift from Dr. Agustin Garcia (Norris Comprehensive Cancer Center, University of Southern California).

2.3. Construction of rCN and VCN expression vectors and recombinant production

rCN and VCN were cloned into pET32a vector downstream of TrxA using a BglII/NcoI set of restriction enzymes. The forward primers for both rCN and VCN introduced a unique TEV protease cleavage site, which made possible the removal of thioredoxin during purification. To build the VCN construct, the nucleotides encoding the C-terminal tail of echistatin were added to CN via an elongated reverse primer. The primers used for rCN were: forward—5′gttccagatctcgagaatctttacttccaaggagacgctcctgcaaatccgtgctgcga3′, and reverse—5′gttattcgccatggcttaggcatggaagggatttctgggacagccagcaga3′. The primers used for VCN were: forward—5′gttccagatctcgagaatctttacttccaaggagacgctcctgcaaatccgtgctgcga3′, and reverse—5′gttattcgccatggcttaagtagctggacccttgtggggatttctgggacagccagcagatatgcc3′. The bacterial transformants were grown and induced as previously described (Minea et al., 2005) then lysed in a microfluidizer (Microfluidics M-110 L, Microfluidics, Newton, MA). The operating conditions of the microfluidizer included applied pressures of 14,000–18,000 psi, bacterial slurry flow rates of 300–400 ml per minute and multiple passes of the slurry through the processor. The lysate insoluble cellular debris was removed by centrifugation ($40,000 \times$ g) and the soluble material containing either Trx-rCN or Trx-VCN collected. The expressed fusion proteins in the collected soluble lysates were then proteolysed by incubation with recombinant TEV protease overnight at room temperature. When proteolysis was complete, the proteolyzed lysates were passed through a 0.22 μm filter, diluted 1:100 in ddH$_2$O, ultrafiltrated through a 50,000 MWCO cartridge (Biomax50, Millipore) and then reconcentrated against a 5000 MWCO cartridge (Biomax5, Millipore) using a tangential flow ultrafiltration device (Labscale TFF system, Millipore).

2.4. Purification of recombinant disintegrins

Purification was accomplished by C-18 reverse phase HPLC using the standard elution conditions previously employed for the purification of native CN (Trikha et al., 1994b). The filtrated lysates processed as described above were loaded onto a Vydac C-18 column (218TP54, Temecula, CA). A 10-min rinse (at 5 ml/min) of the column with an aqueous solution containing 0.1%TFA was followed by a linear gradient (0–100%) elution over 150 min in a mobile phase containing 80% acetonitrile and 0.1%TFA. rCN starts eluting in 30% acetonitrile, while VCN elutes in 35% acetonitrile.

2.5. Inhibition of platelet aggregation

The inhibition of ADP-induced platelet aggregation by recombinant disintegrins was determined by measuring the light absorption of human platelet-rich plasma (PRP) in a specialized spectrophotometer (Chrono-log 490 optical aggregometer, Chrono-log, Havertown, PA) as previously described (Swenson et al., 2004). The FITC-labeled disintegrins (FITC-CN and FITC-VCN) and the liposomal formulations of VCN (LVCN) were also tested for activity against platelets.

2.6. Mass spectrometry (MS) analysis and sequencing by tryptic digestion

The MS analysis (MALDI-TOF and ESI) was initially done by Dr. Kym Faull (University of California at Los Angeles) and the subsequent sequencing by Dr. Ebrahim Zandi (Keck

School of Medicine, University of Southern California). For sequencing, the purified recombinant disintegrin was reduced, alkylated and digested with trypsin at 37 °C overnight. The resultant digestion peptides were then used in the tandem LC/MS/MS for sequence analysis. The LC consists of a reverse phase C-18 column through which peptides were eluted into the mass spectrometer using the following gradients: 5–60% acetonitrile + 0.1% formic acid over 75 min and 50–90% acetonitrile + 0.1% formic acid over 10 min. Tandem MS/MS spectra was acquired with Xcalibur software on a linear ion trap LTQ instrument. Data was analyzed using Bioworks, the SEQUEST algorithm and Sage-N Sorcerer to determine cross-correlation scores between acquired spectra and NCBI protein FASTA databases or any other databases as needed.

2.7. Cell surface binding studies by flow cytometry

HUVEC, MDA-MB-231 or MDA-MB-435 cells were grown to early confluency and starved overnight in serum-free media. The cells were harvested and resuspended in 1 ml of serum-free media (5×10^5 cells/condition) before being incubated with different treatments or controls for 30 min at 37 °C. At the end of the incubation period, the cells were pelleted, washed in ice-cold PBS containing 5% fetal bovine serum and analyzed in a FACSCalibur scanner. All cells were counterstained with propidium iodide to allow gating of necrotic cells.

2.8. Integrin binding kinetics by fluorescence polarization (FP)

Differing concentrations of purified soluble functional integrins (i.e., $\alpha v \beta 3$, $\alpha v \beta 5$ or $\alpha 5 \beta 1$) were incubated with a constant amount of FITC-labeled VCN or CN using an established protocol (Park and Raines, 2004). Upon binding to the much larger integrin, the fluorescent tag on either disintegrin tumbles in solution at a slower rate compared to the unbound state resulting in increased levels of polarization. The measured FP value is a weighted average of FP values of the bound and free fluorescent disintegrins and is therefore a direct measure of the bound fraction. The data were analyzed as for standard radioligand binding, and kinetics of binding determined using Scatchard analysis and a non-linear curve fit. The data were generated in a PTI QuantaMaster QM-4SE spectrofluorometer (Photon Technology International, Birmingham, NJ) using the PTI FeliX32 software for data acquisition and Prism v3.02 (GraphPad Software, La Jolla, CA) for data analysis.

2.9. Cell viability studies

HUVEC, MDA-MB-231 or MDA-MB-435 cells were plated in complete media on either plastic or Matrigel-coated 24-well plates (5×10^4 cells/well) and allowed to adhere. Native CN or VCN were added to the wells at concentrations ranging from 1 to 1000 nM. Cells receiving no treatment or Actinomycin D were used as controls. The number of viable cells for each condition was quantified colorimetrically after 24 h of incubation using the Cell Titer 96 AQueous cell viability kit (Promega, Madison, WI)

according to the manufacturer's protocol. The cell viability was further confirmed by TUNEL staining.

2.10. Inhibition of cell migration (the colloidal gold migration assay)

The ability of disintegrins to interfere with HUVEC, MDA-MB-231 or MDA-MB-435 cell migration was assessed on glass coverslips homogenously covered with a fine layer of colloidal gold salt. This assay represents a modified form of a previously described cellular migration assay (Albrecht-Buehler, 1977; Bowersox and Sorgente, 1982; Zetter, 1980). The cell migration generates particle-free tracks ('phagokinetic tracks') on a densely particle-coated migratory substrate that can act as a permanent record of cellular movement. The gold chloride solution was prepared using 0.342 g Hydrogen Tetrachloroaurate(III) (Sigma–Aldrich) dissolved in 50 ml dH$_2$O. Clean round glass coverslips 2.2 cm diameter (VWR International) were grasped with forceps from the edge and repeatedly dipped into a 1% BSA solution over a period of several minutes. The BSA slowly adhered to the glass and this process allowed for a better and more uniform gold coating. Excess BSA was allowed to drain off the coverslips at an angle after which the slips were dipped once in 100% ethanol. The coverslips were then rapidly dried with a hand held hair dryer at medium settings and then placed into the wells of a 12-well cell culture plate (VWR International) for further coating with gold salt as previously described (Bowersox and Sorgente, 1982; Zetter, 1980). Microscopic visual inspection of the wells was then performed under 100–200 × magnification (Olympus CK2 inverted phase contrast microscope, or Zeiss Axioplan-2 optical microscope). A uniform orange brown speckled appearance on a black background covering the surface of the slides was indicative of a successful preparation. The prepared gold coverslips were further covered with a layer of complete Matrigel (overnight at 37° C). Early passages of serum-starved HUVEC, MDA-MB-231 or MDA-MB-435 cells were then seeded on these coverslips (approximately 3000cells/well) in the presence of various treatments and allowed to migrate at 37 °C in the presence of 5%CO$_2$ for up to 48 h depending on the cell line, after which the cells were fixed in 4% formaldehyde and further imaged. The quantification of cellular migration was done by computer-assisted image analysis in which each pixel corresponding to the 'phagokinetic tracks' was counted digitally using the 'SimplePCI' imaging software (C-Imaging Systems, Cranberry Township, PA). The pixels were counted in 25 randomly selected microscopic fields captured at ×200 magnification for each treatment condition and plotted against the controls.

2.11. Inhibition of HUVEC tube formation

'Endothelial Tube Formation' plates precoated with Matrigel were used according to the manufacturer's protocol. HUVEC were seeded in triplicate (3×10^4 cells/well) in the presence of various concentrations of either native CN or VCN and incubated for 16 h at 37 °C in the presence of 5%CO$_2$. The tube formation inhibitor Suramin was used as a positive control. At the end of incubation

period, cells were stained with Calcein AM and imaged by confocal microscopy (LSM 510 Confocal/Titanium Sapphire Laser). The total length of tubes for each condition was quantitated in multiple fields using the Zeiss LSM Image Browser (Carl Zeiss MicroImaging GmbH, Munich, Germany) and averaged from at least three independent experiments.

2.12. Disruption of actin cytoskeleton organization

HUVEC grown in complete media were seeded in triplicate in 8-well chamber slides coated with complete Matrigel (4×10^4 cells/well) before being incubated with various treatments for 3 h at 37 °C in the presence of 5%CO_2. The actin modifier Cytochalasin D (CytoD) was used as a positive control. At the end of the incubation period, the cells were washed, fixed in 4% formaldehyde, permeabilized in 0.1% Triton X-100 in PBS, and then stained with Rhodamine-Phalloidin and counterstained with Hoechst 33342 before being imaged by confocal microscopy (LSM 510 Confocal/Titanium Sapphire Laser).

2.13. Liposomal encapsulation of VCN

This procedure was carried out as previously described (Minea et al., 2005) by Molecular Express, Inc (Los Angeles, CA) a company specializing in liposomal encapsulation of therapeutic proteins and other drugs. Liposomal VCN (LVCN) particles were generated by either probe sonication at 10% power for 3–5 min in a Branson Probe Sonifier or homogenized in a microfluidizer (M-110 L; Microfluidics, Newton, MA). The homogenized material was processed between 10,000 and 18,000 psi while maintaining an elevated temperature (45–65 °C). Samples from each batch were taken during the process and the size distribution of LVCN was determined with an Ultrafine Particle Analyzer (UPA150; Microtrac, North Largo, FL). After processing, the unencapsulated VCN in each batch was removed by ultrafiltration using an Amicon UF membrane of 100,000 MWCO and the LVCN was further sterilized by filtration through a 0.2 μM PVDF filter.

2.14. In vivo efficacy studies

MDA-MB-231 cells (2.5×10^6 per inoculum) were harvested and resuspended in complete Matrigel before being inoculated into the mammary fat pads of nude mice as previously described (Swenson et al., 2004). The tumors were allowed to grow for 2 weeks or until they became palpable before treatment was initiated. VCN was administered either encapsulated in different liposomal formulations (at the dose-equivalent of 100 μg of VCN per injection) or non-encapsulated, as an aqueous solution (100 μg VCN). All VCN administrations were made intravenously (via tail vein) twice a week for the duration of each study. Avastin was administered intravenously (via tail vein) at the dose of 400 μg per injection (approx. 20 μg/gr) once a week for the duration of the study. Tumor diameters were measured weekly with a caliper in a blind fashion and the tumor volumes calculated using the formula [length (mm) $\times$ width (mm)^2]/2, where the width

and the length were the shortest and longest diameters, respectively (Osborne et al., 1985). The average tumor volume for each study group was plotted as a function of time and type of treatment during the entire course of each study. The animals were handled and euthanized under the strict guidelines of the Institutional Animal Care and Use Committee (IACUC) of the University of Southern California.

2.15. TUNEL staining of tumor sections

For tumor apoptosis, the DeadEnd^{TM} Fluorometric TUNEL assay kit (Promega, Madison, WI) was used according to the manufacturer's protocol. After TUNEL staining, the cell nuclei were counterstained with Hoechst 33342. The nuclei from apoptosis 'hotspot' areas were digitally counted (object counting) using the SimplePCI imaging software on random images (at least 10 images per tumor from multiple tumors per group) captured at $\times 250$. The % of cell death was plotted using the formula 'number of TUNEL$^+$ nuclei/total number of nuclei $\times 100$' for each treatment group.

2.16. Statistical analysis

Statistical significance was analyzed in Prism v.3.2 (GraphPad Software, La Jolla, CA) by unpaired t-test followed by F-test to compare variances. The tumor volume distribution and immunohistochemistry data were assessed by analysis of variance (ANOVA) with a significant overall F-test followed by Dunnett's multiple comparison tests of treatment groups relative to control. Two-tailed $P < 0.05$ were considered significant.

3. Results

3.1. Recombinant production of VCN

3.1.1. Bacterial expression

The expression of recombinant disintegrins was in Origami B (DE3), a strain uniquely designed to address the shortcomings of disulfide-rich recombinant protein production in wild-type E. coli (LaVallie et al., 1993). The pET32a expression vector and the T7 system are designed for robust expression of heterologous proteins fused to the 109 amino acid bacterial thioredoxin A (TrxA) in DE3 lysogens. In wild-type E. coli, TrxA normally functions as a major cytoplasmic reductase under tight regulatory control. However, in the Origami strain, the oxidative redox state perpetuated by defective thioredoxin reductase (TrxB) and glutathione reductase (Gor) enzymes 'tricks' this bacterium into producing compensatory higher amounts of TrxA reductase in an attempt to restore the wild-type redox equilibrium which in turn drives the robust expression of any recombinant protein genetically fused to TrxA. Another advantage of expressing heterologous proteins fused to TrxA is the high solubility of this bacterial protein, the result of which is that TrxA internally chaperones the recombinant protein fused to it thus keeping it in solution and allowing for higher levels of foreign protein accumulation in the cytoplasm (LaVallie et al., 1993).

To explore the recombinant production of disintegrins in Origami B (DE3), we generated a construct based on the native sequence of CN (referred to as rCN) and a chimeric construct, previously designated as rCN+ (Minea et al., 2005), but now referred to as vicrostatin (VCN). The VCN construct was designed by replacing the C-terminal tail of native CN with the tail of another native disintegrin, echistatin (also known as echistatin alpha), a short–length viperid disintegrin (Fig. 1). The rationale for the VCN design was based on the finding that the C-termini of snake venom disintegrins are important structural elements essential for full disintegrin activity. For instance, the co-crystallization of monomeric disintegrin trimestatin with integrin αvβ3 demonstrates that the C-terminus of this disintegrin also engages the receptor, but in a different region than its disintegrin loop (Fujii et al., 2003). In addition, a previous report (Wierzbicka-Patynowski et al., 1999) had demonstrated that the swapping of C-terminal tails between two native disintegrins may actually lead to the generation of novel chimeric molecules capable of recognizing specific integrins with altered binding affinities.

By employing the recombinant system described above, two fusion proteins (Trx-rCN and Trx-VCN) were successfully expressed in the cytoplasm of Origami B (DE3) (Fig. 2). Although the expression of Trx-VCN was robust in Origami B (DE3), by growing these transformants in modified media we have been able to boost the recombinant production level of VCN by at least one order of magnitude to a final expression yield of approximately 200 mg of active purified disintegrin per liter of bacterial culture.

A unique tobacco etch virus (TEV) protease cleavage site was engineered upstream of both disintegrin constructs in order to facilitate their subsequent cleavage from TrxA. TEV is a highly selective protease that recognizes with very high specificity the canonical Glu–Asn–Leu–Tyr–Phe–Gln–Gly amino acid sequence (Carrington and Dougherty, 1988) therefore leaving the target recombinant proteins intact. This high specificity makes TEV an ideal molecular tool for processing recombinant proteins expressed as fusions. The released recombinant disintegrins were further processed and purified by reverse phase HPLC using a protocol originally designed for native disintegrins (see Materials and Methods).

3.1.2. Initial evaluation of recombinant disintegrin activity

The two purified recombinant molecules were initially tested for activity against platelets. Presumably, a main function of snake venom disintegrins in nature is to bind with very high affinity to the activated platelet integrin αIIbβ3, thus efficiently inhibiting (McLane et al., 2008) the last step in blood clotting, the aggregation of platelets, a process mediated by platelet integrin αIIbβ3. However, of the two constructs expressed recombinantly, only chimeric VCN retained full activity against activated αIIbβ3 integrin (with an IC_{50} very similar to native CN), whereas the rCN construct showed no activity in the nanomolar range characteristic of snake venom disintegrins (Fig. 2). Apparently, the latter construct, although soluble, had failed to fold correctly in the region where the binding site of the molecule resides (i.e., the 11-amino acid disintegrin loop), whereas the C-terminal graft in VCN appeared to play an unexpected beneficial role. It is noteworthy that, like VCN, rCN was also expressed as a unique monomeric species as demonstrated on reducing and non-reducing gels (data not shown). Its lack of activity against activated platelets suggests that rCN adopted a non-native disulfide pattern at least in the disintegrin loop region. Although it is unclear why the rCN construct failed to adopt CN's native dimeric conformation in this recombinant system, this was not the result of unsuccessful disulfide bridge formation. Both recombinant constructs have been probed with Ellman's reagent and found to contain no free thiol groups.

3.1.3. Mass spectrometry analysis and sequencing of VCN

Interestingly, the MS analysis (MALDI-TOF and ESI) demonstrated that, unlike native CN, VCN is a monomer (MW = 7146.0). The sequence was subsequently confirmed by tryptic MS sequencing. Based on these data, we speculated that although VCN may have folded correctly in the C-terminal half of the molecule where the disintegrin loop
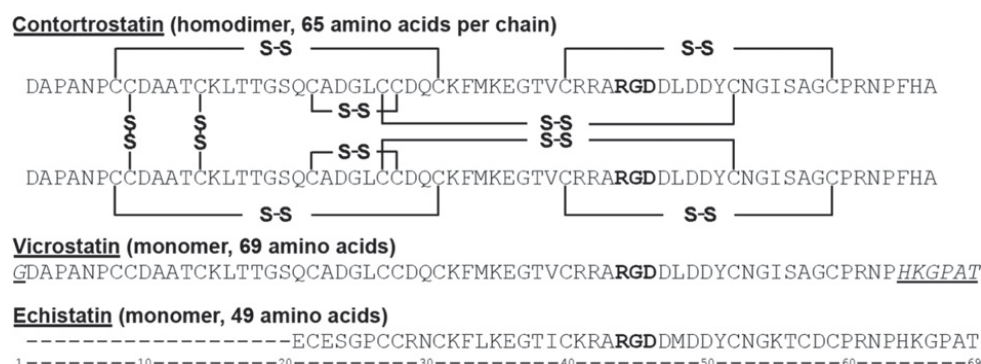

Fig. 1. Sequence alignment of contortrostatin (CN), vicrostatin (VCN), and echistatin. VCN is a modified CN sequence that was generated recombinantly by swapping the C-terminal tail of CN with the tail of echistatin. Mass spectrometry and crystallographic data have shown that CN is a dimer with two identical chains oriented in an antiparallel fashion and held together by two interchain disulfide bonds. Unlike native CN, mass spectrometry has confirmed that VCN is a monomer. In the above sequences, the Arg–Gly–Asp tripeptide motif is depicted in bold whereas the non-native amino acids in VCN are both italicized and underlined.
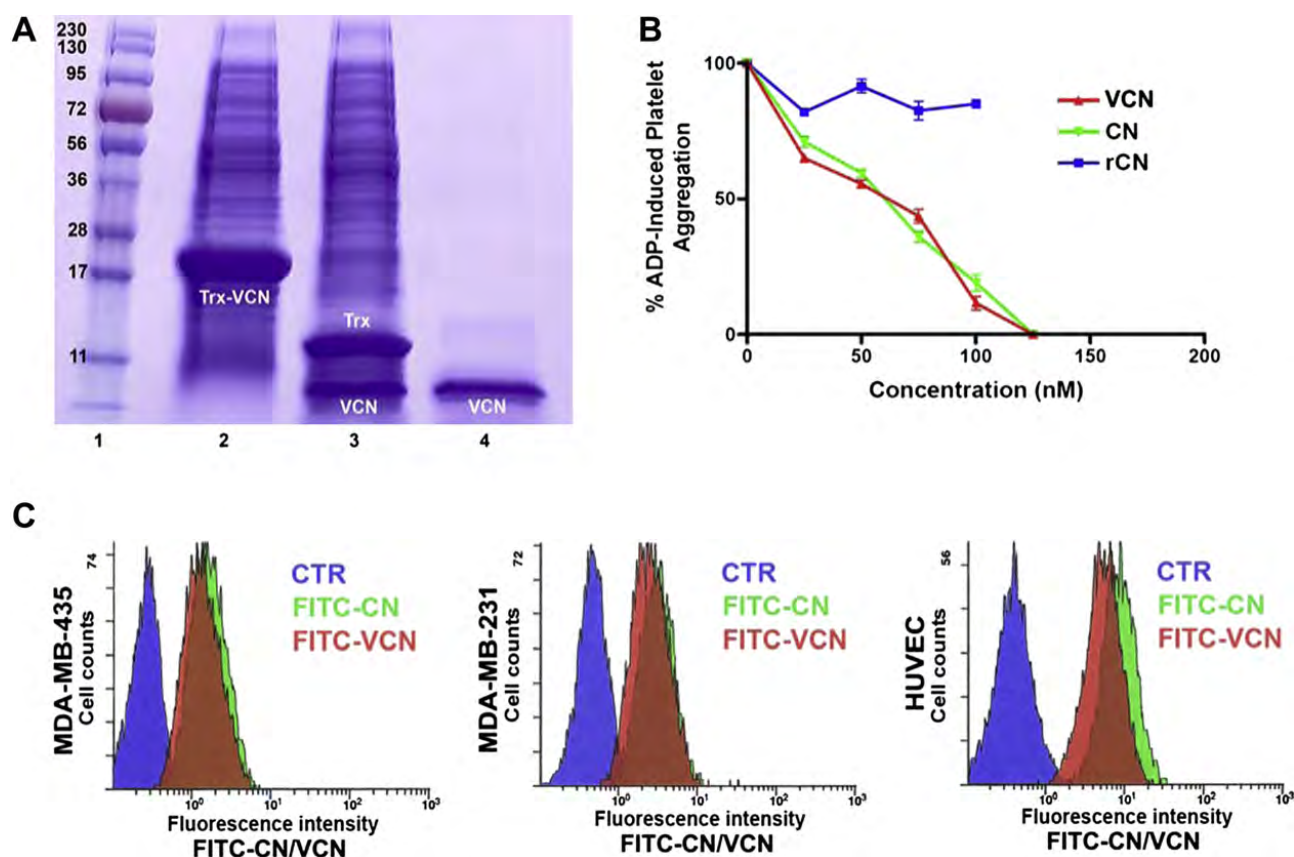
Fig. 2. The expression, purification and binding analysis of FITC-labeled disintegrins by flow cytometry. Panel A—Coomassie stained gel showing the migration of Trx-VCN before and after TEV proteolysis (lanes 2 and 3, respectively) versus C-18 reverse phase-HPLC purified VCN (lane 4). The same amount (5 μl) of cell lysates before and after TEV proteolysis was loaded on a precast gel and Coomassie stained. Panel B—VCN and native CN exhibit an almost identical dose-dependent inhibitory effect against ADP-induced platelet aggregation when incubated with human platelet-rich plasma (with a calculated IC_{50} of ∼60 nM). In contrast, a recombinant construct based on the exact CN sequence (designated rCN), which is also expressed as a soluble polypeptide in Origami B (DE3), shows no inhibitory activity. Panel C—Labeled disintegrins (FITC-CN and FITC-VCN) bind in a similar manner to cells displaying different integrin profiles as determined by flow cytometry. MDA-MB-435, MDA-MB-231 or HUVEC were either incubated with FITC-CN (green) or FITC-VCN (red) or probed with an FITC-labeled irrelevant antibody control (blue). (For interpretation of the references to colour in this figure legend, the reader is referred to the web version of this article).

resides, hence its ability to function like a fully active disintegrin, it might have adopted a non-native cysteine pairing in the N-terminal half of the molecule when compared to native CN (Moiseeva et al., 2008), which compromised its dimerization (see Fig. 1 for disulfide bond configuration of native CN).

3.1.4. Cell surface binding analysis by flow cytometry

The ability of VCN to mimic the binding behavior of native CN against different cell lines was tested by flow cytometry (Fig. 2). Our results show that FITC-labeled VCN has a similar binding profile to CN against HUVEC, MDA-MB-231 and MDA-MB-435 cells.

3.1.5. Integrin binding kinetics by fluorescence polarization

To further determine the specific binding affinities of both native CN and VCN to purified (αvβ3 and αvβ5) or recombinant (α5β1) functional integrins, we measured these interactions in solution by fluorescence polarization. From this set of experiments, the dissociation constants for both native CN and VCN (Table 1) were further

deduced. These data showed that both disintegrins exhibit nearly identical affinities for αvβ3 and a similar affinity for αvβ5. However, the results demonstrated that there is at least an order of magnitude difference in these molecules' Kd values to α5β1 with VCN showing an improved binding affinity for this receptor compared to native CN.

3.2. In vitro functional assays with VCN

3.2.1. Cell viability studies

To understand the impact of VCN on cell viability *in vitro*, we tested a range of VCN concentrations (1–1000 nM) on HUVEC, MDA-MB-231 and MDA-MB-435 cells seeded on top of Matrigel (see Materials and methods) and compared the results to native CN. Neither disintegrin showed any significant impact on cell viability irrespective of the concentration used or the length of the incubation time. The cell viability data was generated using an MTS-based colorimetric assay and further confirmed by TUNEL staining (data not shown).

Table 1
Disintegrin–integrin binding kinetics by fluorescence polarization.

Disintegrin	Integrin Kd (+/−SD).		
	$\alpha v \beta 3$	$\alpha 5 \beta 1$	$\alpha v \beta 5$
CN	6.6 nM (0.8).	191.3 nM(65.2).	19.5 nM(5.7).
VCN	7.4 nM (0.4).	15.2 nM (4.2).	41.2 nM (12.3).

The binding kinetics were calculated by measuring the steady state binding of FITC-labeled disintegrins to either purified ($\alpha v \beta 3$ and $\alpha v \beta 5$) or recombinant ($\alpha 5 \beta 1$) functional human integrins. The dissociation constants for interactions of either CN or VCN with soluble integrins were determined by Scatchard analysis using a non-linear curve fit.

3.2.2. Inhibition of cell migration

Similar to native CN, VCN significantly inhibits HUVEC, MDA-MB-231 or MDA-MB-435 cell migration in a dose-dependent manner (Fig. 3). Cell migration on complete Matrigel is an integrin-dependent mechanism and both disintegrins blocked this process when using different cell lines with significantly different integrin profiles. As determined by us and others, the MDA-MB-435 cells express significantly more copies of $\alpha v \beta 3$ integrin than HUVEC or MDA-MB-231 cells, with the latter expressing the least amount. All three cells also express both $\alpha v \beta 5$ and
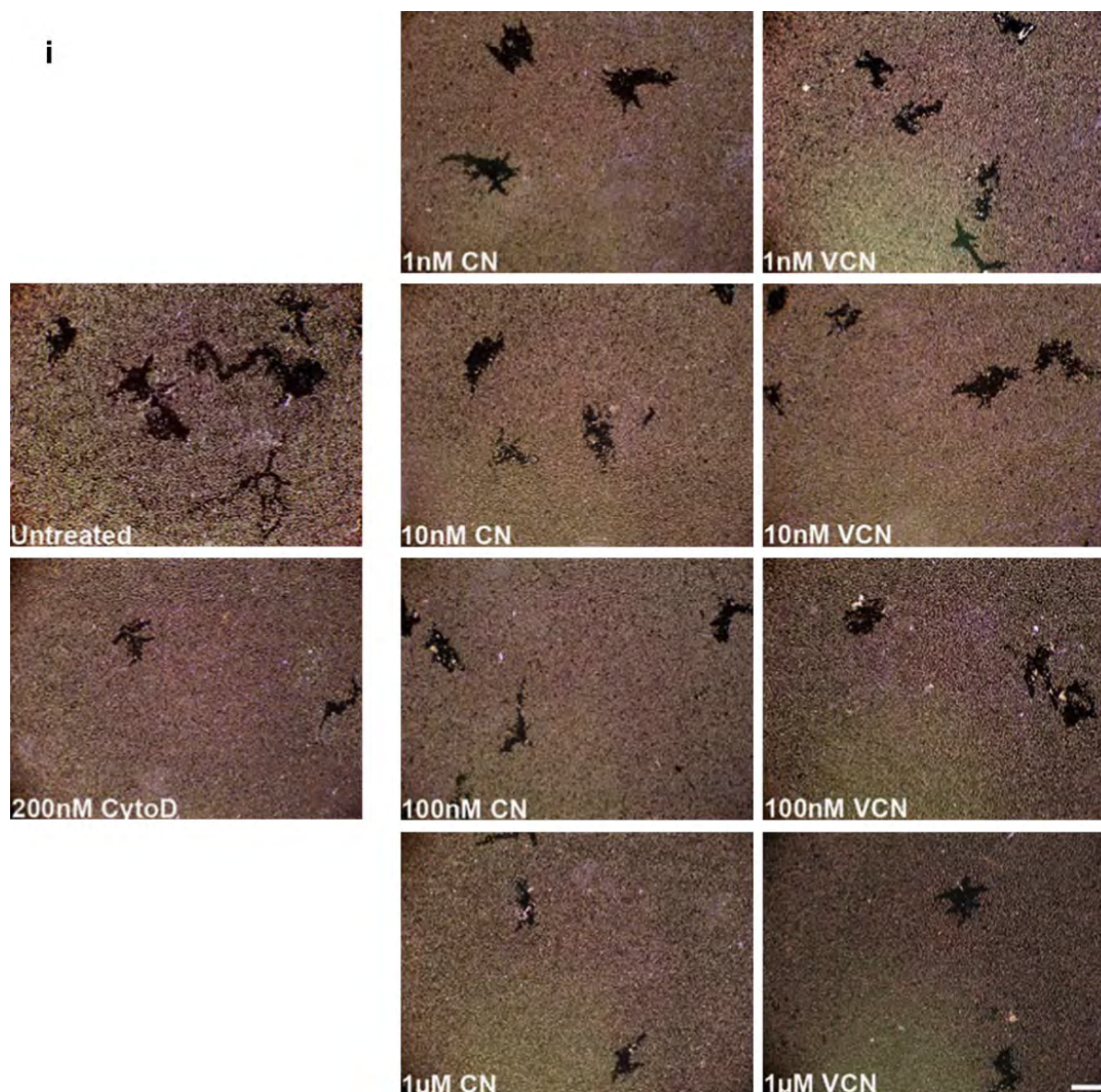

Fig. 3. Inhibition of cell migration (the colloidal gold migration assay) by disintegrins. The ability of VCN to disrupt cell migration was assessed on gold coverslips coated with complete Matrigel on which serum-starved HUVEC, MDA-MB-231 or MDA-MB-435 cells were seeded and allowed to adhere before being incubated for up to 48 h with various concentrations of disintegrins (1–1000 nM). The fungal metabolite Cytochalasin D, a potent inhibitor of actin polymerization, was used as a positive control at a concentration of 200 nM. (i) Representative images of 'phagokinetic tracks' generated on colloidal gold by migratory HUVEC exposed to different concentrations of disintegrins (magnification, ×200; scale bar, 200 μm). (ii) The 'phagokinetic tracks' generated by migratory cells with different integrin profiles (HUVEC, MDA-MB-231 or MDA-MB-435) were quantitated digitally ('SimplePCI' imaging software) by counting the total number of pixels corresponding to every track in multiple photomicrographs for each condition. The above plotted data were averaged from multiple independent experiments for each cell line tested.
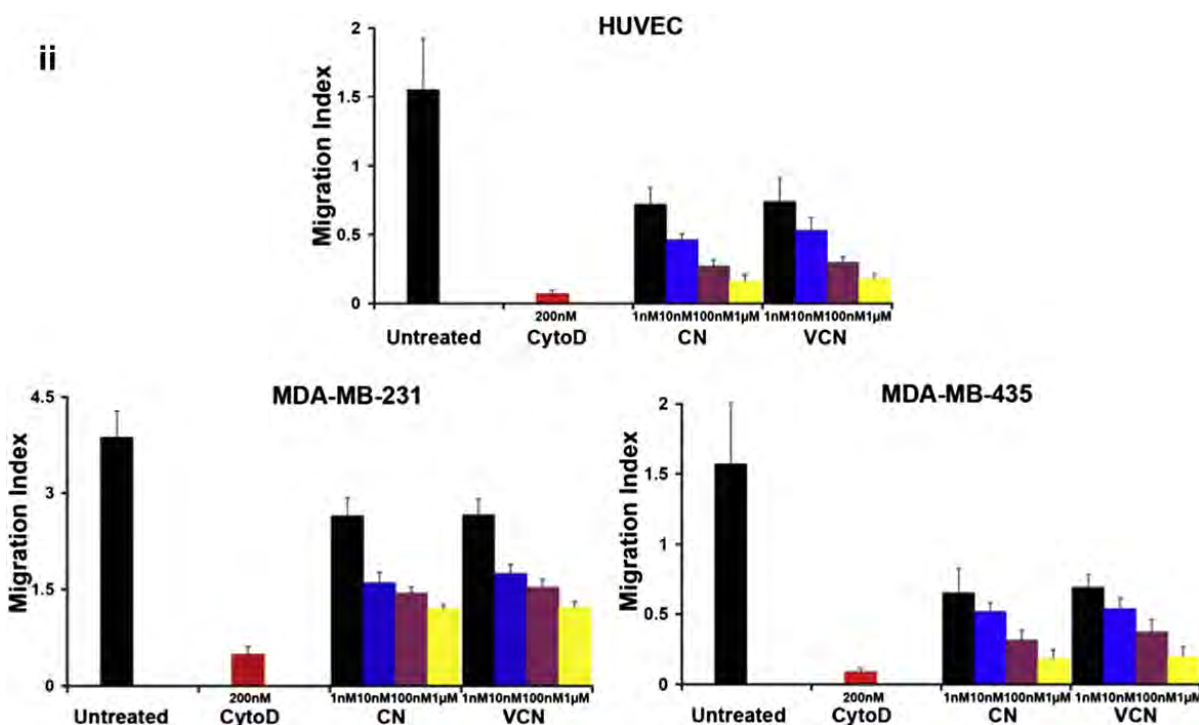
Fig. 3. (*continued*)

α5β1 integrins, with MDA-MB-435 expressing relatively lower amounts of αvβ5 integrin.

3.2.3. Inhibition of HUVEC tube formation

As previously reported with native CN (Golubkov et al., 2003), VCN also potently inhibits HUVEC tube formation in a dose-dependent manner (Fig. 4). In this assay, cells were plated on Matrigel, incubated with various concentrations of each disintegrin, allowed to form tubes, and then compared to either untreated cells or cells treated with a known tube formation inhibitor (Suramin). The cells were stained with Calcein and further visualized by confocal microscopy. Multiple images were captured from at least three independent experiments and the tubes corresponding to each treatment condition were measured digitally by pixel counting using the 'SimplePCI' imaging software. The data was collected by multiple individuals in a blind fashion and the total tube length averaged and plotted for each data set.

3.2.4. Disruption of HUVEC actin cytoskeleton organization

To assess the effect of VCN on cell morphology and actin cytoskeleton organization, HUVEC were allowed to adhere to complete Matrigel before being exposed to various treatments. While VCN does not detach HUVEC plated on Matrigel, our results show that unlike other integrin ligands, including a small cyclic RGD peptide (the cRGDfV) and an anti-integrin β3 monoclonal antibody (7E3), VCN potently collapses the actin cytoskeleton of HUVEC in the nanomolar range (Fig. 5). This effect can be only partially prevented if the cells are preincubated with either the 7E3

antibody or the cyclic RGD peptide cRGDfV before being exposed to VCN (data not shown).

3.3. In vivo studies with VCN

3.3.1. Liposomal encapsulation of VCN

Our previous study showed that liposomal CN has the following characteristics in mice: 1) no immunogenicity, 2) extended circulatory half-life, and 3) undetectable non-target effects (Swenson et al., 2004). In the present study, various batches of LVCN were prepared for *in vivo* testing by either sonication or homogenization under different processing conditions (temperature, pressure etc). The encapsulation efficiency for these batches was determined to be 70% or greater, and the average size of homogenized LVCN was 83 nm.

3.3.2. Efficacy studies with LVCN in vivo

LVCN was previously tested in an MDA-MB-435 animal model (Minea et al., 2005) where we showed that it efficiently delayed tumor growth while exerting a pronounced anti-angiogenic effect. In the current study VCN was further tested in the MDA-MB-231 breast carcinoma model with similar results (Fig. 6). Importantly, in the aggressive MDA-MB-231 model, in addition to the delay in tumor growth, LVCN was a found to also significantly increase the survival of animals with results very similar to those observed with Avastin (all control animals in this model died by the end of week 7). A group that received unencapsulated VCN (at the dose of 100 μg per injection administered twice weekly via tail vein injections) was also evaluated in this breast cancer
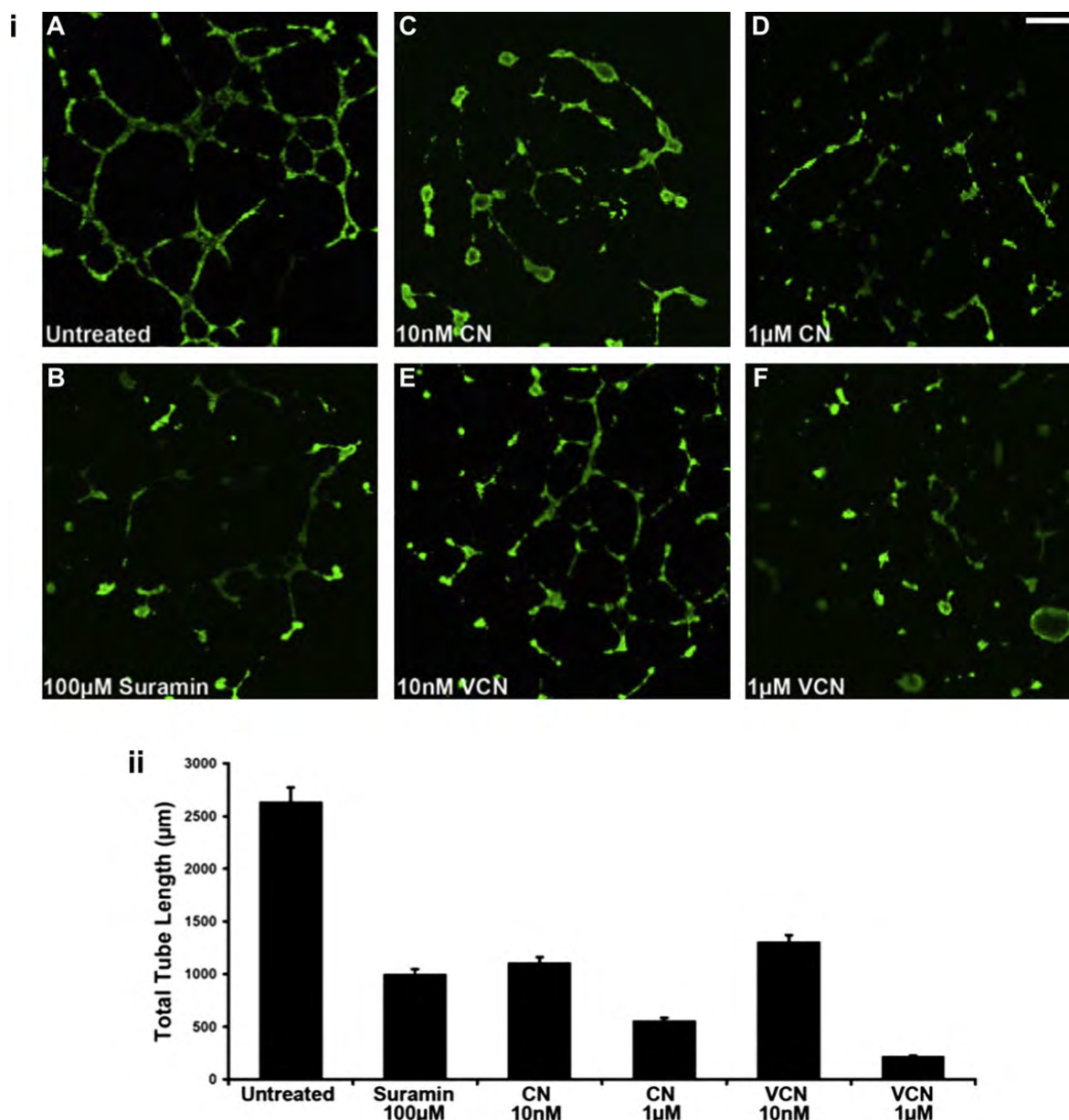
Fig. 4. Inhibition of HUVEC tube formation (tubulogenesis) on Matrigel. HUVEC were plated on 'Endothelial Cell Tube Formation' plates (BD Biosciences) and allowed to adhere before being incubated overnight with various concentrations of either CN or VCN (10–1000 nM) at 37 °C in the presence of 5%CO_2. Suramin, a known tube formation inhibitor, was used as a positive control at a concentration of 100 μM. At the end of incubation period, the cells were stained with Calcein AM and imaged by confocal microscopy. (i) Representative HUVEC images from three independent experiments (magnification, ×25; scale bar, 200 μm). (ii) The degree of tubulogenesis was assessed on multiple photomicrographs for each condition on which the total length of the tubes was measured and computed in multiple fields using the Zeiss LSM Image Browser (Carl Zeiss MicroImaging GmbH) and then averaged to form each data point. The data presented above was assembled from three independent experiments.

model. Interestingly, although the direct injection of unencapsulated VCN at the above dose seemed to be very well tolerated by the animals for the entire duration of the study, at this dose regimen there was no a significant difference in terms of both tumor growth inhibition and survival between the unencapsulated VCN and the control groups (data not shown). The lack of response by unencapsulated VCN is not surprising since this group received the same amount of disintegrin and under the same dosing schedule as the one who received LVCN (i.e., 100 μg twice weekly). Since liposomal VCN has a much longer circulatory half-life than the naked protein (20.4hr for L^{125}I-VCN vs. 0.4 h for ^{125}I-VCN) and a superior tumor accumulation, it is conceivable that the naked VCN group did not receive a therapeutically efficacious dose. Similarly, Cilengitide, a cyclic RGD pentapeptide developed by Merck KGaA, is administered at much higher doses than LVCN due to a shorter circulatory half-life and tumor availability (Mas-
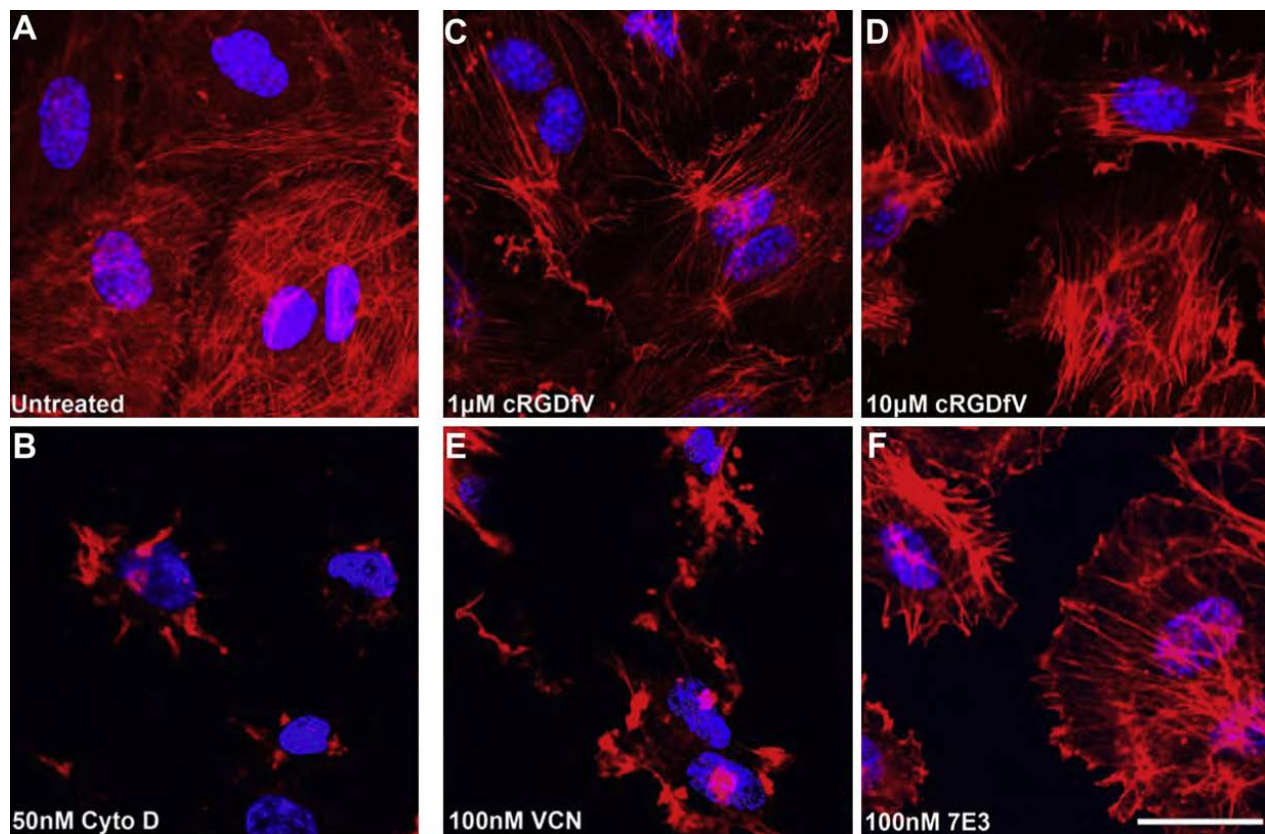
Fig. 5. VCN induces massive actin cytoskeleton reorganization in HUVEC seeded on Matrigel. HUVEC were seeded in multiwell chamber slides in serum-free media on complete Matrigel, allowed to adhere, and then treated for 3 h with various concentrations of either a cRGDfV peptide (1 or 10 μM), VCN (100 nM) or the anti-$\alpha v\beta 3$ monoclonal antibody 7E3 (100 nM). The actin modifier Cytochalasin D was used as a positive control at a concentration of 50 nM. At the end of the incubation period, the cells from all conditions were fixed in 4% formaldehyde, permeabilized in 0.1% Triton X-100, and had their actin cytoskeletons stained with Rhodamine-Phalloidin and nuclei counterstained with Hoechst 33342. Shown above are representative confocal images from multiple experiments taken at the same magnification ($\times 1000$; scale bar, 20 μm).

Moruno et al., 2011). Studies to determine the efficacious dose and dosing regimen for naked VCN in multiple tumor animal models are currently ongoing in the Markland laboratory.

3.3.3. Evaluation of tumor apoptosis activity of LVCN

The current study was also aimed at evaluating the effect of LVCN on tumor apoptosis in the MDA-MB-231 breast cancer model. Unlike the above efficacy study, to evaluate the impact of LVCN on tumor cell death, tumors were allowed to become more established (4 weeks from inoculation) before a short course of treatment (6 doses) with either LVCN or Avastin was started. In this experimental setting, a large and significant difference in the amount of cell death (TUNEL staining) was observed between the LVCN and control groups (Fig. 6). The reason we chose to quantitate the effects of these treatments on tumor apoptosis in more established tumors that received only a short course of therapy rather than in tumors harvested at the end of the above-mentioned efficacy study was that in the latter, despite the significant differences observed in both tumor size and survival, the number of apoptosis events did not appear to be significantly different across the groups at the end of 7 weeks of treatment (data not shown). One possible explanation for this observed discrepancy in the amount of cell death between the two studies might be that in the longer efficacy study, after 7 weeks of treatment, both LVCN and Avastin might have had a tumor stabilization/dormancy effect which might have led to gradual decline in the number of apoptosis events in these treated tumors over the course of treatment. We plan to address this hypothesis in the future by looking at the differences in both tumor apoptosis and cell proliferation in treated and control groups during a time course study.

4. Discussion

As key regulators of cell migration, integrins function as centripetal signaling platforms or functional hubs (Contois et al., 2009) capable of bi-directionally integrating the signaling circuitries elicited by different classes of cell surface receptors (e.g., the semaphorin/plexin/neuropilin, the growth factor/receptor tyrosine kinase and the cell surface protease systems) with the cellular locomotor apparatus (Ivaska and Heino, 2009). The efficient disruption of integrin-mediated interactions between tumorigenic

ECM and angiogenic EC in the tumor microenvironment seems to be critical from the therapeutic standpoint since, as recently reported (Baluk et al., 2005), one important downside of the potent VEGF/PDGF blockade is the persistence of the basement membranes of involuted tumor vessels after both EC and pericytes undergo regression. Thus, the vascular ECM left behind provides a scaffold for the rapid repopulation of these 'tracks' with new EC once the anti-VEGF/PDGF treatment is discontinued.

The critical involvement of integrins in both angiogenesis (Contois et al., 2009; Mahabeleshwar et al., 2006) and tumor invasion (Hood and Cheresh, 2002) provides the rationale for developing therapeutic antagonists aimed at disrupting these molecularly intertwined processes (Folkman, 2007). Most efforts of the past were focused on anti-integrin agents targeting the RGD-binding alphav members, a subclass of integrins thought to play pivotal roles in the regulation of pathological angiogenesis, which prompted the development of a number of small RGD-mimetics and monoclonal antibodies (Nemeth et al., 2007; Tucker, 2006).

In this study, we show that a chimeric disintegrin, vicrostatin (VCN), derived from a member of a well
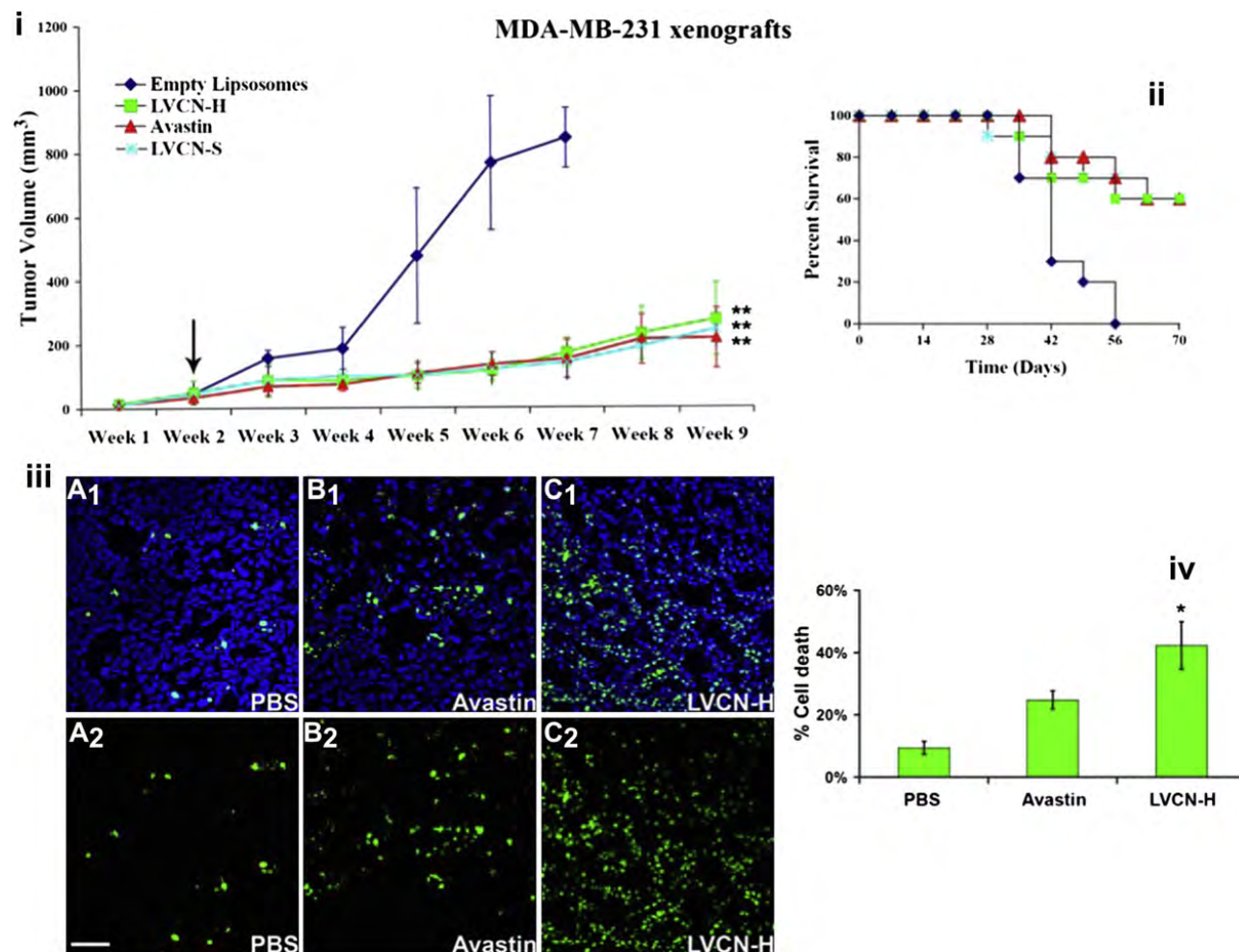

Fig. 6. The anti-tumor activity of liposomal VCN (LVCN) in MDA-MB-231 breast carcinoma xenograft model. Nude mice inoculated orthotopically (mammary fat pads; 2.5×10^6 cells) were allowed to grow palpable tumors before treatment was commenced (indicated by the arrow). Two different liposomal formulation of VCN were tested in this study: LVCN-S (prepared by sonication) and LVCN-H (prepared by homogenization). The groups of animals ($n = 10$) were treated intravenously with either LVCN-H or LVCN-S (the dose-equivalent of 100 μg of VCN per injection) each administered twice a week, or Avastin (400 μg per injection; approx. 20 μg/gr) administered once a week. The control group received empty liposomes only. When compared to the control group, a significant delay in tumor growth (i) and increased survival (ii) was observed in all treated groups. ANOVA was used for statistical analysis followed by Dunnett's multiple comparison tests (** signifies a $P < 0.001$). (iii) In a different study, designed to assess the ability of VCN to induce tumor apoptosis, MDA-MB-231 xenografts were allowed to grow to a significantly larger volume (4 weeks after inoculation) before the treatments were initiated. These animals received 6 consecutive doses of either LVCN (at the dose-equivalent of 100 μg of VCN per injection) or Avastin (400 μg per injection) administered intravenously every other day and compared to a control group that received saline only. Tumor cryostat sections from each group were stained with FITC-TUNEL, and counterstained with Hoechst 33342. Representative confocal images from multiple experiments taken at ×250 magnification are shown above (scale bar, 100 μm; panels A₁–C₁-TUNEL-Hoechst, panels A₂–C₂-TUNEL only). (iv) The amount of cell death was quantitated as 'number of TUNEL⁺ nuclei/total number of nuclei × 100' by counting all nuclei in 'hotspot' areas from multiple fields using a computer-assisted approach (the 'SimplePCI' imaging software). The LVCN group shows a significantly increased amount of cell death compared to either Avastin or PBS control. The data was analyzed with ANOVA followed by post-hoc tests (* signifies a $P < 0.01$).

characterized family of naturally occurring broad-spectrum integrin inhibitors, could be successfully produced recombinantly in large scale in an engineered bacterial system. In a number of *in vitro* functional assays, VCN is shown to retain the anti-migration/anti-invasion properties of the native molecule contortrostatin (CN) it was derived from. Our previous studies with native CN indicate that this disintegrin may behave like a soluble ECM-mimetic, by potently altering the actin cytoskeleton dynamics and inducing the deactivation of key molecular components of focal adhesions in both adherent HUVEC and glioma cells, which in turn results in a net anti-migratory/anti-invasive effect (Schmitmeier et al., 2005). Compared to native CN, VCN also targets integrins αvβ3, αvβ5, and α5β1, while diplaying a higher affinity than CN for integrin α5β1 (an amino acid sequence alteration purposefully engineered into VCN). Similar to native CN, recombinant VCN collapses the actin cytoskeleton in endothelial cells cultured in a rich tumorigenic matrix (complete Matrigel) uniquely endowed to support both survival and migration. These effects distinguish VCN from other integrin ligands tested in this setting, among which were a small cyclic RGD peptide and an integrin-targeting monoclonal antibody. It is important to emphasize that a methylated variant of the cyclic RGD peptide used in our experiments, the cyclo(Arg–Gly–Asp–DPhe–NMeVal) peptide or Cilengitide, displaying an improved specificity for integrins αvβ3 and αvβ5 (Dechantsreiter et al., 1999; Goodman et al., 2002), has already been tested against solid tumors in a number of clinical trials with mixed results (Hariharan et al., 2007; Reardon et al., 2008). By comparing these different integrin ligands, our *in vitro* data seem to suggest that VCN might have additional signaling properties compared to cyclic RGD peptides and integrin-targeting monoclonal antibodies. Additional mechanistic studies are currently underway in our laboratory in an effort to better understand these signaling, and possibly therapeutic, differences between disintegrins and other soluble integrin ligands.

Although VCN retains native CN's ability to bind the activated αIIbβ3 platelet integrin, like CN (Swenson et al., 2004) it does not interact with quiescent platelets, an *in vitro* observation further corroborated by our *in vivo* findings: no side effects were documented following direct intravenous administration of purified VCN up to 1 mg (mice) or to 5 mg (rats). It is noteworthy that there is an established link between activated platelets and metastasis (Jurasz et al., 2004; Nash et al., 2002) and from the therapeutic standpoint it may be advantageous to use a polypeptide like VCN that also has the potential to address this mechanism of metastasis. As a small polypeptide, VCN is not expected to be immunogenic, and our preliminary animal studies showed that VCN indeed failed to elicit an antibody response following intravenous infusion. Despite these findings, for enhanced passive targeting of the drug to the tumor site, we opted for liposomal delivery. VCN can be efficiently encapsulated into unilamellar liposomes and our findings indicate that the liposomal formulations of VCN have far superior efficacy compared to the naked polypeptide in the *in vivo* model tested. On the other hand, liposomal delivery has a number of other advantages including the ability to achieve a good therapeutic response at lower doses administered less frequently. As a unique broad-spectrum anti-invasive drug, VCN may hold an advantage over other anti-tumor therapeutic modalities in that it may be better suited to address the cell survival loops operating in the avascular tissue in the early steps of angiogenesis and metastasis (Kim et al., 2000a, 2000b). For instance, recent studies have demonstrated that the usage of various anti-VEGF/PDGF strategies is linked to an increased risk of early metastasis in animal cancer models (Ebos et al., 2009; Paez-Ribes et al., 2009). Although the clinical relevance of these preclinical studies is not yet clear (Ellis and Reardon, 2009), these data support the idea that not only is there an imperative need to design novel anti-angiogenic drugs with better anti-invasive properties, but also to test the impact of standard of care anti-angiogenics (such as Avastin) on metastasis and/or postoperative survival when they are administered in combination with anti-invasive modalities.

In summary, we developed a novel chimeric disintegrin VCN that can be easily and cost-effectively produced recombinantly and shows excellent anti-tumor efficacy in the breast carcinoma model discussed in this report. Furthermore, the liposomal formulation of VCN is shown to have a profound tumor apoptotic effect when tested on significantly more established tumors in the same breast cancer model.

Conflict of interest statement

RM, SS, and FM are co-founders of Applied Integrin Sciences, Inc. (formerly Aspis Biopharmaceutical, Inc.), a startup company focused on developing disintegrin-based theranostics. The Vicrostatin sequence and its method of production are protected by pending patent applications filed by the University of Southern California.

Ethical statement

All animals involved in this study were handled and euthanized in strict accordance with good animal practice as defined by the strict guidelines of the Institutional Animal Care and Use Committee (IACUC) of the University of Southern California.

References

Albrecht-Buehler, G., 1977. The phagokinetic tracks of 3T3 cells. Cell 11, 395–404.

Baluk, P., Hashizume, H., McDonald, D.M., 2005. Cellular abnormalities of blood vessels as targets in cancer. Curr. Opin. Genet. Dev. 15, 102–111.

Barker, P.L., Bullens, S., Bunting, S., Burdick, D.J., Chan, K.S., Deisher, T., Eigenbrot, C., Gadek, T.R., Gantzos, R., Lipari, M.T., et al., 1992. Cyclic RGD peptide analogues as antiplatelet antithrombotics. J. Med. Chem. 35, 2040–2048.

Bissell, M.J., Rizki, A., Mian, I.S., 2003. Tissue architecture: the ultimate regulator of breast epithelial function. Curr. Opin. Cell Biol. 15, 753–762.

Bowersox, J.C., Sorgente, N., 1982. Chemotaxis of aortic endothelial cells in response to fibronectin. Cancer Res. 42, 2547–2551.

Carrington, J.C., Dougherty, W.G., 1988. A viral cleavage site cassette: identification of amino acid sequences required for tobacco etch virus polyprotein processing. Proc. Natl. Acad. Sci. U.S.A. 85, 3391–3395.

Contois, L., Akalu, A., Brooks, P.C., 2009. Integrins as "functional hubs" in the regulation of pathological angiogenesis. Semin. Cancer Biol.

Dechantsreiter, M.A., Planker, E., Matha, B., Lohof, E., Holzemann, G., Jonczyk, A., Goodman, S.L., Kessler, H., 1999. N-methylated cyclic RGD peptides as highly active and selective alpha(V)beta(3) integrin antagonists. J. Med. Chem. 42, 3033–3040.

Desgrosellier, J.S., Barnes, L.A., Shields, D.J., Huang, M., Lau, S.K., Prevost, N., Tarin, D., Shattil, S.J., Cheresh, D.A., 2009. An integrin alpha(v)beta(3)-c-Src oncogenic unit promotes anchorage-independence and tumor progression. Nat. Med.

Ebos, J.M., Lee, C.R., Cruz-Munoz, W., Bjarnason, G.A., Christensen, J.G., Kerbel, R.S., 2009. Accelerated metastasis after short-term treatment with a potent inhibitor of tumor angiogenesis. Cancer Cell 15, 232–239.

Ellis, L.M., Reardon, D.A., 2009. Cancer: the nuances of therapy. Nature 458, 290–292.

Folkman, J., 2007. Angiogenesis: an organizing principle for drug discovery? Nat. Rev. Drug Discov. 6, 273–286.

Fujii, Y., Okuda, D., Fujimoto, Z., Horii, K., Morita, T., Mizuno, H., 2003. Crystal structure of trimestatin, a disintegrin containing a cell adhesion recognition motif RGD. J. Mol. Biol. 332, 1115–1122.

Gold, H.K., Yasuda, T., Jang, I.K., Guerrero, J.L., Fallon, J.T., Leinbach, R.C., Collen, D., 1991. Animal models for arterial thrombolysis and prevention of reocclusion. Erythrocyte-rich versus platelet-rich thrombus. Circulation 83, IV26–40.

Golubkov, V., Hawes, D., Markland, F.S., 2003. Anti-angiogenic activity of contortrostatin, a disintegrin from Agkistrodon contortrix contortrix snake venom. Angiogenesis 6, 213–224.

Goodman, S.L., Holzemann, G., Sulyok, G.A., Kessler, H., 2002. Nanomolar small molecule inhibitors for alphav(beta)6, alphav(beta)5, and alphav(beta)3 integrins. J. Med. Chem. 45, 1045–1051.

Gould, R.J., Polokoff, M.A., Friedman, P.A., Huang, T.F., Holt, J.C., Cook, J.J., Niewiarowski, S., 1990. Disintegrins: a family of integrin inhibitory proteins from viper venoms. Proc. Soc. Exp. Biol. Med. 195, 168–171.

Hamano, Y., Zeisberg, M., Sugimoto, H., Lively, J.C., Maeshima, Y., Yang, C., Hynes, R.O., Werb, Z., Sudhakar, A., Kalluri, R., 2003. Physiological levels of tumstatin, a fragment of collagen IV alpha3 chain, are generated by MMP-9 proteolysis and suppress angiogenesis via alphaV beta3 integrin. Cancer Cell 3, 589–601.

Hanahan, D., Weinberg, R.A., 2000. The hallmarks of cancer. Cell 100, 57–70.

Hariharan, S., Gustafson, D., Holden, S., McConkey, D., Davis, D., Morrow, M., Basche, M., Gore, L., Zang, C., O'Bryant, C.L., Baron, A., Gallemann, D., Colevas, D., Eckhardt, S.G., 2007. Assessment of the biological and pharmacological effects of the alpha nu beta3 and alpha nu beta5 integrin receptor antagonist, cilengitide (EMD 121974), in patients with advanced solid tumors. Ann. Oncol. 18, 1400–1407.

Hood, J.D., Cheresh, D.A., 2002. Role of integrins in cell invasion and migration. Nat. Rev. Cancer 2, 91–100.

Huang, T.F., Yeh, C.H., Wu, W.B., 2001. Viper venom components affecting angiogenesis. Haemostasis 31, 192–206.

Ivaska, J., Heino, J., 2009. Interplay between cell adhesion and growth factor receptors: from the plasma membrane to the endosomes. Cell Tissue Res.

Jurasz, P., Alonso-Escolano, D., Radomski, M.W., 2004. Platelet–cancer interactions: mechanisms and pharmacology of tumour cell-induced platelet aggregation. Br. J. Pharmacol. 143, 819–826.

Kang, I.C., Kim, D.S., Jang, Y., Chung, K.H., 2000. Suppressive mechanism of salmosin, a novel disintegrin in B16 melanoma cell metastasis. Biochem. Biophys. Res. Commun. 275, 169–173.

Kim, S., Bell, K., Mousa, S.A., Varner, J.A., 2000a. Regulation of angiogenesis in vivo by ligation of integrin alpha5beta1 with the central cell-binding domain of fibronectin. Am. J. Pathol. 156, 1345–1362.

Kim, S., Harris, M., Varner, J.A., 2000b. Regulation of integrin alpha vbeta 3-mediated endothelial cell migration and angiogenesis by integrin alpha5beta1 and protein kinase A. J. Biol. Chem. 275, 33920–33928.

Kim, S.I., Kim, K.S., Kim, H.S., Kim, D.S., Jang, Y., Chung, K.H., Park, Y.S., 2003. Inhibitory effect of the salmosin gene transferred by cationic liposomes on the progression of B16BL6 tumors. Cancer Research 63, 6458–6462.

LaVallie, E.R., DiBlasio, E.A., Kovacic, S., Grant, K.L., Schendel, P.F., McCoy, J.M., 1993. A thioredoxin gene fusion expression system that circumvents inclusion body formation in the E. coli cytoplasm. Biotechnol. (N Y) 11, 187–193.

Mahabeleshwar, G.H., Chen, J., Feng, W., Somanath, P.R., Razorenova, O.V., Byzova, T.V., 2008. Integrin affinity modulation in angiogenesis. Cell Cycle 7, 335–347.

Mahabeleshwar, G.H., Feng, W., Phillips, D.R., Byzova, T.V., 2006. Integrin signaling is critical for pathological angiogenesis. J. Exp. Med. 203, 2495–2507.

Marcinkiewicz, C., Weinreb, P.H., Calvete, J.J., Kisiel, D.G., Mousa, S.A., Tuszynski, G.P., Lobb, R.R., 2003. Obtustatin: a potent selective inhibitor of alpha1beta1 integrin in vitro and angiogenesis in vivo. Cancer Res. 63, 2020–2023.

Mas-Moruno, C., Rechenmacher, F., Kessler, H., 2011. Cilengitide: The first anti-angiogenic small molecule drug candidate design, Synthesis and clinical Evaluation. Anticancer Agents Med. Chem.

McLane, M.A., Joerger, T., Mahmoud, A., 2008. Disintegrins in health and disease. Front. Biosci. 13, 6617–6637.

McLane, M.A., Marcinkiewicz, C., Vijay-Kumar, S., Wierzbicka-Patynowski, I., Niewiarowski, S., 1998. Viper venom disintegrins and related molecules. Proc. Soc. Exp. Biol. Med. 219, 109–119.

McQuade, P., Knight, L.C., Welch, M.J., 2004. Evaluation of 64Cu- and 125I-radiolabeled bitistatin as potential agents for targeting alpha v beta 3 integrins in tumor angiogenesis. Bioconjug. Chem. 15, 988–996.

Minea, R., Swenson, S., Costa, F., Chen, T.C., Markland, F.S., 2005. Development of a novel recombinant disintegrin, contortrostatin, as an effective anti-tumor and anti-angiogenic agent. Pathophysiol. Haemost. Thromb. 34, 177–183.

Mizejewski, G.J., 1999. Role of integrins in cancer: survey of expression patterns. Proc. Soc. Exp. Biol. Med. 222, 124–138.

Moiseeva, N., Bau, R., Swenson, S.D., Markland Jr., F.S., Choe, J.Y., Liu, Z.J., Allaire, M., 2008. Structure of acostatin, a dimeric disintegrin from Southern copperhead (Agkistrodon contortrix contortrix), at 1.7 A resolution. Acta Crystallogr. D. Biol. Crystallogr. 64, 466–470.

Nash, G.F., Turner, L.F., Scully, M.F., Kakkar, A.K., 2002. Platelets and cancer. Lancet Oncol. 3, 425–430.

Nemeth, J.A., Nakada, M.T., Trikha, M., Lang, Z., Gordon, M.S., Jayson, G.C., Corringham, R., Prabhakar, U., Davis, H.M., Beckman, R.A., 2007. Alpha-v integrins as therapeutic targets in oncology. Cancer Invest. 25, 632–646.

Osborne, C.K., Hobbs, K., Clark, G.M., 1985. Effect of Estrogens and Anti-estrogens on growth of human breast cancer cells in Athymic nude mice. Cancer Res. 45, 584–590.

Ouyang, C., Huang, T.F., 1983. Potent platelet aggregation inhibitor from Trimeresurus gramineus snake venom. Biochim. Biophys. Acta 757, 332–341.

Paez-Ribes, M., Allen, E., Hudock, J., Takeda, T., Okuyama, H., Vinals, F., Inoue, M., Bergers, G., Hanahan, D., Casanovas, O., 2009. Anti-angiogenic therapy elicits malignant progression of tumors to increased local invasion and distant metastasis. Cancer Cell 15, 220–231.

Park, S.H., Raines, R.T., 2004. Fluorescence polarization assay to quantify protein–protein interactions. Methods Mol. Biol. 261, 161–166.

Ramos, O.H., Kauskot, A., Cominetti, M.R., Bechyne, I., Salla Pontes, C.L., Chareyre, F., Manent, J., Vassy, R., Giovannini, M., Legrand, C., Selistre-de-Araujo, H.S., Crepin, M., Bonnefoy, A., 2008. A novel alpha(v)beta(3)-blocking disintegrin containing the RGD motive, DisBa-01, inhibits bFGF-induced angiogenesis and melanoma metastasis. Clin. Exp. Metastasis. 25, 53–64.

Reardon, D.A., Nabors, L.B., Stupp, R., Mikkelsen, T., 2008. Cilengitide: an integrin-targeting arginine-glycine-aspartic acid peptide with promising activity for glioblastoma multiforme. Expert Opin. Investig. Drugs 17, 1225–1235.

Reynolds, L.E., Wyder, L., Lively, J.C., Taverna, D., Robinson, S.D., Huang, X., Sheppard, D., Hynes, R.O., Hodivala-Dilke, K.M., 2002. Enhanced

pathological angiogenesis in mice lacking beta3 integrin or beta3 and beta5 integrins. Nat. Med. 8, 27–34.

Saudek, V., Atkinson, R.A., Pelton, J.T., 1991. Three-dimensional structure of echistatin, the smallest active RGD protein. Biochemistry 30, 7369–7372.

Schmitmeier, S., Markland, F.S., Schonthal, A.H., Chen, T.C., 2005. Potent mimicry of fibronectin-induced intracellular signaling in glioma cells by the homodimeric snake venom disintegrin contortrostatin. Neurosurgery 57, 141–153. discussion 141–153.

Serini, G., Valdembri, D., Bussolino, F., 2006. Integrins and angiogenesis: a sticky business. Exp. Cell Res. 312, 651–658.

Shebuski, R.J., Ramjit, D.R., Sitko, G.R., Lumma, P.K., Garsky, V.M., 1990. Prevention of canine coronary artery thrombosis with echistatin, a potent inhibitor of platelet aggregation from the venom of the viper, *Echis carinatus*. Thromb. Haemost. 64, 576–581.

Silva, R., D'Amico, G., Hodivala-Dilke, K.M., Reynolds, L.E., 2008. Integrins: the keys to unlocking angiogenesis. Arterioscler. Thromb. Vasc. Biol. 28, 1703–1713.

Swenson, S., Costa, F., Minea, R., Sherwin, R.P., Ernst, W., Fujii, G., Yang, D., Markland Jr., F.S., 2004. Intravenous liposomal delivery of the snake venom disintegrin contortrostatin limits breast cancer progression. Mol. Cancer Ther. 3, 499–511.

Trikha, M., De Clerck, Y.A., Markland, F.S., 1994a. Contortrostatin, a snake venom disintegrin, inhibits beta 1 integrin-mediated human metastatic melanoma cell adhesion and blocks experimental metastasis. Cancer Res. 54, 4993–4998.

Trikha, M., Rote, W.E., Manley, P.J., Lucchesi, B.R., Markland, F.S., 1994b. Purification and characterization of platelet aggregation inhibitors from snake venoms. Thromb. Res. 73, 39–52.

Tucker, G.C., 2006. Integrins: molecular targets in cancer therapy. Curr. Oncol. Rep. 8, 96–103.

Wierzbicka-Patynowski, I., Niewiarowski, S., Marcinkiewicz, C., Calvete, J.J., Marcinkiewicz, M.M., McLane, M.A., 1999. Structural requirements of echistatin for the recognition of alpha(v)beta(3) and alpha(5)beta(1) integrins. J. Biol. Chem. 274, 37809–37814.

Zetter, B.R., 1980. Migration of capillary endothelial cells is stimulated by tumour-derived factors. Nature 285, 41–43.

Zhou, Q., Nakada, M.T., Arnold, C., Markland, F.S., 1999. Contortrostatin, a dimeric disintegrin from *Agkistrodon contortrix contortrix*, inhibits angiogenesis. Angiogenesis 3, 259–269.

Zhou, Q., Nakada, M.T., Brooks, P.C., Swenson, S.D., Ritter, M.R., Argounova, S., Arnold, C., Markland, F.S., 2000. Contortrostatin, a homodimeric disintegrin, binds to integrin alphavbeta5. Biochem. Biophys. Res. Commun. 267, 350–355.

Chapter 19
Anti-Angiogenesis and Disintegrins

Stephen Swenson, Radu Minea, Samuel Zidovetzki, Corey Helchowski, Fritz Costa, and Francis S. Markland

Abstract Angiogenesis is a critical process in tumor and disease progression. A number of features are central to both tumor growth and development, and the recruitment and invasion of a growing vascular network supplying the tumor with nutrients and a mechanism of escape to allow meastatic growth. One class of molecules important to both tumor growth and blood vessel recruitment are a family of cell surface receptors identified as integrins. Integrins are α/β heterodimeric glycoproteins in which the different α subunits combine with distinct β subunits resulting in a range of specificities toward various extracellular matrix (ECM) proteins. The RGD sequence found in a number of ECM proteins is recognized by several classes of integrins, allowing for linkage of cytoskeletal proteins associated with the integrins to the ECM which leads to involvement in bi-directional signaling that displays profound effects on cellular functions. Among these integrin mediated interactions are the adhesion of both endothelial cells and cancer cells to ECM proteins, an interaction that is integral to metastasis, tumor growth and angiogensis. Antibodies targeted to integrins have been shown to retard tumor growth and subsequent tumor induced angiogenesis. One concern with this approach is that the antibody targets a single integrin, which may allow the tumor to utilize other non-targeted integrins to circumvent this type of blockage. A more broad spectrum agent is available that binds to and blocks the function of several different integrins at a time, this agents is identified as a disintegrin. Originally purified from the venom of *Viperidae* family of snakes, a disintegrins role in nature is presumably to block platelet aggregation following envenomation based on interaction of an integrin on the activated platelet surface with an RGD sequence in the disintegrin. It has been observed that integrins overexpressed on some tumor types and angiogenic vasculature have similar affinity for RGD motifs found in ECM proteins. Based on

S. Swenson (✉)
USC/Norris Comprehensive Cancer Center, University of Southern California, Keck School of Medicine, Cancer Research Laboratory #106, 1303 N. Mission Road, Los Angeles, CA 90033, USA
e-mail: sswenson@usc.edu

disintegrin structure we have developed a recombinant form of a snake venom disintegrin, which we call vicrostatin (VCN). VCN is a potent anti-angiogenic/anti-tumor agent in in vitro and in vivo laboratory studies. Further development of the recombinant venom derived disintegrin along with new technology looking at additional disintegrin-like proteins may offer a novel therapeutic approach in targeting tumor induced angiogenesis.

Introduction

Angiogenesis, the ingrowth of new blood vessels into a growing tumor, is critical to cancer progression and spread. A number of cancer types such as breast and prostate cancer affect up to 10% of the US population at some point in their lifetime (Jemal et al., 2009). In the description of the development of a novel form of anti-cancer therapy, prostate cancer will be used as the model. With the exception of skin cancer, prostate cancer (PC) is the most prevalent cancer in American men and the second leading cause of cancer death after lung cancer. The American Cancer Society estimates there will be about 192,280 men diagnosed with PC and 27,360 deaths from PC in the United States in 2009 (Jemal et al., 2009). As of 2004 the five year survival rate for men in whom PC has spread to distant sites at time of diagnosis was 32% (Jemal et al., 2009). In advanced PC, different treatment combinations in the past have failed because as prostate cancer progresses it becomes resistant to treatment (Di Lorenzo and De Placido, 2006; Gleave et al., 2005; Harris et al., 2009; Sharifi et al., 2008). It is critical, therefore, that new treatment options be made available for patients with metastatic PC. While cytotoxic therapeutics form the backbone of PC treatment, there are other approaches that may allow for even more effective treatment of PC. For example, the inhibition of blood vessel growth into the tumor, anti-angiogenic therapy, is one of the more promising strategies for enhanced long-term inhibition of PC progression (Aragon-Ching and Dahut, 2008; Choy and Rafii, 2001; Madan and Dahut, 2009; van Moorselaar and Voest, 2002). Abnormal expression of angiogenic factors, such as vascular endothelial growth factor (VEGF), and their receptors have been associated with PC (Aragon-Ching and Dahut, 2009; Fox et al., 2002). Both PC and vascular endothelial cells produce growth factors, including VEGF and basic fibroblast growth factor (bFGF), that promote neovascularization (Beekman and Hussain, 2006; Kwabi-Addo et al., 2004; Pallares et al., 2006; Polnaszek et al., 2003; Strohmeyer et al., 2004; Sun et al., 2004). Angiogenesis is a critical prerequisite for progression to advanced disease and plays a pivotal role for growth and metastasis of PC (Cox et al., 2005; Choy and Rafii, 2001; Madan and Dahut, 2009). Tumor vascularity has been shown to be a prognostic factor in PC, with highly vascular PC having a poor prognosis (Concato et al., 2009; Erbersdobler et al., 2009; Mucci et al., 2009; Weidner et al., 1993). Further, there is a specific correlation between blood vessel density in PC and the metastatic potential (Weidner et al., 1993). PC is identified as an angiogenesis-dependent cancer and an excellent target for anti-angiogenic therapy (Aragon-Ching and Dahut, 2008; Cox et al., 2005; Jimenez et al., 2006; Madan

and Dahut, 2009). Anti-angiogenic therapy can produce prolonged tumor dormancy and is cytostatic, which will lead to reduced side effects commonly associated with chemotherapeutic agents (Boehm et al., 1997; Wu and Moses, 2000). However, anti-angiogenic agents when used as monotherapy are not as effective as in combination, suggesting that anti-angiogenic strategies in combination with cytotoxic agents, should be an effective therapeutic approach in PC.

Integrins: Targets for Anti-Angiogenic Therapies

Cell–cell and cell–matrix interactions are of critical importance to newly established cancer cell colonies. These interactions are extremely complex and involve surface interactions between tumor cells and surrounding tissues (Liotta and Kohn, 2001). The integrin class of molecules is particularly important to these interactions. All integrins are α/β heterodimeric glycoproteins (Cheresh, 1992). The 18 α subunits combine with 8 β subunits to create 24 unique αβ heterodimers resulting in a range of specificities toward various extracellular matrix (ECM) proteins (Hynes, 1992; Pignatelli et al., 1992). Several classes of integrins recognize the RGD sequence present in ECM proteins (Ruoslahti, 1991), allowing integrins to link cytoskeletal proteins with the ECM and to be involved in bi-directional signaling that alters cellular functions. Among these interactions are the adhesion of both endothelial cells and cancer cells to ECM proteins (Ruoslahti, 1991), interactions that are integral to tumor growth, metastasis and angiogenesis; integrins also mediate endothelial cell proliferation and migration (Beekman et al., 2006). Importance of the vitronectin receptors, integrins αvβ3 and αvβ5, in angiogenesis is well known. A monoclonal antibody to αvβ3, as well as a cyclic RGD-containing peptide (Brooks et al., 1994), perturbed angiogenesis and produced regression of a human cancer growing on a chick embryo chorioallantoic membrane (CAM). Administration of antagonists of αvβ3 cause apoptosis of vascular endothelial cells responsible for angiogenesis, following selective activation of p53 and increased expression of the p53-inducible cell cycle inhibitor p21WAF1/CIP1 in vivo (Strömblad et al., 1996). In vivo survival of vascular endothelial cells is dependent on attachment and spreading on the ECM. αvβ5 has also been found to play a role in angiogenesis. An anti-αvβ3 antibody blocked angiogenesis induced by bFGF, whereas an anti-αvβ5 antibody blocked VEGF induced angiogenesis (Friedlander et al., 1995). This suggests that down-stream signal transduction pathways of the two growth factors are distinct; there appears to be two angiogenic pathways mediated by αv integrins. α5β1 antagonists inhibit tumor angiogenesis, and block metastases in an animal tumor model (Stoeltzing et al., 2003). Both α5β1 and αvβ3 have been shown to participate in important angiogenic pathways (Bayless et al., 2000); inhibition of endothelial cell lumen formation was only achieved by blocking both αvβ3 and α5β1. Yet integrins are not only central to angiogenesis. In PC, integrins are known to be involved in metastases and exhibit differential expression on PC cells (Demirgoz et al., 2008; Goel et al., 2008; Romanov and Goligorsky, 1999). Zheng et al. (1999) and Sun et al. (2007) observed that the highly invasive human PC cell line, PC-3, expresses αvβ3,

which mediated cell adhesion and migration on vitronectin. In contrast, noninvasive LNCaP cells did not express αvβ3, nor adhere to and migrate on vitronectin, although these cells expressed α5β1 (Demirgoz et al., 2008). Exogenous expression of αvβ3 in LNCaP induced the cells to adhere and migrate on vitronectin. Also, primary human PC cells isolated from 16 surgical specimens expressed αvβ3, whereas normal prostate epithelial cells did not (Zheng et al., 1999). This report pointed to αvβ3 as a potential target in PC cell migration and metastasis. Metastasis to remote sites, primarily to the bone, is a major cause of death in prostate cancer. A significant component of metastasis involves adhesion of cancer cells within the vasculature. Adhesion depends on integrins and is dependent on integrin activation. Integrin αvβ3 supports prostate cancer cell attachment under blood flow conditions in an activation-dependent manner (Nemeth et al., 2003; Zheng et al., 1999), and evidence suggests that transition from a locally invasive phenotype to metastatic behavior may be dependent on increased expression of αvβ3 (Sun et al., 2007). Other findings suggest that integrin αvβ3 expression in PC cells accelerates the development of bone metastasis (Cooper et al., 2002), presumably through increased invasion of and adhesion to bone (Kumar, 2003; Nemeth et al., 2003). Other integrins appear to be involved in cancer invasion as well (Cress et al., 1995; Witkowski et al., 1993). Since a single antagonist, targeting a broad range of integrins, can be envisioned to disrupt many of these tumor cell–tissue interactions, integrins present a very attractive target for anticancer drug development. Disintegrins (Gould et al., 1990) avidly attach to a range of human integrins, disrupting normal cellular functions. These findings suggest that metastasis and angiogenesis inhibition should be a feasible treatment strategy in PC. Thus, agents such as the disintegrin vicrostatin (VCN) an antagonist of integrins αvβ3/α5β1/αvβ5 (Minea et al., 2005), as described below should be an effective therapeutic agent for inhibition of metastasis and angiogenesis in PC if targeted to the tumor, and should be highly effective when administered in combination with cytotoxic agents.

Disintegrins as Molecular Weapons Against Cancer

Disintegrins are small, disulfide-rich, RGD-containing peptides that bind to integrins on the surface of normal and malignant cells (Dennis et al., 1990; Huang et al., 1989; McLane et al., 2008; Scarborough et al., 1993). Disintegrins have been characterized from many snake venoms and were originally categorized as platelet aggregation inhibitors (McLane et al., 1998; Niewiarowski et al., 1994; Phillips et al., 1991; Trikha et al., 1994b). Nuclear magnetic resonance has been used to determine the structures of several disintegrins (Adler et al., 1991; Saudek et al., 1991); they display little secondary structure, and are characterized by an RGD or other tripeptide sequence at the tip of a flexible loop protruding from the main body of the peptide chain and anchored by disulfide bonds at the base (Niewiarowski et al., 1994). The Markland lab originally isolated contortrostatin (CN), a homodimeric disintegrin, from the venom of the southern copperhead snake (Trikha et al., 1994b). CN is a homodimer with a molecular mass (Mr) of 13,500; each chain has

an RGD sequence and a Mr of 6,750 (Trikha et al., 1994a, b). CN binds competitively to integrins of the β1, β3 and β5 subclasses, including receptors for fibronectin (α5β1), vitronectin (αvβ3, αvβ5), and fibrinogen (αIIbβ3) (Trikha et al., 1994a, b; Zhou et al., 2000a). Human umbilical vein endothelial cells (HUVEC) were exposed to CN for 0–3 days and then tested for processes critical to angiogenesis; migration, invasion, and tube formation (Golubkov et al., 2003). All three activities were inhibited by up to 90%. Further, immunochemical staining showed both actin and VE-cadherin organization to be disrupted by CN in HUVEC (Golubkov et al., 2003). In addition, CN disrupts angiogenesis induced by both bFGF and VEGF, consistent with the observation that cyclic RGD-peptides have no selectivity among αv family members (Friedlander et al., 1995). The lack of integrin specificity by CN is believed to be an advantage in controlling cancer dissemination. PC cell lines, as well as vascular endothelial cells, have been shown to display integrins αvβ3, αvβ5, and α5β1, and the antitumor and anti-angiogenic activity of CN is based on its high affinity interaction with these integrins. CN blocks the function of integrins on both tumor and endothelial cells and has a distinct advantage over many anti-angiogenic agents, which act by blocking a single angiogenic pathway. In animal models of cancer, CN demonstrates anti-angiogenic and antimetastatic activities (Markland et al., 2001; Pyrko et al., 2005; Trikha et al., 1994a; Zhou et al., 2000b). In vivo studies carried out by the Markland lab and other groups have shown that disintegrins are well tolerated and can be infused without detrimental effect on blood pressure, body temperature, or other physiological parameters (Cousins et al., 1995; Shebuski et al., 1989; Yasuda et al., 1991). Acute disintegrin toxicity was studied by the Markland lab in the canine in collaboration with Dr. Benedict Lucchesi, University of Michigan Medical School; disintegrin treated animals did not exhibit changes in heart rate, EKG, or blood coagulation parameters, and there was no evidence of toxicity at the doses tested (Cousins et al., 1995). Although the pharmacological properties of CN have made it an intriguing molecule for potential anticancer therapeutic strategies, the fact that only limited quantities are available from snake venom have highlighted the need to produce a recombinant form of CN. Dr. Minea in Markland's lab designed and engineered a novel recombinant disintegrin, VCN, whose structure is based on the sequence of CN. Interestingly, we found that VCN when expressed in bacteria is a monomer unlike the homodimer CN. Due to the monomeric structure of VCN and the fact that it retains full biological activity, the recombinant system has been used to provide VCN in large quantities. VCN has proven to be a potent anti-angiogenic agent with impressive anticancer activity, as shown in murine models of human breast and prostate cancer (Minea et al., 2005; Pinski et al., 2003). VCN is as active as native CN both in vitro and in vivo and has an additional benefit in that the design of VCN includes a slight carboxyl-terminal sequence alteration that produces much higher affinity for integrin α5β1, which is known to be over expressed on angiogenic endothelial cells and prostate cancer cell lines (Witkowski et al., 1993). In addition, agents that induce endothelial cell apoptosis by antagonizing integrin binding are considered potential therapeutic agents for PC via their ability to inhibit tumor vascularization (Garrison and Kyprianou, 2004). Recent studies by the Markland lab indicate that VCN induces apoptosis of

HUVEC, further supporting its role as an effective anti-angiogenic agent (Minea et al., In Press). Importantly, VCN also induced disruption of the actin cytoskeleton in HUVEC and mediated the dissociation of talin from the cytoplasmic domain of the β1 integrin (unpublished results). These findings provide insight into the molecular mechanism of anti-angiogenic action of VCN, separate from its ability to disrupt integrin adhesion to ECM proteins. In chronic studies in nude mice, a liposomal formulation of VCN (LVCN) was administered by twice weekly intravenous (i.v.) injection over a four week period. There were no visible side effects or signs of internal bleeding, indicating that mice tolerate chronic administration of LVCN very well (Minea et al., 2005). Since there was no evidence of an immune response to a liposomal formulation of CN (LCN), we expect similar results with LVCN. With the availability of the recombinant method for production of VCN, the development of this disintegrin into a commercially viable product is feasible.

Advantages of VCN as an Antitumor/Anti-Angiogenic Agent

The antitumor activity of VCN is based not only on blocking integrin adhesion but also by disrupting the actin cytoskeleton and dissociating the complex between talin and the β1 integrin cytoplasmic tail. Importantly, the binding of talin to integrin β tails represents the final common step in integrin activation (Calderwood, 2004). The effect on integrins mediated by VCN leads to dramatic depression of invasive ability of tumor cells, and of the angiogenic vasculature. Advantages of the disintegrin approach for cancer therapy include: an exclusive and unique recombinant production method that is robust, low cost and easily scalable; the disintegrin sequence can be modified to alter affinity and specificity for integrins; the recombinant expression system can produce venom-derived disintegrins in sufficient quantity to advance this technology to the clinic. Metastasis is a major killer of cancer victims and there are no good anti-metastatic drugs available. We have shown that VCN inhibits processes involved in tumor metastasis (adhesion and invasion) and in a breast cancer model we found that CN inhibited >65% of spontaneous lung metastasis (Zhou et al., 1999), and we are confident VCN will as well.

Importantly, we have shown in rats, dog and mice that there are few if any side effects after chronic exposure to CN or VCN. This indicates that normal, non-migrating cells do not display activated integrins and they are, therefore, not accessible to disintegrin binding. This is particularly true in mature vasculature, which does not display αvβ3. By contrast, αvβ3 is prominently displayed by neovasculature, which serves as the basis for integrin-mediated anti-angiogenic therapy (Gasparini et al., 1998; Gutheil et al., 2000; Hood et al., 2002). This was further emphasized by studies carried out with platelets in vitro wherein we showed that CN only binds to platelets after their exposure to ADP, which induces intracellular signals switching integrins into a ligand competent state (activates integrins by inducing a conformational change in their extracellular domain) (Banno and Ginsberg, 2008; Humphries, 1996; Sun et al., 2007; Xiong et al., 2003), thereby making them accessible to CN.

Avastin (bevacizumab) is a monoclonal antibody that neutralizes VEGF and has shown preclinical evidence of anti-angiogenic efficacy for prostate cancer (Ranieri et al., 2006), it is approved for use in combination therapy in several types of cancer (Courtney and Choueiri, 2009; Grothey and Galanis, 2009). We have shown in head to head comparison of VCN with avastin that there was equivalent efficacy and anti-angiogenic activity of the two agents in a human breast cancer xenograft model. However, whereas avastin has one target (VEGF), VCN targets three pathways based on integrins αvβ3, αvβ5, and α5β1 displayed by tumor cells and angiogenic blood vessels, which could be important when tumor cells develop alternative pathways to bypass VEGF. We expect to see this difference translate to an increased effectiveness of VCN against metastatic disease when compared to avastin. Further, the peptide VCN should be considerably less expensive to manufacture than the antibody avastin. The tyrosine kinase inhibitors (TKIs) sunitinib and sorafenib have shown good efficacy in clinical use, particularly in metastatic renal cell carcinoma, a highly vascular disease (Courtney and Choueiri, 2009; Hiles and Kolesar, 2008; Merseburger et al., 2009; Zhu et al., 2009). Nonetheless, patients treated by all three of these anti-angiogenic agents (avastin and the TKIs) have experienced significant rates of adverse events (AE) (Choueiri et al., 2009). Although many of these AE are minor and clinically manageable, some are severe and life-threatening (Chen and Cleck, 2009). However, two recent reports throw an even more serious spotlight on potential problems with the VEGF/VEGFR targeting agents, including Avastin and the TKIs. In the first report by Kerbel's group (Ebos et al., 2009), sunitinib was shown to accelerate metastatic tumor growth and decrease overall survival in mice receiving short-term therapy in several metastasis assays. Their results suggested possible metastatic conditioning in multiple organs. Similar findings with other TKIs suggest a class-specific effect. Another study (Paez-Ribes et al., 2009) confirmed these findings and provided results suggesting that VEGF-targeting angiogenesis inhibitors initially elicit an antitumor response, but then the tumors appear to adapt and progress to a state of greater malignancy with increased invasiveness and in some cases increased distant metastases. This process is referred to as "evasive resistance". This newly found connection could explain why most current anti-angiogenics have only shown a modest increase in survival in cancer patients (Montagnani et al., 2009). It is important to note that the therapeutic strategy employing VCN is not based solely on the VEGF/VEGFR axis and involves a mechanism that dramatically inhibits the invasive capacity of endothelial and tumor cells, as well as inhibiting growth in the bone in a PC metastatic model (as described below). Thus, the use of disintegrins represents a truly novel therapeutic concept. Finally, cilengitide, cyclo(L-arginyl-L-glycyl-L-aspartyl-D-phenylalanyl-N-methyl-L-valyl), is a potent selective αvβ3-αvβ5 integrin antagonist that has been shown to inhibit integrin-mediated cell adhesion and block in vitro endothelial cell migration. Cilengitide inhibits cytokine-induced bFGF- and VEGF-mediated angiogenesis in a dose-dependent manner, and inhibits tumor growth in several in vivo systems (Beekman et al., 2006). In glioblastoma multiforme (GBM) cilengitide monotherapy is well tolerated with minimal toxicity and exhibits antitumor activity against recurrent disease. It was concluded that integrating cilengitide into

combination regimens for GBM is warranted (Reardon et al., 2008). However, when comparing CN and VCN to the parental cyclic RGD peptide cilengitide was derived from, cRGDfV, we found that this cyclic peptide neither induced the profound actin cytoskeleton disruption nor the signaling activity exhibited by CN and VCN. In experiments designed to investigate the mechanism of the anti-invasive activity of CN, we found CN induced dissociation of talin from β1 integrin cytoplasmic tail leading to massive disruption of the actin cytoskeleton in HUVEC plated on Matrigel, whereas cRGDfV had no such activity. Similarly, confocal images of HUVEC plated on Matrigel show a clear discrepancy between VCN and cRGDfV treatment in their ability to collapse the actin cytosleleton of these cells. In further support of these findings, the design of cyclic RGD peptides and RGD mimetics is based on the exposed RGD tripeptide motif in ECM proteins that plays an important role in ligand recognition by integrins, particularly αvβ3 and αvβ5. However, our findings indicate that the presence of the RGD motif alone, although it contributes significantly to the ligand–receptor interaction, may not be sufficient to efficiently and fully modulate the downstream signaling of integrins. Unlike cyclic RGD peptides and peptidomimetics, disintegrins have additional structural elements which enable them to modulate integrin signaling in an efficient and unique manner (Brown et al., 2009; Calvete et al., 2005; Fujii et al., 2003; Marcinkiewicz et al., 1997; Sanz et al., 2005; Yahalom et al., 2002). Thus, unlike cilengitide, the RGD-containing disintegrin loop (11 amino acids) in CN and VCN has additional flanking residues, a structural feature which enables it to make more extensive contacts with the receptor. Furthermore, NMR and crystallographic studies have revealed that the C-terminal tail in disintegrins folds with the RGD-containing disintegrin loop, such that these two structural elements are linked together and form an extended conformational epitope in the three-dimensional structure of disintegrins. This strongly indicates that these two functional regions are engaged in extensive interactions with the target integrin receptor (Brown et al., 2009; Sanz et al., 2005). These observations led us to conclude that, unlike cyclic RGD peptides and peptidomimetics that act only as receptor antagonists, integrin modulation in the case of disintegrins is far more complex. Therefore, by using structural and functional regions in addition to the RGD motif, a tripeptide amino acid sequence that serves as the sole basis for the design of cyclic RGD peptides and non-peptide RGD mimetics, disintegrins are expected to exhibit novel antitumor activities as compared to cyclic RGD peptides and peptidomimetics.

Necessity for Liposomal Delivery of VCN

Due to the short circulatory half-life of peptides such as VCN a delivery system other than direct i.v. administration was needed. Liposomes are submicroscopic nanospheres composed of thin but durable membranes made primarily of phospholipids and cholesterol. The composition, number of lipid layers, size, charge and permeability of the membrane can be altered to enhance delivery of a variety of therapeutic agents encapsulated inside the nanoparticle (Fujii, 1996; Woodle, 1993).

With respect to disintegrin delivery to the tumor bed, we hypothesize that our liposomes are degraded by phospholipases or other enzymes generated in the tumor microenvironment. Due to the incorporation of phospholipids such as phosphatidylcholine or phosphatidylglycerol in the membrane of these unilamellar liposomes, action of these enzymes leads to disruption of the membrane structure with release of the disintegrin payload and subsequent binding of the disintegrin to integrins at the surface of the endothelial and tumor cells. Other advantages associated with our lipid encapsulation process include: (1) enhanced drug delivery to the desired site, (2) prolonged drug half-life and thus reduced dosing frequency, and (3) reduced drug and carrier related toxicities. In the following experimental evidence section, a description of the success is presented for the development of a stable expression system for VCN, a scalable liposomal encapsulation method to prepare LVCN and in vitro and in vivo biological efficacy studies using cells in culture and two PC animal cancer models.

Experimental Evidence for Efficacy of VCN as an Anti-Tumor/Anti-Angiogenic Agent

Recombinant Expression of a Venom Derived Disintegrin

For a number of years the Markland laboratory has worked with contortrostatin (CN), a disintegrin isolated from *Agkistrodon contortrix contortrix* venom. A major obstacle in the pathway to clinical development of CN was the supply of the protein, it is only present as a very small fraction of the total venom protein (∼0.01%). Further, for recombinant production, its peculiar structure stabilized by numerous disulfide bonds makes its expression in commonly-employed recombinant systems a very difficult task. Nonetheless, we have successfully employed a recombinant expression system for which we developed a proprietary production method capable of generating approximately 200 mg of purified active recombinant disintegrin per liter of bacterial culture in small-scale laboratory conditions. To generate recombinant disintegrins, we have successfully adapted a commercially-available *E. coli* expression system consisting of the Origami B (DE3) expression host in combination with the pET32a vector (Novagen) for our production needs. A sequence-engineered form of CN, called vicrostatin (VCN), has been directionally cloned into pET32a expression vector incorporating a unique tobacco etch virus (TEV) protease cleavage site, which facilitates the removal of the thioredoxin fusion partner from the expressed VCN.

Following establishment of primary cultures, large scale cultures were inoculated and grown to an OD of 0.6–1.0 and induced with IPTG. Following a 4–5 h induction period the cultures are centrifuged and bacterial pellets lysed by a scalable homogenization method. The insoluble cellular debris was then removed by centrifugation and the soluble cell lysate collected and further analyzed by SDS-PAGE for recombinant protein expression. The expressed fusion protein, thioredoxinA-VCN (Trx-VCN), was proteolysed by adding recombinant TEV protease to the

soluble cell lysates. TEV protease treatment efficiently cleaved VCN from its TrxA fusion partner; the status of proteolytic cleavage was monitored by SDS-PAGE. When proteolysis was complete, as assessed by SDS-PAGE, the proteolyzed lysate was filtered, diluted in H_2O and ultrafiltrated through a 50 kDa molecular weight cut-off cartridge that removed most of the higher molecular weight bacterial proteins. The resulting ultrafiltrate was then re-concentrated against a 5 kDa molecular weight cut-off cartridge. VCN was further purified by reverse phase HPLC. The recombinant disintegrin we have produced through this system is recognized by polyclonal antisera raised against native CN and inhibits ADP induced platelet aggregation in a dose dependent manner with an IC50 identical to native CN (∼60 nM). Moreover, VCN inhibits tumor cell adhesion, inhibits endothelial cell and tumor cell invasion and inhibits endothelial cell tube formation in a manner indistinguishable from native venom derived contortrostatin. However, VCN is a monomer with a molecular weight of 6,750 Da, whereas CN is a homodimer with a molecular weight of 13,500 Da (Minea et al., 2005)

Liposomal Encapsulation of VCN Using a Homogenization Method

To prepare liposomal vicrostatin (LVCN), stock solutions of phospholipids and cholesterol were prepared by dissolving the lipids in a chloroform/methanol solvent mixture. Thin lipid films were created by pipetting aliquots of the lipid solutions into round bottom glass tubes followed by solvent evaporation. The dried lipids and cholesterol were further dried under vacuum. This process yields lipid powder mixtures that were used to prepare LVCN. For liposome preparation by homogenization, VCN was dissolved in a hydration buffer and added to the dried lipids and incubated briefly at 50°C. LVCN was formed by passing the material through a microfluidizer. The material was processed between 10,000 and 18,000 psi while maintaining an elevated temperature (45–65°C). Samples of the liposome batch were removed during the process and the size distribution of LVCN was determined with an Ultrafine Particle Analyzer. After processing, unencapsulated VCN was removed by 100,000 MWCO ultrafiltration and LVCN sterilized by filtration through a 0.2 μM PVDF filter. We are encouraged that LVCN can be scaled to volumes necessary for commercialization by the homogenization technique.

In Vitro Evaluation of VCN in Limiting Tumor Progression and Angiogenesis

Binding Affinities of VCN to Integrins

To assess the binding affinities of VCN with soluble integrins, fluorescence polarization (FP) was utilized (Jameson and Seifried, 1999). In this method, differing concentrations of functional integrin were incubated with a constant amount of FITC labeled VCN. As VCN is a small molecule it rapidly depolarizes the excitation light. Upon binding to the large integrin, the fluorescent tag on VCN tumbles

Table 19.1   Dissociation constants for interactions of VCN and CN with soluble integrins

Disintegrin	Integrin Kd		
	αvβ3	α5β1	αvβ5
CN	6.6 nM	191.3 nM	19.5 nM
VCN	7.4 nM	15.2 nM	41.2 nM

Values calculated through fluorescence polarization measurements following steady state binding

in solution at a slower rate resulting in increased levels of polarization. The measured FP value is a weighted average of FP values of the bound and free fluorescent VCN and is therefore a direct measure of the fraction bound. Data generated in these experiments can be analyzed like standard radioligand binding, and kinetics of binding can be determined as with Scatchard analysis using a non-linear curve fit. From this set of experiments we determined the dissociation constants for VCN and CN with integrins αvβ3, α5β1 and αvβ5 (Table 19.1). Recombinant VCN was purposely designed with a carboxy terminal extension, which was expected to enhance affinity for α5β1. This was confirmed as CN and VCN exhibit nearly identical affinities for αvβ3 and similar affinity for αvβ5, but there is an order of magnitude difference in the Kd values for binding to α5β1 when comparing VCN (higher affinity binding) to CN.

Inhibition of Cellular Processes Critical to Tumor Progression

To assess the ability of VCN to block processes critical to tumor survival and progression (adhesion, migration and invasion) we have measured the inhibitory effect on different tumor cell lines, as well as endothelial cells. Inhibition of adhesion is evaluated through the ability of VCN to block cell attachment to a number of different extracellular matrix proteins. We observed a dose-dependence in the inhibition of adhesion of PC-3 cells as well as HUVEC, to both vitronectin and fibronectin, ECM proteins that are ligands for integrins targeted by VCN (data not shown). Cellular migration is also inhibited by VCN in a dose dependent manner. To evaluate tumor and endothelial cell migration a phagokinetic tracking assay is employed. In this assay cells are plated on a collagen coated cover-slip with an overlay of colloidal gold. As the cells move they displace or ingest the colloidal gold leaving tracks on the surface of the cover-slip. Then, using dark-field microscopy the tracks can be visualized and photographed. Using image analysis software the area of the tracks in a photographed field can be determined and a "migration index" can be calculated as a percentage of the field lacking gold. Following treatment by increasing concentrations of VCN the migration of both tumor and endothelial cells is significantly limited. Finally, the ability of cells to invade through the ECM was evaluated using modified Boyden chambers. These chambers contain a Matrigel coated porous membrane (pore size 8 μm). A chemoattractant is placed in the lower chamber and untreated cells invade through the membrane toward the attractant. Both CN and

VCN block the invasion of endothelial (HUVEC) and PC-3 cells in a dose dependent manner with IC_{50} at low nM concentrations. These results show that VCN has essentially identical activity to CN in inhibiting invasion of endothelial and prostate cancer (PC-3) cells. The results also convincingly demonstrate one of the important attributes of VCN, that it inhibits endothelial cell as well as tumor cell invasion in the low nM range.

Inhibition of HUVEC Tube Formation

To assess the ability of VCN to interfere with tube formation (an in vitro assay of anti-angiogenic activity), HUVEC were maintained in EGM-2 complete media and grown to confluency. HUVEC cells were harvested and resuspended in basal media. After being maintained in suspension for 15–30 min, cells were seeded onto Endothelial Cell Tube Formation plates, an in vitro endothelial tubulogenesis system, at a concentration of 25,000 cells per well and immediately treated with various concentrations of VCN, CN (positive control), or Suramin (positive control) and incubated for 18 h at 37°C. At the end of the incubation period, cells were washed and then stained with Calcein AM in PBS at 37°C. After 30 min the cells were washed again and imaged (Fig. 19.1) using confocal microscopy at 2.5X and 10X magnifications. On the captured images, the total length of tubes was
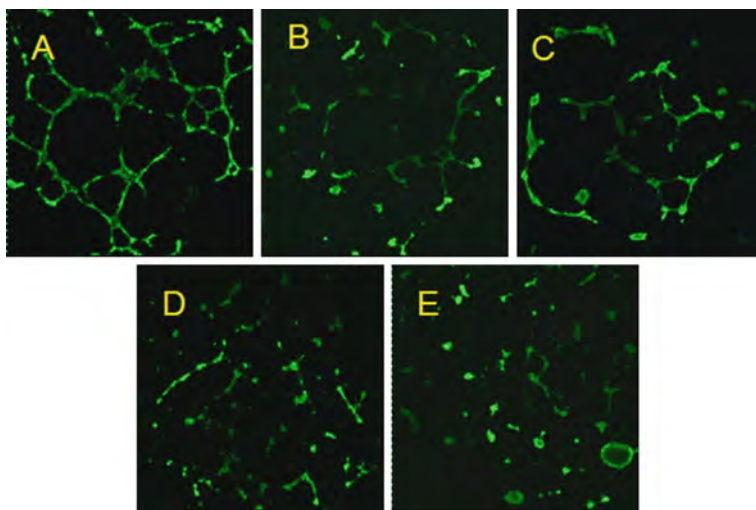

Fig. 19.1 Inhibition of HUVEC tube formation by VCN (representative images from multiple experiments). HUVEC cells were plated on "Endothelial Cell Tube Formation" plates (BD Biosciences) in the presence of various concentrations of VCN (0–1,000 nM), or a known tube formation inhibitor Suramin (used as a positive control). Representative figures from independent experiments were shown above: *panel a* – untreated control; *panel b* – 100 µM suramin; *panel c* – 1 nM VCN; *panel d* –10 nm VCN; and *panel e* – 1,000 nm VCN. Cells were stained with Calcein AM and imaged using confocal microscopy
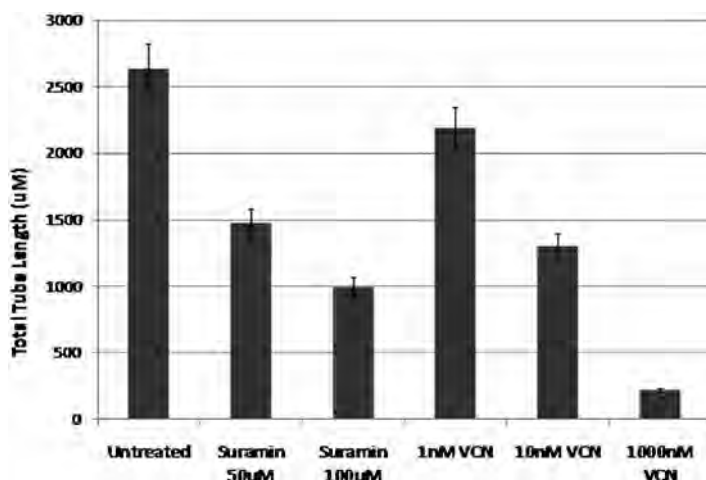
Fig. 19.2 Quantitation of tube formation inhibition by varying concentrations of VCN. The tubes formed by HUVECs were quantitated in multiple fields collected from three repeated experiments by computing the total tube length with Zeiss LSM image software and averaged to form each data point. The data shown above was assembled from multiple independent experiments

quantitated with Zeiss LSM image software and data plotted against the total length of tubes (in μm) generated by untreated cells. Representative tubes from 6 different wells were measured by 3 individuals and averaged to form each data point (Fig. 19.2). VCN exhibits potent dose-dependent inhibition of tube formation at low nM concentrations

Alterations of FAK Phosphorylation Induced by VCN

It has been proposed that the mechanism of action of VCN (delivered as LVCN) involves alterations in integrin mediated signal transduction pathways. Changing the phosphorylation status of FAK has previously been identified as a target of disintegrin action on both tumor and endothelial cells. To carry out these experiments using MDA-MB-435 cancer cells, the cells were grown to confluency and harvested. Cells were then maintained in suspension for 1 h in 2% bovine serum albumin/serum free medium. Various concentrations of VCN or CN (positive control) were used to treat the cells for 10–30 min while still in suspension. Following incubation with disintegrins and washing to remove unbound CN or VCN, cells were lysed with modified radioimmunoprecipitation assay (RIPA) buffer. For further analysis the total amount of protein in lysates was standardized before immunoprecipitation. Rabbit anti-FAK polyclonal antibodies were incubated with the whole cell lysates for 9–12 h at 4°C, and immune complexes were recovered by incubation with protein G immobilized on agarose beads overnight at 4°C. The precipitated protein complexes were centrifuged and the pellets washed, resuspended in SDS-PAGE sample buffer, and
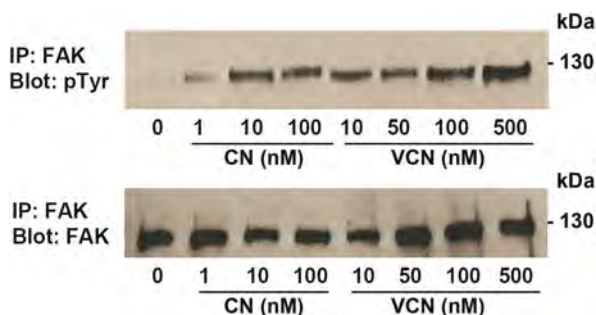
Fig. 19.3 FAK phosphorylation levels in MDA-MB-435 cells treated with disintegrins. Cells were kept in suspension in serum-free media and incubated with various amounts of CN or VCN for 10–30 min. The agonistic activity of both CN and VCN was assessed based on their effect on the global level of FAK phosphorylation by Western blotting. The level of total FAK in the treated cells does not change

boiled. For immunoblotting, proteins were resolved on 10% SDS gels and transferred to nitrocellulose membranes. Blots were incubated with either total anti-FAK monoclonal antibodies or p-TYR antibodies for 2 h at RT. Bound primary antibodies were detected with horseradish peroxidase-conjugated anti-mouse secondary antibodies, followed by enhanced chemiluminescence (Fig. 19.3). Experiments were repeated at least three times to verify results. These studies indicate that the level of phospho-FAK increases with increased concentration of treatment agent, VCN or CN; the difference between CN and VCN is almost indistinguishable, again indicating that the recombinant disintegrin (VCN) has identical bioactivity to the natural protein CN.

Actin Cytoskeleton and Focal Adhesion Disruption

In view of the finding that CN and VCN alter FAK phosphorylation, the effect of disintegrin treatment on focal adhesions and the actin cytoskeleton was evaluated. This was accomplished by visualization of the actin cytoskeleton and talin-based focal adhesions in HUVEC which were actively forming focal adhesions in a polymerized growth factor reduced (GFR) matrigel layer after treatment with either CN or a cyclic RGD peptide (cRGDfV). Eight well chamber slides were coated with GFR matrigel and left to polymerize. Residual media was aspirated out of the chamber slides and HUVECs (2.5×10^4) were seeded in serum free media onto the polymerized matrigel layer. Cells were incubated for 1-h at 37°C before being treated with either 100 nM CN or 10 μM cRGDfV. After overnight incubation, cells were washed with PBS, fixed in ice-cold acetone for 10 min at 4°C, and allowed to air dry for 2 min at 20°C. Each chamber was then blocked with PBS containing 5% BSA for 1 h. Talin was stained with a mouse monoclonal Ab, still in the presence of 5% BSA for 2 h. After washing with PBS, each chamber was counter stained with anti-mouse FITC-conjugated secondary Ab. The nucleus was stained with Hoechst

stain and the actin cytoskeleton was stained with rhodamine phalloidin. Following washing in PBS the chambers were separated and mounted with fluorescent mounting media for confocal microscopy. The immunofluorescent staining of talin clearly shows focal adhesions forming when HUVEC cells are plated on polymerized GRF matrigel. For the untreated group, focal adhesions are well-defined, small, cylindrical structures that are easily visualized under the zoomed panel (Fig. 19.4). Every cell also has numerous focal contacts in the leading edge of their lamellipodia. In addition, the actin cytoskeleton of the untreated group is highly organized. In every aspect, from the number of focal contacts made by talin to the organization of the actin cytoskeleton, the staining for cells treated with 10 μM cRGDfV is identical to the untreated group (Fig. 19.4). However, the CN treatment group reveled less
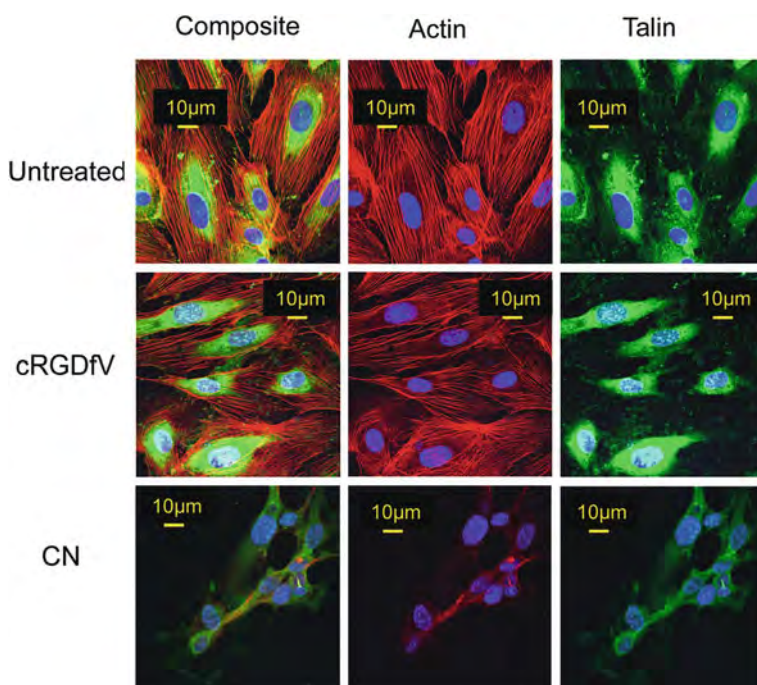

Fig. 19.4 Immunofluorescence of actin cytoskeleton and focal adhesions. Chamber slides coated with growth factor reduced matrigel were seeded with HUVEC (2.5×10^4) in serum free media. Cells were incubated for 1 h at 37°C before either no treatment (*top row*), treatment with 100 nM CN (*bottom row*), or 10 μM cRGDfV (*middle row*). After overnight incubation, cells were washed with PBS, fixed in acetone for 10 min at 4°C, and allowed to air dry for 2 min at 20°C. Each chamber was then blocked with PBS containing 5% BSA for 1 h at 20°C. Talin was stained with a mouse monoclonal Ab (clone TA205) for 2 h at 20°C. Followed by counter staining with anti-mouse FITC-conjugated secondary Ab (488 nM), Hoechst stain (460 nM), and rhodamine phalloidin (580 nM). After three washes in PBS the chambers were separated and mounted with fluorescent mounting media for confocal microscopy (63x). Composite column: superimposed images shown after counter-staining by all three agents; Actin column: rhodamine phalloidin staining; Talin column: talin staining. A 10 μm scale bar is included in each image

defined talin staining of broader sized structures that were hard to classify as focal adhesions (Fig. 19.4). Also, the number of focal contacts each lamellipodia has is greatly reduced. Moreover, the actin cytoskeleton for the CN treatment group is highly disorganized and looks to be under extreme stress conditions. This data indicates that cRGDfV treatment has virtually no effect on cytoskeletal organization and focal adhesions based on their associations with talin, while CN treatment drastically disrupts both of these structures. We assume that VCN will show identical activity based on its similarity to CN.

VCN Induction of Apoptosis in Tubulogenic HUVEC

VCN does not affect HUVEC viability if adherent cells are plated on Matrigel, but VCN exhibits significant anti-migratory effects (i.e., inhibition of tube formation) on HUVEC grown on Matrigel. Interestingly, when HUVEC are sandwiched between two layers of complete Matrigel, a significant apoptotic effect is also observed in the presence of VCN, but not with other integrin ligands (Fig. 19.5). Surprisingly, a similar effect was also seen with Avastin in this setting, though less pronounced than with VCN. It is noteworthy that HUVEC sandwiched between two Matrigel layers migrate and form tubes much faster than when plated on top of Matrigel. Thus, it appears that the rapidly migrating cells sandwiched in Matrigel may be more dependent (than those plated on top of Matrigel) on their ability to assemble a dynamic actin cytoskeleton and this seems to be a requirement not only for migration, but also for survival. Thus, the ability of VCN to efficiently disrupt the actin cytoskeleton of rapidly migrating cells may explain the discrepancy seen in cell survival between the two experimental settings. It is also important to note that, unlike the two integrin binding antibodies, 7E3 and LM609, the c(RGDfV) peptide did alter the morphology of the tubes formed by HUVEC when sandwiched in Matrigel, although to a lesser extent than VCN and with no impact on cell viability.

In Vivo Evaluation of the Anti-Angiogenic Anti-Tumor Activity of VCN

Circulatory Half-Life of LVCN

Previously we had determined the circulatory half-life of CN and liposomal CN (Swenson et al., 2004). We repeated these studies for VCN and LVCN. Blood samples were taken 0.5, 1, 3, 6, 18, 24, 48 and 72 h following i.v. administration of ^{125}I-VCN or L-^{125}I-VCN. Gamma counting of collected blood samples revealed that there was a rapid decrease to <0.1% of the administered counts in the blood 6 h after i.v. injection of ^{125}I-VCN. However, in animals given L-^{125}I-VCN, the percentage of total injected counts in the blood drops to a level of 63% of the injected counts 6 h post-injection and gradually decreases over the following 66 h. By plotting the decrease in radioactivity in blood over time following i.v. administration in tumor-free mice, we observed a circulatory half-life of 0.4 h for ^{125}I-VCN and
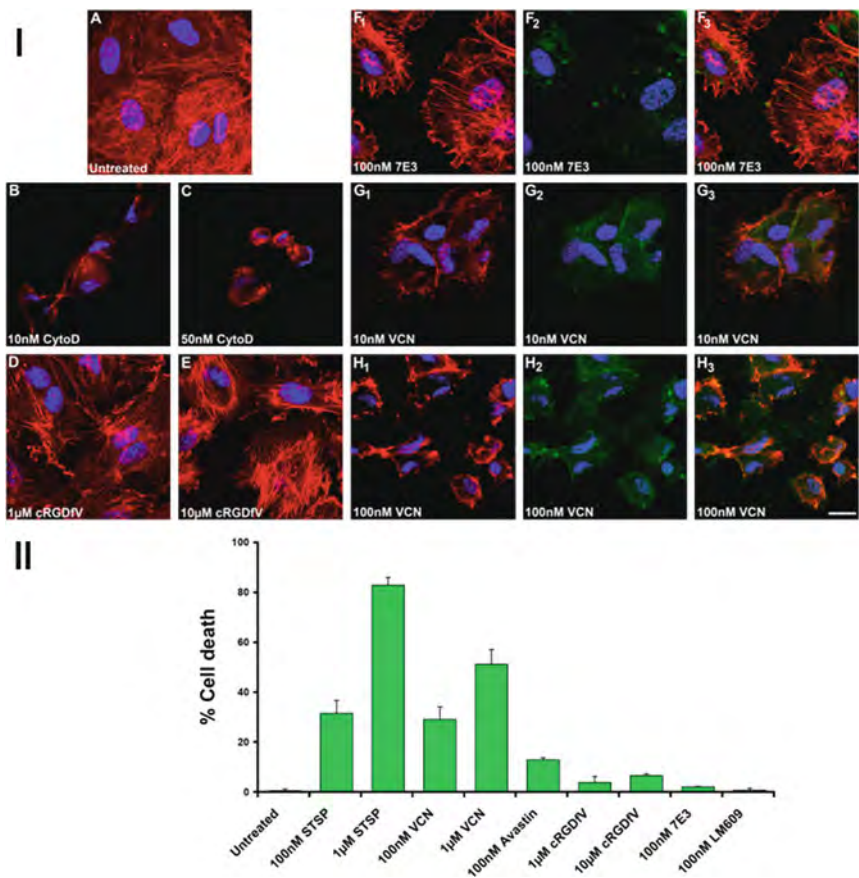
Fig. 19.5 VCN induces massive actin cytoskeleton reorganization in HUVEC seeded on Matrigel. HUVEC were seeded in serum-free media in multiwell chamber slides on complete Matrigel, allowed to adhere, and then treated for 3 h with various concentrations of cRGDfV peptide (1 and 10 μM) or FITC-VCN (10 and 100 nM) or the αvβ3-integrin binding antibody fragment 7E3 (100 nM) followed by a FITC-conjugated secondary antibody. The actin modifier Cytochalasin D was used as a positive control at two different concentrations (10 and 50 nM). At the end of the incubation period, the cells from all conditions were fixed in 4% formaldehyde, permeabilized in 0.1% Triton X-100, stained with Rhodamine-Phalloidin and Hoechst 33342, and imaged by confocal microscopy. The cells in panels F-H (treated with FITC-labeled 7E3 or VCN) are triple stained. The images shown above are Rhodamine-Hoechst (panels A–E and F1–H1), FITC-Hoechst (panels F2–H2) or all three fluorophores (panels F3–H3). Unlike the cRGDfV peptide or the integrin-binding 7E3 antibody fragment (or LM609, not shown), VCN collapses the actin cytoskeleton in HUVEC plated on Matrigel. Representative confocal images from multiple experiments taken at the same magnification (x630) are shown above (scale bar, 20 μm)

20.4 h for L-^{125}I-VCN similar to our previous findings with CN and LCN. Thus, encapsulation of VCN in liposomes not only protects the protein but also maintains it in the circulation for a much longer period of time than unencapsulated VCN, enabling more effective access to the tumor.

Preferential Tumor Binding of VCN

In order to determine if there was preferential tumor binding of VCN as compared to a cyclic peptide cyclo(-RGDfV-), similar to Cilengitide, which is currently in clinical trials for glioma therapy, we evaluated VCN as a PET imaging agent. This experiment was designed to show tumor specific binding of VCN in existing bone metastases, using the androgen dependent PC CWR22. CWR22 cells were injected into the tibia of nude mice and were allowed to grow untreated for ∼5 weeks until the tumors were 10–14 mm in diameter. Animals were then injected with ^{64}Cu labeled VCN or cyclo(-RGDfV-), and imaged using a Concorde Systems micro-PET imaging system. As can be seen in Fig. 19.6, injected VCN localizes to the tumor with much higher affinity than the cyclic RGD peptide. This indicates that VCN binds to the tumor and could serve as an effective imaging agent, as well as a therapeutic agent.

In Vivo Biological Efficacy Assay on Both Tumor and Angiogenic Vessel Growth

We examined the effect of treatment of a xenograft model of human PC using LVCN prepared by homogenization. Human prostate cancer cells (PC-3, 2×10^6) were implanted subcutaneously in the hip flank of 5-week old male nude mice. Tumors were allowed to grow until palpable (14 days) at which time drug administration was
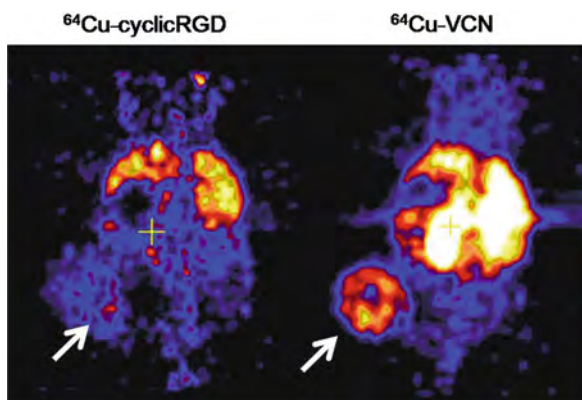

Fig. 19.6 VCN binds to prostate tumor. Comparison of binding efficacy of ^{64}Cu labeled VCN and a cyclic RGD peptide to an existing prostate tumor implanted in the tibia of a nude mouse (*white arrow* points to tumor. As can be seen the VCN binds with higher affinity than the RGD peptide to the existing PC tumor. With VCN a significant amount of the injected radioactivity is associated with the tumor but there also is a high level of non-specific binding in the kidneys liver and intestines. The level of non-specific binding with the RGD peptide appears lower but this can be due to the much shorter circulatory half-life of the RGD as compared to VCN. This indicated that VCN can potentially be used as both a therapeutic or PET imaging agent in prostate cancer. The image registration cross hatch is seen in the RGD panel

initiated. A preparation of LVCN as well as unencapsulated VCN were administered twice weekly via intravenous injection (100 µg per dose for 5 weeks); PBS and empty liposome controls were also included. Tumors were measured weekly via caliper in a blind fashion. At the end of the treatment period there is a significant inhibitory effect on tumor growth ($\sim$75% inhibition) when comparing the LVCN treated animals with the PBS treated and empty liposome controls (Fig. 19.7). In addition unencapsulated VCN displayed essentially no anti-tumor activity, which may in part be explained by its relatively short circulatory half-life. In additional PC-3 therapeutic efficacy studies we evaluated the efficacy of LVCN in combination with docetaxel. In these studies we used therapeutic doses of both docetaxel and LVCN and observed no additional effect on inhibition of tumor growth over that of LVCN alone. These studies will be repeated using a reduced LVCN dose and several different doses of docetaxel.

In addition to the inhibitory effect on tumor growth we also evaluated the anti-angiogenic effect of LVCN in the PC-3 model utilizing immunohistochemistry (IHC). Briefly, tumors were embedded in OCT using standard techniques. The frozen blocks were sectioned on a cryostat. The sections were taken from three regions of the tumor, the first, second and third 20 µm segment of the tumor. The thickness per section was 5 µm. This method was used to make sure that the
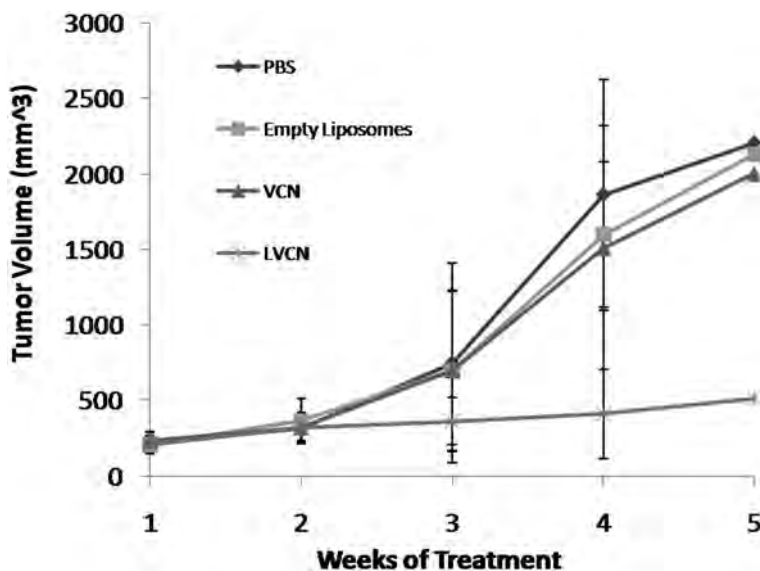

Fig. 19.7 PC-3 xenografts treated with LVCN. Tumor volume measurements in athymic nude mice bearing subcutaneous xenografts of the prostate cancer cell line PC-3 during treatment with LVCN or VCN administrated twice weekly via i.v. injection (100 µg/dose) Control animals were injected with PBS or empty liposomes. Treatment lasted for 5 weeks. Vertical bars indicate SEM. There is statistical significance, with p values less than 0.05 between the LVCN treatment group and the control

staining was representative of the entire tumor, and not due to the specific portion of the tumor tested. Following sectioning, tumor sections were fixed in acetone followed by blocking with 5% goat serum. The primary antibody utilized was a polyclonal rat anti-mouse CD31/PECAM. Following primary antibody incubation, the slides were washed and probed with the secondary antibody, biotinylated goat anti-rat antibody. Slides were then washed in PBS, and incubated with Avidin Binding Complex (ABC), and then stained with 3-amino-9-ethylcarbazole (AEC) chromogen solution. Slides were counterstained with Mayers Hemotoxylin to visualize nuclei. To quantitate the blood vessels the stained sections were subject to "random field" analysis. Four randomly assigned fields were chosen and digitally captured. To insure objectivity, the pictures were taken "blindly" without prior knowledge of treatment group. Four images per section and three sections per tumor (1 from 0–20 μm, 1 from 20–40 μm and 1 from 40–60 μm) were typically analyzed, twelve images per each tumor. Between 2 and 4 tumors per animal group of 5 animals were analyzed to obtain the microvessel density average in each of the experimental groups. Once the images were captured, and loaded onto the computer, they were quantitated using Simple PCI software. Blood vessels were defined as any endothelial cell or endothelial cell cluster, which was distinctly separated from tumor cells or connective tissue. The simple PCI imaging software allows the observer to pick a range of pixel colors denoting blood vessels. Those pixels are then quantified as both a raw number and % pixels per field of view. The images were analyzed in a blind fashion to reduce bias. As illustrated in Fig. 19.8, the microvessel density present in the control (PBS) group represents ~7% of the total pixels in a field being positive. Treatment of the animals with the LVCN resulted in a dramatic decrease in tumor-associated microvessel density to 1.5–2.5% of the visualized fields. The statistical significance between the PBS group and the LVCN treatment group reached P values on the order of 10^{-18}. This data further illustrates the anti-angiogenic potential of LVCN.

In separate studies we evaluated the therapeutic efficacy of LVCN in treating existing PC bone metastases. In these studies PC cells were implanted in the study
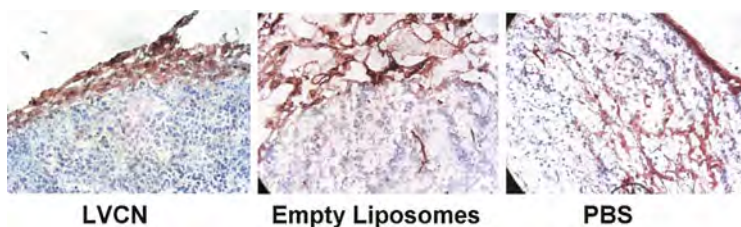

Fig. 19.8 Immunohistochemical Staining of Microvessels with CD31. Tumors were embedded in OCT and frozen prior to sectioning. Blocks were sectioned at 5 μm and probed with an anti-CD31 antibody. Following washing and after initial detection with a secondary antibody the chromagen AEC was used to visualize CD31 mAb. In both the PBS and empty liposome samples numerous vessels are observed while in the LVCN sample considerably fewer vessels are observed. LVCN is an effective antiangiogenic agent in prostate cancer
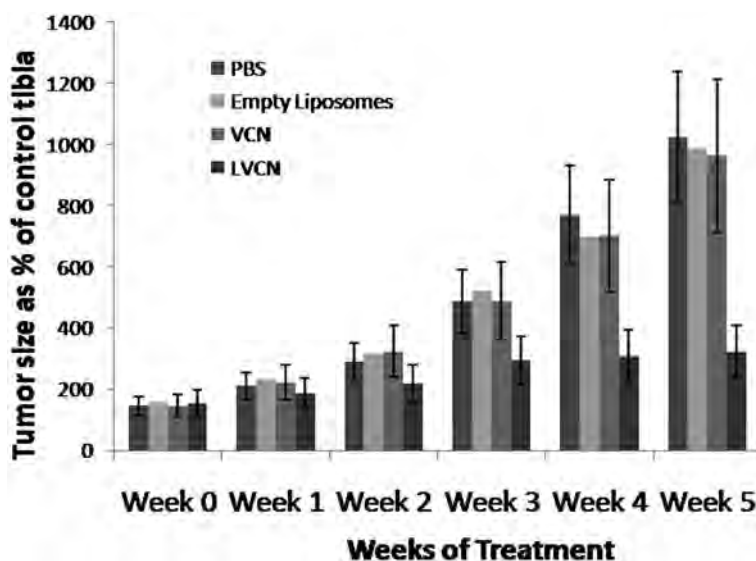
Fig. 19.9 CWR22 model of prostate cancer bone metastasis treated with LVCN. Shown are the tumor sizes as a percentage of the control tibia in athymic nude mice bearing experimental CWR22 PC bone metastasis treated with LVCN or VCN administrated twice weekly via i.v. injection (100 μg/dose). Control animals were injected with PBS or empty liposomes. Treatment lasted for 5 weeks. Vertical bars indicate SEM. There is statistical significance, with p values less than 0.05 between the LVCN treatment group and the control

animals by intra-tibial injection. Briefly, CWR22 prostate cancer cells were suspended in a solution of matrigel in modified Eagles media (MEM) at 2.5×10^6 cells/ ml and 25 μl of this suspension was directly injected into the proximal left tibia of immunodeficient mice. Following injection the diameter of both the left and right (control) tibias were measured by caliper twice weekly. Since the CWR22 cell line is androgen dependent, animals received daily i.p. injections of testosterone suspended in DMSO (1 mg/kg, daily). The tumors grew slowly over the initial 20 days, but at this point tumors were evident and treatment began. As in the subcutaneous model studies, LVCN as well as unencapsulated VCN were administered twice weekly via i.v. injection (100 μg per dose for 5 weeks). LVCN displayed a significant inhibition of tumor growth as compared to VCN, PBS and empty liposomes (Fig. 19.9). Studies to evaluate bone loss are ongoing.

Preliminary Evaluation of LVCN Acute Toxicity

The toxicity of a single intravenous dose of VCN or LVCN prepared by homogenization was evaluated using a rat model. Wistar rats (120–130 g) were assigned to 12 groups of 3 animals each, including 2 control groups (PBS and empty liposome control), and 10 experimental groups that received VCN or LVCN preparations (3, 10, 25, and 75 mg/kg for VCN and 1, 3, 10, 25, 50, and 75 mg/kg for LVCN).

Table 19.2 Average hematologic values for VCN LVCN toxicity test

Agent	Dose	Weight (g)	WBC ($\times 10^3$/μl)	RBC ($\times 10^6$/μl)	HGB (g/dl)	MCV (10^{-15} l)	MCHC (g/dl)	PLT ($\times 10^3$/μl)	MPV (10^{-15} l)
Saline		186±7	5.7±0.6	5.9±0.5	12.2±0.4	55.9±0.6	34.7±1.0	988±39	5.4±0.6
Liposomes		179±9	7.3±1.3	7.1±0.6	13.9±0.8	58.9±0.9	35.0±0.9	1028±44	5.4±0.5
VCN	3 mg/kg	183±7	4.7±0.8	6.8±0.4	13.1±0.9	55.8±0.5	34.6±1.1	1160±83	5.1±0.7
VCN	75 mg/kg	176±9	4.4±0.7	6.5±0.6	12.7±0.6	56.2±0.8	35.2±1.2	1193±64	5.2±0.5
LVCN	3 mg/kg	182±6	5.7±0.6	6.3±0.7	13.0±0.7	55.5±0.6	35.0±1.1	976±59	5.4±0.4
LVCN	75 mg/kg	188±7	5.4±0.9	6.6±0.4	13.6±0.5	57.3±0.9	35.1±0.9	1022±46	5.3±0.3

Weight = animal weight in grams (g); WBC = white blood cell count; RBC = Red Blood Cell count, HGB = Hemoglobin; MCV = Mean corpuscular volume, MCHC = Mean Cell Hemoglobin Concentration, PLT = Platelet Count; MPV = Mean platelet volume

Animals were given a single administration of the test agents and evaluated for signs of physical toxicity or stress over 14 days, and then sacrificed at day 14. Signs of toxicity were monitored via physical status, activity level and total body weight; following sacrifice, gross and microscopic pathology was performed and hematological properties were analyzed. There were no adverse effects observed in the any of the treated animals. Animals in all treatment groups thrived and gained weight indistinguishable from the control groups. There were no observed changes in behavior immediately following agent administration, nor throughout the 14 day study. Gross examination following sacrifice revealed no changes in tissue or organ histopathology between control and treated animals. There were no significant differences in hematological parameters between even the highest dose (75 mg/kg) and control (Table 19.2). Microscopic examination of major body organs revealed that there was no observable inflammation, no significant cellular alterations and no visible hemorrhagic changes in the microscopic sections.

Conclusions and Future Directions of Disintegrins as Anti-Angiogenics

Anti-angiogenic agents currently in clinical trials and clinical use including monoclonal antibodies, such as bevacizumab, which specifically inhibits the VEGF-A signaling cascade, or small-molecule inhibitors of signaling pathways, are limited in that they target a specific single pathway within the tumor or angiogenic vasculature. While such specific targeting strategies may be initially effective, tumors can develop resistance to anti-angiogenic therapies, reviewed by Kerbel (2001a, 2001b). For example, VEGF-A can be replaced by other redundant signaling mechanisms, including other VEGF family members or pathways unrelated to VEGF, during tumor progression. This would enable a tumor to escape the effects of the single target VEGF-A blockade. In addition, targeting a single pathway applies a positive selective pressure upon tumor cells such that resistant variants may be generated through mutation. Tumors can also evade anti-angiogenic agents through the emergence of hypoxia-resistant mutants that are less dependent on angiogenesis. Changes in the structure of tumor vasculature towards a more mature phenotype might also promote resistance. Therefore, the development of drug resistance is a significant concern in the design of novel anti-angiogenic therapies.

As previously discussed, integrins play a central role in a number of key pathways in tumor progression, including cell migration, invasion, adhesion, metastasis and angiogenesis. Integrin antagonists can therefore be expected to impact all of these pathways and have a more broad-spectrum effect upon tumor cells. Such an approach alleviates the problem of drug resistance since multiple pathways are being targeted simultaneously. Since the disintegrin class of integrin antagonists are small peptides, which do not appear to be toxic nor do they activate the immune system, and thus potential side effects are minimized. Utilizing liposome technology, a clinically relevant method for the administration and delivery of the disintegrins has been developed and has proven to be effective in a number of mouse

models without significant toxicity. Employing a fully functional recombinant variant of CN, VCN, expressed in a highly modified *E. coli* expression system, which has been described elsewhere (Minea et al., 2005) provides a clear path for the clinical translation of this molecule . This advance in the production and validation of recombinant VCN solves an important supply problem faced by the natural venom purified disintegrin and will allow further development as a clinical agent. Therefore, while current therapies have been promising, disintegrins represent an attractive alternative to conventional anti-angiogenic agents.

References

Adler, M., Lazarus, R.A., Dennis, M.S., Wagner, G., 1991. Solution structure of kistrin, a potent platelet aggregation inhibitor and GP IIb-IIIa antagonist. Science 253, 445–448.

Aragon-Ching, J.B., Dahut, W.L., 2008. The role of angiogenesis inhibitors in prostate cancer. Cancer. J. 14, 20–25.

Aragon-Ching, J.B., Dahut, W.L., 2009. VEGF inhibitors and prostate cancer therapy. Curr. Mol. Pharmacol. 2, 161–168.

Banno, A., Ginsberg, M.H., 2008. Integrin activation. Biochem. Soc. Trans. 36, 229–34.

Bayless, K.J., Salazar, R., Davis, G.E., 2000. RGD-dependent vacuolation and lumen formation observed during endothelial cell morphogenesis in three-dimensional fibrin matrices involves the αvβ3 and α5β1 integrins. Am. J. Pathol. 156, 1673–1683.

Beekman, K.W., Colevas, A.D., Cooney, K., Dipaola, R., Dunn, R.L., Gross, M., Keller, E.T., Pienta, K.J., Ryan, C.J., Smith, D., Hussain, M., 2006. Phase II evaluations of cilengitide in asymptomatic patients with androgen-independent prostate cancer: scientific rationale and study design. Clin. Genitourin. Cancer 4, 299–302.

Beekman, K.W., Hussain, M., 2006. Targeted approaches for the management of metastatic prostate cancer. Curr. Oncol. Rep. 8, 206–212.

Boehm, T., Folkman, J., Browder, T., O'Reilly, M.S., 1997. Antiangiogenic therapy of experimental cancer does not induce acquired drug resistance. Nature 390, 404–407.

Brooks, P.C., Montgomery, A.M., Rosenfeld, M., Reisfeld, R.A., Hu, T., Klier, G., Cheresh, D.A., 1994. Integrin αvβ3 antagonists promote tumor regression by inducing apoptosis of angiogenic blood vessels. Cell 79, 1157–1164.

Brown, M.C., Eble, J.A., Calvete, J.J., Marcinkiewicz, C., 2009. Structural requirements of KTS-disintegrins for inhibition of $\alpha_1\beta_1$ integrin. Biochem. J. 417, 95–101.

Calderwood, D.A., 2004. Talin controls integrin activation. Biochem. Soc. Trans. 32, 434–437.

Calvete, J.J., Marcinkiewicz, C., Monleon, D., Esteve, V., Celda, B., Juarez, P., Sanz, L., 2005. Snake venom disintegrins: evolution of structure and function. Toxicon 45, 1063–1074.

Chen, H.X., Cleck, J.N., 2009. Adverse effects of anticancer agents that target the VEGF pathway. Nat. Rev. Clin. Oncol. 6, 465–477.

Cheresh, D.A., 1992. Structural and biologic properties of integrin-mediated cell adhesion. Clin. Lab. Med. 12, 217–236.

Choueiri, T.K., Duh, M.S., Clement, J., Brick, A.J., Rogers, M.J., Kwabi, C., Shah, K., Percy, A. G., Antras, L., Jayawant, S.S., Chen, K., Wang, S.T., Luka, A., Neary, M.P., McDermott, D., Oh, W.K., 2009. Angiogenesis inhibitor therapies for metastatic renal cell carcinoma: effectiveness, safety and treatment patterns in clinical practice-based on medical chart review. BJU Int. 105(9), 1247–1254.

Choy, M., Rafii, S., 2001. Role of angiogenesis in the progression and treatment of prostate cancer. Cancer Invest. 19, 181–91.

Concato, J., Jain, D., Uchio, E., Risch, H., Li, W.W., Wells, C.K., 2009. Molecular markers and death from prostate cancer. Ann. Intern. Med. 150, 595–603.

Cooper, C.R., Chay, C.H., Pienta, K.J., 2002. The role of $\alpha_v\beta_3$ in prostate cancer progression. Neoplasia 4, 191–194.

Courtney, K.D., Choueiri, T.K., 2009. Optimizing recent advances in metastatic renal cell carcinoma. Curr. Oncol. Rep. 11, 218–226.

Cousins, G.R., Sudo, Y., Friedrichs, G.R., Markland, F.S., Lucchesi, B.R., 1995. Contortrostatin prevents reocclusion after thrombolytic therapy in a canine model of carotid artery thrombosis. FASEB J. 9, A938.

Cox, M.C., Permenter, M., Figg, W.D., 2005. Angiogenesis and prostate cancer: important laboratory and clinical findings. Curr. Oncol. Rep. 7, 215–219.

Cress, A.E., Rabinovitz, I., Zhu, W., Nagle, R.B., 1995. The alpha 6 beta 1 and alpha 6 beta 4 integrins in human prostate cancer progression. Cancer Metastasis Rev. 14, 219–228.

Demirgoz, D., Garg, A., Kokkoli, E., 2008. PR_b-targeted PEGylated liposomes for prostate cancer therapy. Langmuir 24, 13518–13524.

Dennis, M.S., Henzel, W.J., Pitti, R.M., Lipari, M.T., Napier, M.A., Deisher, T.A., Bunting, S., Lazarus, R.A., 1990. Platelet glycoprotein IIb/IIIa protein antagonists from snake venoms: evidence for a family of platelet-aggregation inhibitors. Proc. Natl. Acad. Sci. U.S.A. 87, 2471–2475.

Di Lorenzo, G., De Placido, S., 2006. Hormone refractory prostate cancer (HRPC): present and future approaches of therapy. Int. J. Immunopathol. Pharmacol. 19, 11–34.

Ebos, J.M., Lee, C.R., Cruz-Munoz, W., Bjarnason, G.A., Christensen, J.G., Kerbel, R.S., 2009. Accelerated metastasis after short-term treatment with a potent inhibitor of tumor angiogenesis. Cancer Cell 15, 232–239.

Erbersdobler, A., Isbarn, H., Dix, K., Steiner, I., Schlomm, T., Mirlacher, M., Sauter, G., Haese, A., 2009. Prognostic value of microvessel density in prostate cancer: a tissue microarray study. World J. Urol. In Press

Fox, W.D., Higgins, B., Maiese, K.M., Drobnjak, M., Cordon-Cardo, C., Scher, H.I., Agus, D.B., 2002. Antibody to vascular endothelial growth factor slows growth of an androgen-independent xenograft model of prostate cancer. Clin. Cancer Res. 8, 3226–3231.

Friedlander, M., Brooks, P.C., Shaffer, R.W., Kincaid, C.M., Varner, J.A., Cheresh, D.A., 1995. Definition of two angiogenic pathways by distinct αv integrins. Science 270, 1500–1502.

Fujii, G., 1996. Liposomal amphotericin B(AmBisome): realization of the drug delivery concept, in: Rosoff, M. (Ed.), Vesicles. Marcel Dekker, New York, pp. 491–526.

Fujii, Y., Okuda, D., Fujimoto, Z., Horii, K., Morita, T., Mizuno, H., 2003. Crystal structure of trimestatin, a disintegrin containing a cell adhesion recognition motif RGD. J. Mol. Biol. 332, 1115–1122.

Garrison, J.B., Kyprianou, N., 2004. Novel targeting of apoptosis pathways for prostate cancer therapy. Curr. Cancer Drug Targets 4, 85–95.

Gasparini, G., Brooks, P.C., Biganzoli, E., Vermeulen, P.B., Bonoldi, E., Dirix, L.Y., Ranieri, G., Miceli, R., Cheresh, D.A., 1998. Vascular integrin $\alpha_v\beta_3$: a new prognostic indicator in breast cancer. Clin. Cancer. Res. 4, 2625–2634.

Gleave, M., Miyake, H., Chi, K., 2005. Beyond simple castration: targeting the molecular basis of treatment resistance in advanced prostate cancer. Cancer Chemother. Pharmacol. 56 Suppl 1, 47–57.

Goel, H.L., Li, J., Kogan, S., Languino, L.R., 2008. Integrins in prostate cancer progression. Endocr. Relat. Cancer 15, 657–664.

Golubkov, V., Hawes, D., Markland, F.S., 2003. Anti-angiogenic activity of contortrostatin, a disintegrin from *Agkistrodon contortrix contortrix* snake venom. Angiogenesis 6, 213–224.

Gould, R.J., Polokoff, M.A., Friedman, P.A., Huang, T.F., Holt, J.C., Cook, J.J., Niewiarowski, S., 1990. Disintegrins: a family of integrin inhibitory proteins from viper venoms. Proc. Soc. Exptl. Biol. Med. 195, 168–171.

Grothey, A., Galanis, E., 2009. Targeting angiogenesis: progress with anti-VEGF treatment with large molecules. Nat. Rev. Clin. Oncol. 6, 507–518.

Gutheil, J.C., Campbel, T.N., Pierce, P.R., Watkins, J.D., Huse, W.D., Bodkin, D.J., Cheresh, D.A., 2000. Targeted antiangiogenic therapy for cancer using vitaxin: a humanized monoclonal antibody to the integrin $\alpha v\beta 3$. Clin. Cancer Res. 6, 3056–3061.

Harris, W.P., Mostaghel, E.A., Nelson, P.S., Montgomery, B., 2009. Androgen deprivation therapy: progress in understanding mechanisms of resistance and optimizing androgen depletion. Nat. Clin. Pract. Urol. 6, 76–85.

Hiles, J.J., Kolesar, J.M., 2008. Role of sunitinib and sorafenib in the treatment of metastatic renal cell carcinoma. Am. J. Health Syst. Pharm. 65, 123–131.

Hood, J.D., Bednarski, M., Frausto, R., Guccione, S., Reisfeld, R.A., Xiang, R., Cheresh, D.A., 2002. Tumor regression by targeted gene delivery to the neovasculature. Science 296, 2404–2407.

Huang, T.F., Holt, J.C., Kirby, E.R., Niewiarowski, S., 1989. Trigramin: primary structure and its inhibition of von willebrand factor binding to glycoprotein IIb-IIIa complex on human platelets. Biochemistry 28, 661–666.

Humphries, M.J., 1996. Integrin activation: the link between ligand binding and signal transduction. Curr. Opin. Cell Biol. 8, 632–640.

Hynes, R.O., 1992. Integrins: versatility, modulation, and signaling in cell adhesion. Cell 69, 11–25.

Jameson, D.M., Seifried, S.E., 1999. Quantification of protein–protein interactions using fluorescence polarization. Methods 19, 222–233.

Jemal, A., Siegel, R., Ward, E., Hao, Y., Xu, J., Thun, M.J., 2009. Cancer statistics, 2009. CA. Cancer J. Clin. 59, 225–249.

Jimenez, J.A., Kao, C., Raikwar, S., Gardner, T.A., 2006. Current status of anti-angiogenesis therapy for prostate cancer. Urol. Oncol. 24, 260–268.

Kerbel, R.S., 2001a. Clinical trials of antiangiogenic drugs: opportunities, problems, and assessment of initial results. J. Clin. Oncol. 19, 45S–51S.

Kerbel, R. S., 2001b. Molecular and physiologic mechanisms of drug resistance in cancer: an overview. Cancer Metastasis Rev. 20, 1–2.

Kumar, C.C., 2003. Integrin alpha v beta 3 as a therapeutic target for blocking tumor-induced angiogenesis. Curr. Drug. Targets. 4, 123–311.

Kwabi-Addo, B., Ozen, M., Ittmann, M., 2004. The role of fibroblast growth factors and their receptors in prostate cancer. Endocr. Relat. Cancer 11, 709–724.

Liotta, L.A., Kohn, E.C., 2001. The microenvironment of the tumour-host interface. Nature 411, 375–379.

Madan, R.A., Dahut, W.L., 2009. Angiogenesis inhibition in the treatment of prostate cancer. Anticancer Agents Med. Chem. 27, 5627–5633.

Marcinkiewicz, C., Vijay-Kumar, S., McLane, M.A., Niewiarowski, S., 1997. Significance of RGD loop and C-terminal domain of echistatin for recognition of $\alpha_{IIb}\beta_3$ and $\alpha_v\beta_3$ integrins and expression of ligand-induced binding site. Blood 90, 1565–1575.

Markland, F.S., Shieh, K., Zhou, Q., Golubkov, V., Sherwin, R.P., Richters, V., Sposto, R., 2001. A novel snake venom disintegrin that inhibits human ovarian cancer dissemination and angiogenesis in an orthotopic nude mouse model. Haemostasis 31, 183–191.

McLane, M.A., Joerger, T., Mahmoud, A., 2008. Disintegrins in health and disease. Front. Biosci. 13, 6617–6637.

McLane, M.A., Marcinkiewicz, C., Vijay-Kumar, S., Wierzbicka-Patynowski, I., Niewiarowski, S., 1998. Viper venom disintegrins and related molecules. Proc. Soc. Exp. Biol. Med. 219, 109–119.

Merseburger, A.S., Simon, A., Waalkes, S., Kuczyk, M.A., 2009. Sorafenib reveals efficacy in sequential treatment of metastatic renal cell cancer. Expert Rev. Anticancer Ther. 9, 1429–1434.

Minea, R., Swenson, S., Costa, F., Chen, T.C., Markland, F.S., 2005. Development of a novel recombinant disintegrin, contortrostatin, as an effective anti-tumor and anti-angiogenic agent. Pathophysiol. Haemost. Thromb. 34, 177–183.

Montagnani, F., Migali, C., Fiorentini, G., 2009. Progression-free survival in bevacizumab-based first-line treatment for patients with metastatic colorectal cancer: is it a really good end point? J. Clin. Oncol. 27, e132–e133; author reply e134–e135.

Mucci, L.A., Powolny, A., Giovannucci, E., Liao, Z., Kenfield, S.A., Shen, R., Stampfer, M.J., Clinton, S.K., 2009. Prospective study of prostate tumor angiogenesis and cancer-specific mortality in the health professionals follow-up study. J. Clin. Oncol. 9, 1070–1078.

Nemeth, J.A., Cher, M.L., Zhou, Z., Mullins, C., Bhagat, S., Trikha, M., 2003. Inhibition of $\alpha_v\beta_3$ integrin reduces angiogenesis, bone turnover, and tumor cell proliferation in experimental prostate cancer bone metastases. Clin. Exp. Metastasis 20, 413–420.

Niewiarowski, S., McLane, M.A., Kloczewiak, M., Stewart, G.J., 1994. Disintegrins and other naturally occurring antagonists of platelet fibrinogen receptors. Semin. Hematol. 31, 289–300.

Paez-Ribes, M., Allen, E., Hudock, J., Takeda, T., Okuyama, H., Vinals, F., Inoue, M., Bergers, G., Hanahan, D., Casanovas, O., 2009. Antiangiogenic therapy elicits malignant progression of tumors to increased local invasion and distant metastasis. Cancer Cell 15, 220–231.

Pallares, J., Rojo, F., Iriarte, J., Morote, J., Armadans, L.I., de Torres, I., 2006. Study of microvessel density and the expression of the angiogenic factors VEGF, bFGF and the receptors Flt-1 and FLK-1 in benign, premalignant and malignant prostate tissues. Histol. Histopathol. 21, 857–865.

Phillips, D.R., Charo, I.F., Scarborough, R.M., 1991. GP IIb-IIIa: the responsive integrin. Cell 65, 359–362.

Pignatelli, M., Cardillo, M.R., Hanby, A., Stamp, G.W., 1992. Integrins and their accessory adhesion molecules in mammary carcinomas: loss of polarization in poorly differentiated tumors. Human Pathol. 23, 1159–1166.

Pinski, J., Markland, F., Wang, Q., Horiatis, D., Swenson, S., Costa, F. (2003). A novel therapy for prostate cancer based on the disintegrin contortrostatin. ASCO Annual Meeting. Chicago, IL.

Polnaszek, N., Kwabi-Addo, B., Peterson, L.E., Ozen, M., Greenberg, N.M., Ortega, S., Basilico, C., Ittmann, M., 2003. Fibroblast growth factor 2 promotes tumor progression in an autochthonous mouse model of prostate cancer. Cancer Res. 63, 5754–5760.

Pyrko, P., Wang, W., Markland, F.S., Swenson, S.D., Schmitmeier, S., Schonthal, A.H., Chen, T.C., 2005. The role of contortrostatin, a snake venom disintegrin, in the inhibition of tumor progression and prolongation of survival in a rodent glioma model. J. Neurosurg. 103, 526–537.

Ranieri, G., Patruno, R., Ruggieri, E., Montemurro, S., Valerio, P., Ribatti, D., 2006. Vascular endothelial growth factor (VEGF) as a target of bevacizumab in cancer: from the biology to the clinic. Curr. Med. Chem. 13, 1845–1857.

Reardon, D.A., Fink, K.L., Mikkelsen, T., Cloughesy, T.F., O'Neill, A., Plotkin, S., Glantz, M., Ravin, P., Raizer, J.J., Rich, K.M., Schiff, D., Shapiro, W.R., Burdette-Radoux, S., Dropcho, E.J., Wittemer, S.M., Nippgen, J., Picard, M., Nabors, L.B., 2008. Randomized phase II study of cilengitide, an integrin-targeting arginine-glycine-aspartic acid peptide, in recurrent glioblastoma multiforme. J. Clin. Oncol. 26, 5610–5617.

Romanov, V.I., Goligorsky, M.S., 1999. RGD-recognizing integrins mediate interactions of human prostate carcinoma cells with endothelial cells in vitro. Prostate 39, 108–118.

Ruoslahti, E., 1991. Integrins. J. Clin. Invest. 87, 1–5.

Sanz, L., Chen, R.Q., Perez, A., Hilario, R., Juarez, P., Marcinkiewicz, C., Monleon, D., Celda, B., Xiong, Y.L., Perez-Paya, E., Calvete, J.J., 2005. cDNA cloning and functional expression of jerdostatin, a novel RTS-disintegrin from *Trimeresurus jerdonii* and a specific antagonist of the α1β1 integrin. J. Biol. Chem. 280, 40714–40722.

Saudek, V., Atkinson, R.A., Lepage, P., Pelton, J.T., 1991. The secondary structure of echistatin from ^{1}H-NMR. Eur. J. Biochem. 202, 329–338.

Scarborough, R.M., Rose, J.W., Naughton, M.A., Phillips, D.R., Nannizzi, L., Arfsten, A., Campbell, A.M., Charo, I.F., 1993. Characterization of the integrin specificities of disintegrins isolated from American pit viper venoms. J. Biol. Chem. 268, 1058–1065.

Sharifi, N., Dahut, W.L., Figg, W.D., 2008. The genetics of castration-resistant prostate cancer: what can the germline tell us? Clin. Cancer Res. 14, 4691–4693.

Shebuski, R.J., Ramjit, D.R., Bencen, G.H., Polokoff, M.A., 1989. Characterization and platelet inhibitor activity of bitistatin, a potent arginine-glycine-aspartic acid-containing peptide from the venom of viper *Bitis arietans*. J. Biol. Chem. 264, 21550–21556.

Stoeltzing, O., Liu, W., Reinmuth, N., Fan, F., Parry, G.C., Parikh, A.A., McCarty, M.F., Bucana, C.D., Mazar, A.P., Ellis, L.M., 2003. Inhibition of integrin α5β1 function with a small peptide (ATN-161) plus continuous 5-FU infusion reduces colorectal liver metastases and improves survival in mice. Int. J. Cancer 104, 496–503.

Strohmeyer, D., Strauss, F., Rossing, C., Roberts, C., Kaufmann, O., Bartsch, G., Effert, P., 2004. Expression of bFGF, VEGF and c-met and their correlation with microvessel density and progression in prostate carcinoma. Anticancer Res. 24, 1797–1804.

Strömblad, S., Becker, J.C., Yebra, M., Brooks, P.C., Cheresh, D. A., 1996. Suppression of p53 activity and p21WAF1/CIP1 expression by vascular cell integrin αvβ3 during angiogenesis. J. Clin. Invest. 98, 426–433.

Sun, X.T., Ding, Y.T., Yan, X.G., Wu, L.Y., Li, Q., Cheng, N., Qiu, Y.D., Zhang, M.Y., 2004. Angiogenic synergistic effect of basic fibroblast growth factor and vascular endothelial growth factor in an in vitro quantitative microcarrier-based three-dimensional fibrin angiogenesis system. World J. Gastroenterol. 10, 2524–2528.

Sun, Y.X., Fang, M., Wang, J., Cooper, C.R., Pienta, K.J., Taichman, R.S., 2007. Expression and activation of αvβ3 integrins by SDF-1/CXC12 increases the aggressiveness of prostate cancer cells. Prostate 67, 61–73.

Swenson, S., Costa, F., Minea, R., Sherwin, R.P., Ernst, W., Fujii, G., Yang, D., Markland, F.S., Jr., 2004. Intravenous liposomal delivery of the snake venom disintegrin contortrostatin limits breast cancer progression. Mol. Cancer. Ther. 3, 499–511.

Trikha, M., De Clerck, Y.A., Markland, F.S., 1994a. Contortrostatin, a snake venom disintegrin, inhibits β1 integrin-mediated human metastatic melanoma cell adhesion and blocks experimental metastasis. Cancer Res. 54, 4993–4998.

Trikha, M., Rote, W.E., Manley, P.J., Lucchesi, B.R., Markland, F.S., 1994b. Purification and characterization of platelet aggregation inhibitors from snake venoms. Thromb. Res. 73, 39–52.

van Moorselaar, R.J., Voest, E.E., 2002. Angiogenesis in prostate cancer: its role in disease progression and possible therapeutic approaches. Mol. Cell. Endocrinol. 197, 239–250.

Weidner, N., Carroll, P.R., Flax, J., Blumenfeld, W., Folkman, J., 1993. Tumor angiogenesis correlates with metastasis in invasive prostate carcinoma. Am. J. Pathol. 143, 401–409.

Witkowski, C.M., Rabinovitz, I., Nagle, R.B., Affinito, K.S., Cress, A.E., 1993. Characterization of integrin subunits, cellular adhesion and tumorgenicity of four human prostate cell lines. J. Cancer. Res. Clin. Oncol. 119, 637–644.

Woodle, M.C., 1993. Surface-modified liposomes: assessment and characterization for increased stability and prolonged blood circulation. Chem. Phys. Lipids 64, 249–262.

Wu, I., Moses, M.A., 2000. Angiogenic molecules and mechanisms in breast cancer. Curr. Oncol. Rep. 2, 566–571.

Xiong, J.P., Stehle, T., Goodman, S.L., Arnaout, M.A., 2003. New insights into the structural basis of integrin activation. Blood 102, 1155–1159.

Yahalom, D., Wittelsberger, A., Mierke, D.F., Rosenblatt, M., Alexander, J.M., Chorev, M., 2002. Identification of the principal binding site for RGD-containing ligands in the $\alpha_v\beta_3$ integrin: a photoaffinity cross-linking study. Biochemistry 41, 8321–8331.

Yasuda, T., Gold, H.K., Leinbach, R.C., Yaoita, H., Fallon, J.T., Guerrero, L., Napier, M.A., Bunting, S., Collen, D., 1991. Kistrin, a polypeptide platelet GPIIb/IIIa receptor antagonist, enhances and sustains coronary arterial thrombolysis with recombinant tissue-type plasminogen activator in a canine preparation. Circulation 83, 1038–1047.

Zheng, D.Q., Woodard, A.S., Fornaro, M., Tallini, G., Languino, L.R., 1999. Prostatic carcinoma cell migration via $\alpha_v\beta_3$ integrin is modulated by a focal adhesion kinase pathway. Cancer Res. 59, 1655–1664.

Zhou, Q., Nakada, M.T., Arnold, C., Markland, F.S., 1999. Contortrostatin, a dimeric disintegrin from *Agkistrodon contortrix contortrix*, inhibits angiogenesis. Angiogenesis 3, 259–269.

Zhou, Q., Nakada, M.T., Brooks, P.C., Swenson, S.D., Ritter, M.R., Argounova, S., Arnold, C., Markland, F.S., 2000a. Contortrostatin, a homodimeric disintegrin, binds to integrin $\alpha_v\beta_5$. Biochem. Biophys. Res. Commun. 267, 350–355.

Zhou, Q., Sherwin, R.P., Parrish, C., Richters, V., Groshen, S.G., Tsao-Wei, D., Markland, F.S., 2000b. Contortrostatin, a dimeric disintegrin from *Agkistrodon contortrix contortrix*, inhibits breast cancer progression. Breast Cancer Res. Treat. 61, 249–260.

Zhu, A.X., Duda, D.G., Sahani, D.V., Jain, R.K., 2009. Development of sunitinib in hepatocellular carcinoma: rationale, early clinical experience, and correlative studies. Cancer J. 15, 263–268.

PLoS ONE

Vicrostatin – An Anti-Invasive Multi-Integrin Targeting Chimeric Disintegrin with Tumor Anti-Angiogenic and Pro-Apoptotic Activities

Radu O. Minea, Corey M. Helchowski, Samuel J. Zidovetzki, Fritz K. Costa, Stephen D. Swenson, Francis S. Markland, Jr.*

Department of Biochemistry and Molecular Biology and Norris Comprehensive Cancer Center, Keck School of Medicine, University of Southern California, Los Angeles, California, United States of America

Abstract

Similar to other integrin-targeting strategies, disintegrins have previously shown good efficacy in animal cancer models with favorable pharmacological attributes and translational potential. Nonetheless, these polypeptides are notoriously difficult to produce recombinantly due to their particular structure requiring the correct pairing of multiple disulfide bonds for biological activity. Here, we show that a sequence-engineered disintegrin (called vicrostatin or VCN) can be reliably produced in large scale amounts directly in the oxidative cytoplasm of Origami B *E. coli*. Through multiple integrin ligation (i.e., $\alpha v\beta 3$, $\alpha v\beta 5$, and $\alpha 5\beta 1$), VCN targets both endothelial and cancer cells significantly inhibiting their motility through a reconstituted basement membrane. Interestingly, in a manner distinct from other integrin ligands but reminiscent of some ECM-derived endogenous anti-angiogenic fragments previously described in the literature, VCN profoundly disrupts the actin cytoskeleton of endothelial cells (EC) inducing a rapid disassembly of stress fibers and actin reorganization, ultimately interfering with EC's ability to invade and form tubes (tubulogenesis). Moreover, here we show for the first time that the addition of a disintegrin to tubulogenic EC sandwiched *in vitro* between two Matrigel layers negatively impacts their survival despite the presence of abundant haptotactic cues. A liposomal formulation of VCN (LVCN) was further evaluated *in vivo* in two animal cancer models with different growth characteristics. Our data demonstrate that LVCN is well tolerated while exerting a significant delay in tumor growth and an increase in the survival of treated animals. These results can be partially explained by potent tumor anti-angiogenic and pro-apoptotic effects induced by LVCN.

Introduction

Despite the tremendous progress made in the last decades in deciphering the molecular intricacies of various signaling circuitries that operate aberrantly in cancers and the therapeutic advancement seen with some of the newer anti-cancer modalities recently approved by the FDA, such as humanized monoclonal antibodies directed at VEGF-A (vascular endothelial growth factor A) and receptor tyrosine kinases [1,2] or non-peptide tyrosine kinase inhibitors [3,4], the 5-year prognosis for most solid tumors remains reserved. Consequently, there is still a significant need to identify new drug candidates with broader spectrums of activity directed at signaling platforms (regulatory molecular hubs) shared by distinct cancer processes, which are, thus, able to simultaneously target multiple pathological aspects of cancer (for instance, both tumor angiogenesis and metastasis) with fewer side effects. The ability of transformed cells to evade the restrictive

environmental control exerted by the normal tissue architecture and grow in an anchorage-independent fashion is one of cancer's hallmarks [5]. One class of cell-surface receptors known to play a critical role in the process leading to the acquisition of an anchorage-independent phenotype is represented by the integrins [6].

Integrins are heterodimeric receptors that evolved to mediate the complex cell-ECM interactions that regulate the ability of cells to mechanically sense their environment by assembling complex multimolecular platforms capable of integrating multiple signaling pathways initiated by extracellular cues with the cellular cytoskeleton. In the ecology of multicelular organisms integrins are major contributors to the homeostasis of tissue architecture by keeping epithelial cells in a differentiated, specialized state [7]. Conversely, as epithelia transition to malignancy they evade the microenvironmental constraints by both altering their integrin affinity and avidity for ECM proteins (inside-out signaling) and/or

shifting their integrin expression [6,8]. The precise roles, however, played by different integrin subunits in various aspects of tumor progression and why some integrins appear to be especially supportive of tumor progression [9] are still not fully understood. Despite these limitations, due to their pivotal roles in cancer biology, integrins represent attractive therapeutic targets. For instance, although it doesn't seem to be essential for the formation of vasculature during development [10], nor during physiological angiogenesis associated with wound healing or tissue repair [11,12], the β3 integrin appears to be critically involved in the regulation of pathological angiogenesis [13]. Therefore, the pharmacological blockade of the β3 integrin has been demonstrated to significantly reduce tumor angiogenesis in numerous cancer models, a finding that has eventually led to the development of several drug candidates currently in clinical trials [14,15]. Similarly, αvβ5 and α5β1 as well as a number of other integrins (notably α2β1, α4β1, and α6β4) have also been shown to play important roles in tumor angiogenesis, their pharmacological targeting by soluble ligands or monoclonal antibodies leading to reduced tumor microvessel density in various cancer models [12,16]. Furthermore, at least some of the complex effects elicited by several endogenous ECM-derived antiangiogenic fragments (e.g., endostatin, tumstatin, endorepellin, etc) are attributed to direct integrin engagement [17,18]. In this report, we provide further evidence in support of the above therapeutic paradigm by showing that the efficient disruption by a member of the disintegrin family of multiple integrin pathways upregulated in cancer is followed by significant tumor anti-angiogenic and pro-apoptotic effects.

Disintegrins are among the most potent soluble ligands of integrins representing a class of cysteine-rich polypeptides historically isolated from the venoms of snakes belonging to the *Viperidae* family [19]. These small polypeptides hold a significant translational potential as anti-cancer agents based on their anti-angiogenic and anti-metastatic effects demonstrated in various experimental settings [20,21,22]. The integrin-binding activity of disintegrins depends on the appropriate pairing of several cysteine residues responsible for the disintegrin fold, a mobile 11-amino acid loop protruding from the polypeptide core displaying a tri-peptide motif, usually RGD (Arg-Gly-Asp), that is conserved in many disintegrins [23,24]. Although these molecules naturally evolved to efficiently bind to the activated platelet-specific integrin αIIbβ3, thus disrupting the process of platelet aggregation (the final step in blood clotting), most purified snake venom disintegrins are rather promiscuous in that they bind to several β1, β3 or β5 integrin members, albeit with different affinities and selectivity [25]. Two of the most studied native disintegrins are the homodimeric contortrostatin (CN) [26] and the monomeric echistatin [20]. Similar to echistatin, the anti-tumor activity of CN is based on its high affinity interaction with integrins α5β1, αvβ3 and αvβ5 on both cancer and angiogenic endothelial cells [27,28,29]. In a previous study [22] we showed that a liposomal formulation of CN limited tumor growth and significantly reduced microvascular density in a xenograft animal cancer model. We provided evidence that CN can be safely and effectively administered intravenously by a clinically acceptable delivery method (i.e., liposomal delivery) and, by doing so, CN passively accumulates at the tumor site. Furthermore, liposomal CN did not interact with the components of blood coagulation system nor elicit a neutralizing antibody immune response. For eventual clinical use, however, the direct isolation of native CN from crude venom would be laborious and prohibitively expensive since this polypeptide only exists as a very minor fraction relative to other venom components.

Vicrostatin (VCN) is a chimeric disintegrin generated recombinantly by grafting the C-terminal tail of **vi**perid snake venom disintegrin echistatin to the sequence of **cro**talid disintegrin contortrostatin (CN); we have previously shown [30] that this novel sequence could be produced as an active polypeptide in Origami B *E. coli*. Here, we show that VCN retains the binding profile of CN yet it engages integrins in a unique manner. As previously shown with native CN, VCN also appears to engage integrins agonistically thus behaving like a soluble ECM-mimetic. Via agonistic integrin ligation in the absence of tethering, VCN appears to inappropriately elicit a cascade of signaling events rapidly leading to actin stress fibers disassembly in HUVEC (human umbilical vein endothelial cells) plated on complete Matrigel. Moreover, in a manner reminiscent of some ECM-derived endogenous anti-angiogenic fragments [31,32,33], VCN interferes with the assembly of a dynamic actin cytoskeleton in tubulogenic HUVEC sandwiched between two Matrigel layers, negatively impacting the survival of these cells. Finally, in an effort to address our main goal of developing an efficient and clinically relevant delivery method for recombinant disintegrins, VCN was packaged in a liposomal formulation (LVCN) and further evaluated for *in vivo* efficacy.

Materials and Methods

Ethics Statement
All animals involved in this study were handled and euthanized in strict accordance with good animal practice as defined by the strict guidelines of the Institutional Animal Care and Use Committee (IACUC) of the University of Southern California.

Controtrostatin purification
Venom of *Agkistrodon contortrix contortrix* was purchased from Miami Serpentarium (Punta Gorda, FL). CN was purified in a four-step high-performance liquid chromatography (HPLC) procedure according to an established protocol [26].

Cells and reagents
The MDA-MB-435 cells were obtained from Dr. Janet Price (MD Anderson Cancer Center, Houston, TX) and the MDA-MB-231 cells from Dr. Toshiyuki Yoneda (Osaka University, Osaka, Japan). HUVEC were purchased from PromoCell (Heidelberg, Germany) and maintained according to the manufacturer's protocol. The Origami B (DE3) *E. coli* strain and pET32a expression vector carrying the bacterial thioredoxin A gene (*trxA*) were purchased from Novagen (San Diego, CA). The oligonucleotide primers used for rCN and VCN cloning were synthesized by Operon Biotechnologies, Inc. (Huntsville, AL). A southern copperhead venom gland cDNA library, a mouse CN monoclonal antibody, and rabbit CN polyclonal antiserum (Alpha Diagnostic Intl., San Antonio, TX) are available in the Markland laboratory at the University of Southern California. 'Endothelial Cell Tube Formation' plates were purchased from BD Biosciences (Bedford, MA). The tube formation inhibitor Suramin, the actin modifier Cytochalasin D (CytoD), and the cyclo(Arg-Gly-Asp-DPhe-Val) peptide (cRGDfV) were purchased from Calbiochem (San Diego, CA). The fluorometric cell invasion assay kit (QCM™ 24-Well Cell Invasion) was from Millipore (Billerica, MA). The complete Matrigel was from BD Biosciences. Recombinant tobacco etch virus (TEV) protease, Calcein AM, and Rhodamine-Phalloidin were purchased from Invitrogen (Carlsbad, CA). A column-based fluorescein isothiocyanate (FITC)-labeling kit (EZ-Label) and an endotoxin removal kit were purchased from Pierce (Rockford, IL). The DeadEnd™ Fluorometric TUNEL (terminal deoxynucleoti-

dyl transferase dUTP nick end labeling) assay kit was from Promega (Madison, WI). The non-selective protein kinase inhibitor Staurosporine (STSP) was from Cayman Chemical (Ann Arbor, MI). The murine β3 integrin 7E3 antibody was a gift from Dr. Marian Nakata (Centocor, Horsham, PA). The murine αvβ3 integrin antibody LM609 was from Millipore. The CD31 polyclonal antibody (MEC13.3) was from BD Pharmingen (Franklin Lakes, NJ). The Ki-67 (H-300), a focal adhesion kinase (FAK) polyclonal (A-17), and all secondary antibodies were purchased from Santa Cruz Biotechnology (Santa Cruz, CA). A FAK monoclonal antibody (clone 77) was from BD Biosciences. A phosphotyrosine monoclonal antibody (P-Tyr-102) was from Cell Signaling Technology (Danvers, MA). Purified soluble αvβ3 and αvβ5 integrins were purchased from Millipore and soluble recombinant α5β1 integrin from R&D Systems (Minneapolis, MN). All other reagents were purchased from Sigma Chemical Co. (St. Louis, MO). Avastin was a gift from Dr. Agustin Garcia (Norris Comprehensive Cancer Center, University of Southern California).

Construction of rCN and VCN expression vectors and recombinant production

rCN and VCN were cloned into pET32a vector downstream of thioredoxin A (TrxA) using a BglII/NcoI set of restriction enzymes. The forward primers for both rCN and VCN introduced a unique TEV protease cleavage site, which made possible the removal of thioredoxin during purification. To build the VCN construct, the nucleotides encoding the C-terminal tail of echistatin were added to CN via an elongated reverse primer. The primers used for rCN were: forward - 5′gttccagatctcgagaatctttacttccaaggagacgctcctgcaaatccgtgctgcga3′, and reverse - 5′gttattcgccatggcttaggcatggaagggatttctgggacagccagcaga3′. The primers used for VCN were: forward - 5′gttccagatctcgagaatctttacttccaaggagacgctcctgcaaatccgtgctgcga3′, and reverse - 5′gttattcgccatggcttaagtagctggacccttgtgggatttctgggacagccagcagatatgcc3′. Both plasmids were initially amplified in DH5α E. coli, purified and sequenced, and then transferred into Origami B (DE3) E. coli. Multiple cultures were established for each construct from individual colonies of transformed BL21 (DE3), AD494 (DE3) or Origami B (DE3) in LB media containing either carbenicillin (50 μg/mL) alone, or carbenicillin (50 μg/mL) plus kanamycin (15 μg/mL) or carbenicillin (50 μg/mL) plus tetracycline (12.5 μg/mL), plus kanamycin (15 μg/mL) and grown at 37°C and 250 rpm in a shaker-incubator until they reached an OD_{600} of 0.6-1. At this point, the cells were induced in 1 mM IPTG (isopropyl-1-β-D-thio-1-galactopyranoside) and incubated for another 4–5 hours at 37°C and 250 rpm. At the end of the induction period, the cells were pelleted at 4000×g and lysed in a microfluidizer (Microfluidics M-110L, Microfluidics, Newton, MA). The operating conditions of the microfluidizer included applied pressures of 14,000–18,000 psi, bacterial slurry flow rates of 300–400 ml per minute and multiple passes of the slurry through the processor. The lysate insoluble cellular debris was removed by centrifugation (40,000×g) and the soluble material containing either Trx-rCN or Trx-VCN collected. The expressed fusion proteins in the collected soluble lysates were then proteolysed by incubation with recombinant TEV protease overnight at room temperature which efficiently cleaved off rCN or VCN from TrxA as monitored by SDS-PAGE (sodium dodecyl sulfate-polyacrylamide gel electrophoresis). When proteolysis was complete, the proteolyzed lysates were passed through a 0.22 μm filter, diluted 1:100 in ddH$_2$O, ultrafiltrated through a 50,000 MWCO cartridge (Biomax50, Millipore) and then reconcentrated against a 5,000 MWCO cartridge (Biomax5, Millipore) using a tangential flow ultrafiltration device (Labscale TFF system, Millipore).

Purification of recombinant disintegrins

This was done by C18-reverse phase HPLC using the standard elution conditions previously employed for the purification of native CN [26]. The filtrated lysates processed as described above were loaded onto a Vydac C18 column (218TP54, Temecula, CA). A ten-minute rinse (at 5 ml/min) of the column with an aqueous solution containing 0.1%TFA was followed by a linear gradient (0–100%) elution over 150 min in a mobile phase containing 80% acetonitrile and 0.1%TFA. rCN starts eluting in 30% acetonitrile, while VCN elutes in 35% acetonitrile.

Inhibition of platelet aggregation

The inhibition of ADP-induced platelet aggregation by recombinant disintegrins was determined by measuring the light absorption of human platelet-rich plasma (PRP) in a specialized spectrophotometer (Chrono-log 490 optical aggregometer, Chrono-log, Havertown, PA) as previously described [22]. The FITC-labeled disintegrins (FITC-CN and FITC-VCN) and the liposomal formulations of VCN were also tested for activity against platelets.

Mass spectrometry (MS) analysis and sequencing by tryptic digestion

The MS analysis (MALDI-TOF and ESI) was initially done by Dr. Kym Faull (University of California at Los Angeles) and the subsequent sequencing by Dr. Ebrahim Zandi (Keck School of Medicine, University of Southern California). For sequencing, the purified recombinant disintegrins were reduced, alkylated and digested with trypsin at 37°C overnight. The resultant digestion peptides were then used in the tandem LC/MS/MS for sequence analysis. The LC consists of a reverse phase C-18 column through which peptides were eluted into the mass spectrometer using the following gradients: 5–60% acetonitrile +0.1% formic acid over 75 min and 50–90% acetonitrile +0.1% formic acid over 10 min. Tandem MS/MS spectra was acquired with Xcalibur software on a linear ion trap LTQ instrument. Data was analyzed using Bioworks, the SEQUEST algorithm and Sage-N Sorcerer to determine cross-correlation scores between acquired spectra and NCBI protein FASTA databases or any other databases as needed.

FAK phosphorylation studies

Serum-starved MDA-MB-435 cells were harvested by limited trypsin/EDTA treatment [34] and maintained in suspension before being exposed for 10–30 min to different concentrations of either native CN or VCN. The cells were lysed and the soluble fraction immunoprecipitated with a polyclonal FAK antibody (clone A-17) and further assayed by Western blotting [34,35]. The transferred proteins were probed with either a p-Tyr antibody (P-Tyr-102, Cell Signaling Technology, Danvers, MA) or a monoclonal FAK antibody (clone 77).

Cell surface binding studies by flow cytometry

HUVEC, MDA-MB-231 or MDA-MB-435 cells were grown to early confluency and starved overnight in serum-free media. The cells were harvested and resuspended in 1 ml of serum-free media (5×10^5 cells/condition) before being incubated with different treatments or controls for 30 min at 37°C. At the end of the incubation period, the cells were pelleted, washed in ice-cold PBS containing 5% fetal bovine serum and either analyzed in a FACSCalibur scanner or, depending on the assay, further incubated at 4°C for 30 min intervals with additional treatments.

All cells were counterstained with propidium iodide to allow gating of necrotic cells. For each reading, 10,000 cells per sample were analyzed.

Integrin binding kinetics by fluorescence polarization (FP)

Differing concentrations of purified soluble functional integrins (i.e., $\alpha v\beta 3$, $\alpha v\beta 5$ or $\alpha 5\beta 1$) were incubated with a constant amount of FITC-labeled VCN or CN using an established protocol [36]. Upon binding to the much larger integrin, the fluorescent tag on either disintegrin tumbles in solution at a slower rate compared to the unbound state resulting in increased levels of polarization. The measured FP value is a weighted average of FP values of the bound and free fluorescent disintegrins and is therefore a direct measure of the bound fraction. The data were analyzed as for standard radioligand binding, and kinetics of binding determined using Scatchard analysis and a non-linear curve fit. The data were generated in a PTI QuantaMaster QM-4SE spectrofluorometer (Photon Technology International, Birmingham, NJ) using the PTI FeliX32 software for data acquisition and Prism v3.02 (GraphPad Software, La Jolla, CA) for data analysis.

Cell viability studies

HUVEC, MDA-MB-231 or MDA-MB-435 cells were plated in serum-free media on Matrigel-coated multi-well glass chamber slides (5×10^4 cells/well) and allowed to adhere. Native CN or VCN were added to the wells at concentrations ranging from 1–1000 nM. Cells receiving no treatment or a known apoptosis inducer (Staurosporine) were used as controls. The cell viability for each condition was assessed after incubation times up to 48 hr both colorimetrically using the Cell Titer 96 AQueous cell viability kit (Promega, Madison, WI) according to the manufacturer's protocol and by TUNEL staining. For TUNEL, the cells were stained using the DeadEnd^{TM} Fluorometric kit (Promega, Madison, WI), and then counterstained with Hoechst 33342. The TUNEL- and Hoechst-stained areas were quantitated digitally by pixel counting on images taken from multiple slides per condition using the 'SimplePCI' imaging software (Hamamatsu Corporation, Sewickley, PA).

Inhibition of cell invasion

The ability of disintegrins to block the invasion of HUVEC, MDA-MB-231 or MDA-MB-435 cells through a reconstituted basement membrane was assessed using the fluorometric QCM^{TM} 24-Well Cell Invasion kit (Millipore, Billerica, MA). The cells were serum-starved overnight, harvested, resuspended in serum-free media (1×10^6 cell/ml) and incubated in the presence of various concentrations (0–1000 nM) of either native CN or VCN for 10 min at 37°C. The assay was done according to the manufacturer's protocol and used HT1080 conditioned media as a chemoattractant. The invasion plates were incubated for up to 48 hr (depending on the cell line) at 37°C in the presence of 5% CO_2. At the end of the incubation period, the invaded cells were detached, lysed and quantitated using the DNA-binding fluorescent dye CyQUANT. The relative fluorescence was measured in a SPECTRAmax GeminiEM fluorescent plate reader (Molecular Devices, Sunnyvale, CA) and the numbers averaged and plotted for each condition.

Inhibition of HUVEC tube formation

'Endothelial Tube Formation' plates precoated with Matrigel (BD Biosciences, Bedford, MA) were used according to the

manufacturer's protocol. HUVEC were seeded in triplicate (3×10^4 cells/well) in the presence of various concentrations (0–1000 nM) of either native CN or VCN and incubated for 16 hr at 37°C in the presence of 5%CO_2. The tube formation inhibitor Suramin was used as a positive control. At the end of incubation period, cells were stained with Calcein AM and imaged by confocal microscopy (LSM 510 Confocal/Titanium Sapphire Laser). The total length of tubes for each condition was quantitated in multiple fields using the Zeiss LSM Image Browser (Carl Zeiss MicroImaging GmbH, Munich, Germany) and averaged from at least three independent experiments.

Disruption of actin cytoskeleton organization

HUVEC grown in complete media were seeded in triplicate in 8-well chamber slides coated with complete Matrigel (4×10^4 cells/well). Each well received different concentrations of various treatments {including FITC-CN, FITC-VCN, the cyclic RGD peptide cyclo(Arg-Gly-Asp-DPhe-Val) (abbreviated cRGDfV), the murine 7E3 or LM609 monoclonal antibodies}. The actin modifier Cytochalasin D (CytoD) was used as a positive control. The cells were incubated with the treatments for 3 hr at 37°C in the presence of 5%CO_2. At the end of the incubation period, the cells were washed, incubated with secondary treatments (depending on the condition), fixed in 4% formaldehyde, permeabilized in 0.1% Triton X-100 in PBS, and then stained with Rhodamine-Phalloidin and counter-stained with Hoechst 33342 before being imaged by confocal microscopy (LSM 510 Confocal/Titanium Sapphire Laser).

In vitro Matrigel-embedded HUVEC apoptosis studies

HUVEC seeded in serum-free media in 8-well chamber slides coated with complete Matrigel (4×10^4 cells/well) were allowed to adhere before being sandwiched with another layer of Matrigel that was uniformly pipetted on top of the adherent cells. The second Matrigel layer was allowed to settle before various treatments were added and chambers incubated at 37°C in the presence of 5%CO_2 for approximately 16 hr. At the end of the incubation period, the cells were fixed in 4% formaldehyde, permeabilized in 0.2% Triton X-100 in PBS, TUNEL stained using the DeadEnd^{TM} Fluorometric kit (Promega, Madison, WI), and counterstained with Rhodamine-Phalloidin and Hoechst 33342. The % cell death was quantitated in random fields taken at ×250 magnification using the formula 'number of TUNEL$^+$ nuclei/total number of nuclei x100' for each treatment group. The TUNEL- and Hoechst-stained areas were quantitated digitally by pixel counting on images taken in random fields from multiple slides per condition using the 'SimplePCI' imaging software (Hamamatsu Corporation, Sewickley, PA).

Liposomal encapsulation of VCN

This procedure was carried out by Molecular Express, Inc (Los Angeles, CA) a company specializing in liposomal encapsulation of therapeutic proteins and other drugs. Briefly, stock solutions of phospholipids and cholesterol were prepared by dissolving each lipid in a chloroform/methanol solvent mixture. Thin lipid films were created by pipetting aliquots of the lipid solutions into round bottom glass tubes followed by solvent evaporation at 65°C under a stream of nitrogen gas with the lipids and cholesterol further dried under vacuum for 48 hours. Dried VCN was then dissolved in a hydration buffer (10 mM sodium phosphate and 262 mM sucrose, pH 7.2) and added to the dried lipids. After 5 min incubation at 50°C, liposomal VCN (LVCN) particles were generated by either probe sonication at 10% power for 3 to 5 min in a Branson Probe Sonifier or homogenized in a

microfluidizer (M110L; Microfluidics, Newton, MA). The homogenized material was processed between 10,000 and 18,000 psi while maintaining an elevated temperature (45–65°C). Samples from each batch were taken during the process and the size distribution of LVCN was determined with an Ultrafine Particle Analyzer (UPA150; Microtrac, North Largo, FL). After processing, the unencapsulated VCN in each batch was removed by ultrafiltration using an Amicon UF membrane of 100,000 MWCO and the LVCN was further sterilized by filtration through a 0.2 µM PVDF filter.

In vivo efficacy studies

MDA-MB-435 cells (5×10^5 per inoculum) or MDA-MB-231 cells (2×10^6 per inoculum) were harvested and resuspended in complete Matrigel and injected in the mammary fat pads of nude mice as previously described [22]. The tumors were allowed to grow for 2 weeks or until they became palpable before treatment was initiated. VCN was administered either encapsulated in different liposomal formulations (at the dose-equivalent of 100 µg of dry VCN per injection) or non-encapsulated, as an aqueous solution (100 µg VCN). All VCN administrations were made intravenously (via tail vein) twice a week for the duration of each study. Avastin was administered intravenously (via tail vein) at the dose of 400 µg per injection (approx. 20 µg/gr.) once a week for the duration of the MDA-MB-231 study. Tumor diameters were measured weekly with a caliper in a blind fashion and the tumor volumes calculated using the formula [length (mm) × width $(mm)^2]/2$, where the width and the length were the shortest and longest diameters, respectively [37]. The average tumor volume for each study group was plotted as a function of time and type of treatment during the entire course of each study.

Tumor microvessel quantitation

Acetone-fixed 5 µm-thick cryostat sections cut from MDA-MB-231 tumors were air dried for 30 min before being blocked in 5% BSA in PBS and incubated overnight with a rat polyclonal CD31 antibody (clone MEC13.3) at room temperature. The working dilution for this antibody was 1/100 in 5%BSA in PBS. After washing off the unbound CD31 antibody, a biotinylated goat anti-rat antibody (1/150 in 5%BSA in PBS) was applied for 45 min at room temperature followed by the Avidin Binding Complex (Vector Laboratories, Burlingame, CA) for another 30 min and the addition of 3-amino-9-ethylcarbazole chromogen (a peroxidase substrate). The slides were counterstained with hematoxylin. To quantitate the CD31-stained microvessels, the slides were subjected to 'random field' analysis [38,39]. Random field images were captured at ×200 (10 images were analyzed per tumor and 4 random tumors were analyzed from each animal group). The CD31-positive areas were quantitated for each random field as % of total stained area by pixel counting using the 'SimplePCI' imaging software (Hamamatsu Corporation, Sewickley, PA). To eliminate bias, the random field image capture and the subsequent processing and analysis were carried out in a blind fashion.

TUNEL and Ki-67 staining of tumor sections

For tumor apoptosis, the DeadEnd[TM] Fluorometric TUNEL assay kit (Promega, Madison, WI) was used according to the manufacturer's protocol. Importantly, we found that the TUNEL staining was optimal only when the cryostat sections were fixed and permeabilized in a cold ethanol/acetic acid (2/1) bath for 5 min at −20°C. Any other fixation and/or permeabilization technique yielded suboptimal staining results. However, this above approach is not compatible with CD31 antibody staining, which works best on either not-fixed or acetone-fixed tissues. After

TUNEL staining, the nuclei were counterstained with Hoechst 33342. The nuclei from apoptosis 'hotspot' areas were digitally counted (object counting) using the SimplePCI imaging software on random images (at least 10 images per tumor from multiple tumors per group) captured at ×250. The % of cell death was plotted using the formula 'number of TUNEL$^+$ nuclei/total number of nuclei x100' for each treatment group. For Ki-67 staining, a primary rabbit antibody (clone H-300) and a biotinylated anti-rabbit secondary were used. The sections were acetone-fixed, incubated with the antibodies and prepared for immunoperoxidase staining as described above for CD31 staining. The Ki-67$^+$ nuclei were quantitated by pixel counting as % of total stained area as described above for CD31.

Statistical analysis

Statistical significance was analyzed in Prism v.3.2 (GraphPad Software, La Jolla, CA) by unpaired t-test followed by F-test to compare variances. The tumor volume distribution and immunohistochemistry data were assessed by analysis of variance (ANOVA) with a significant overall F-test followed by Dunnett's multiple comparison tests of treatment groups relative to control. Two-tailed $P < 0.05$ were considered significant.

Results

The recombinant production of VCN as an active soluble protein

The expression of recombinant disintegrins was done in Origami B (DE3), a strain uniquely designed to address the shortcomings of disulfide-rich recombinant protein production in wild-type E. coli. This strain is engineered to produce defective forms of two redox enzymes that are critically involved in controlling the major reductive pathways in this bacterium: thioredoxin reductase (TrxB) and glutathione reductase (Gor). In the absence of functional cytoplasmic TrxB and Gor enzymes, the redox equilibrium in this E. coli strain is shifted towards oxidation, a redox state that greatly promotes disulfide bond formation in heterologous proteins expressed in this compartment [40].

The Origami B strain is better suited for recombinant protein expression than most other commercially available E. coli strains since, in addition to providing a favorable environment for disulfide bond formation, by being a derivative of the BL21 strain it is also deficient in ompT and lon proteases. Moreover, this strain is lac permease (lacY1) deficient, a feature that enables a uniform entry of IPTG (a lactose derivative commonly employed to trigger the expression of recombinant proteins engineered downstream of a lac promoter) into cells with a more homogenous level of induction and, consequently, adjustable levels of protein expression.

The pET32a expression vector and the T7 system are designed for robust expression of heterologous proteins fused to the 109 amino acid bacterial thioredoxin A (TrxA) in DE3 lysogens. In wild-type E. coli, TrxA normally functions as a major cytoplasmic reductase under tight regulatory control. However, in the Origami strain, the oxidative redox state perpetuated by defective TrxB and Gor enzymes 'tricks' this bacterium into producing compensatory higher amounts of TrxA reductase in an attempt to restore the wild-type redox equilibrium which in turn drives the robust expression of any recombinant protein genetically fused to TrxA. Another advantage of expressing heterologous proteins fused to TrxA is the high solubility of this bacterial protein, the result of which is that TrxA internally chaperones the recombinant protein fused to it thus keeping it in solution and allowing for higher levels of foreign protein accumulation in the cytoplasm [40].

To explore the recombinant production of disintegrins in Origami B (DE3) we generated two constructs: one based on the exact sequence of native CN (referred to as rCN) and a chimeric construct, previously designated as rCN+ [30], but now referred to as vicrostatin (VCN). The VCN construct was designed by replacing the C-terminal tail of native CN with the tail of another native disintegrin, echistatin, a short length viperid disintegrin. The sequence alignment of CN, rCN, VCN and echistatin (also known as echistatin alpha) [20] are shown in **Fig. 1**. The rationale for the VCN design was based on the finding that the C-termini of snake venom disintegrins are important structural elements essential for full disintegrin activity, and have been shown to participate in the ligation of the receptor together with the disintegrin loop [41]. In addition, a previous report [42] had demonstrated that the swapping of C-terminal tails between two native disintegrins may actually lead to the generation of novel chimeric molecules capable of recognizing specific integrins with altered binding affinities. Our expectation for VCN was that, by carrying a modified C-terminus, it would display an improved affinity compared to the native molecule for integrin α5β1, a major player in angiogenesis. The participation of multiple regions in disintegrins in receptor binding emphasizes the complexity of these bigger polypeptides compared to small cyclic RGD peptides or RGD-peptidomimetics. Moreover, these structural differences are also expected to be reflected at the functional level, and in this report we provide the evidence that this is the case.

By employing the recombinant system described above, two fusion proteins (Trx-rCN and Trx-VCN) were successfully expressed in the cytoplasm of Origami B (DE3) (see **Fig. 2A** for a comparison of Trx-VCN expression levels in different expression hosts; the data on Trx-rCN is not shown). Although the expression of Trx-VCN was robust in Origami B (DE3), by growing these transformants in a modified media recipe we have been able to boost the recombinant production level of VCN by at least one order of magnitude to a final expression yield of approximately 200 mg of active purified disintegrin per liter of bacterial culture.

A unique tobacco etch virus (TEV) protease cleavage site was engineered upstream of both disintegrin constructs in order to facilitate their subsequent cleavage from TrxA. TEV is a highly selective protease that recognizes with very high specificity the canonical Glu-Asn-Leu-Tyr-Phe-Gln-Gly amino acid sequence [43] therefore leaving the target recombinant proteins intact. This high specificity makes TEV an ideal molecular tool for processing recombinant proteins expressed as fusions. Moreover, TEV is a cysteine protease that relies on reducing equivalents (e.g., dithiothreitol) in order to be regenerated and act continuously. The addition of reducing equivalents during the purification process, however, could be detrimental to the integrity of any expressed recombinant proteins that rely on multiple disulfide bonds for activity. However, we found that the addition of exogenous reducing equivalents to Origami B lysates enriched in Trx-VCN or Trx-rCN was in fact not necessary for efficient proteolysis, since the bacterial lysates provided enough reducing equivalents for TEV regeneration. Therefore, the mere addition of a few units of recombinant TEV was sufficient to optimally process large quantities of expressed fusions (**Fig. 2B**). The released recombinant disintegrins were further processed and purified by reverse phase HPLC using a protocol originally designed for native disintegrins (see Materials and Methods).

Initial evaluation of recombinant disintegrins for activity

The two purified recombinant molecules were initially tested for activity against platelets. Presumably, the main function of snake venom disintegrins in nature is to bind with very high affinity to the activated platelet αIIbβ3 integrin, thus efficiently inhibiting [20] the last step in the blood clotting, platelet aggregation, a process mediated by platelet integrin αIIbβ3. To our surprise, the platelet aggregation assay showed that only chimeric VCN retained full activity against activated αIIbβ3 integrin (with a calculated IC$_{50}$ of ~60 nM), whereas the rCN construct showed no activity in the nanomolar range characteristic of snake venom disintegrins (**Fig. 2C**). It appears that the latter construct, although soluble, had failed to fold correctly in the region where the binding site of the molecule resides (i.e., the 11-amino acid disintegrin loop).

Mass spectrometry analysis and sequencing of VCN

Interestingly, the MS analysis (MALDI-TOF and ESI) demonstrated that, unlike native CN, VCN is a monomer (MW = 7146.0). The sequence was subsequently confirmed by tryptic MS sequencing. Based on these data, we speculated that although VCN folded correctly in the C-terminal half of the molecule, hence being a functional disintegrin, it may have adopted a non-native cysteine pairing in the N-terminal half of the molecule compared to CN [24] which compromised its dimerization (see **Fig. 1** for disulfide bond configuration of native CN).
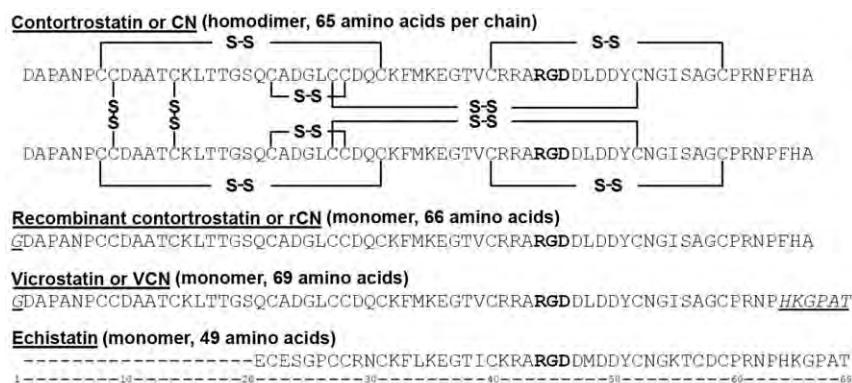

Figure 1. Comparison between contortrostatin (CN), recombinant contortrostatin (rCN), vicrostatin (VCN), and echistatin sequences. Mass spectrometry and crystallographic data have confirmed that CN is a dimer with two identical chains oriented in an antiparallel fashion and held together by two interchain disulfide bonds. Unlike native CN, mass spectrometry showed that both rCN and VCN are monomers. In the above sequences, the Arg-Gly-Asp tripeptide motif is depicted in bold whereas the non-native amino acids in rCN and VCN are both italicized and underlined.
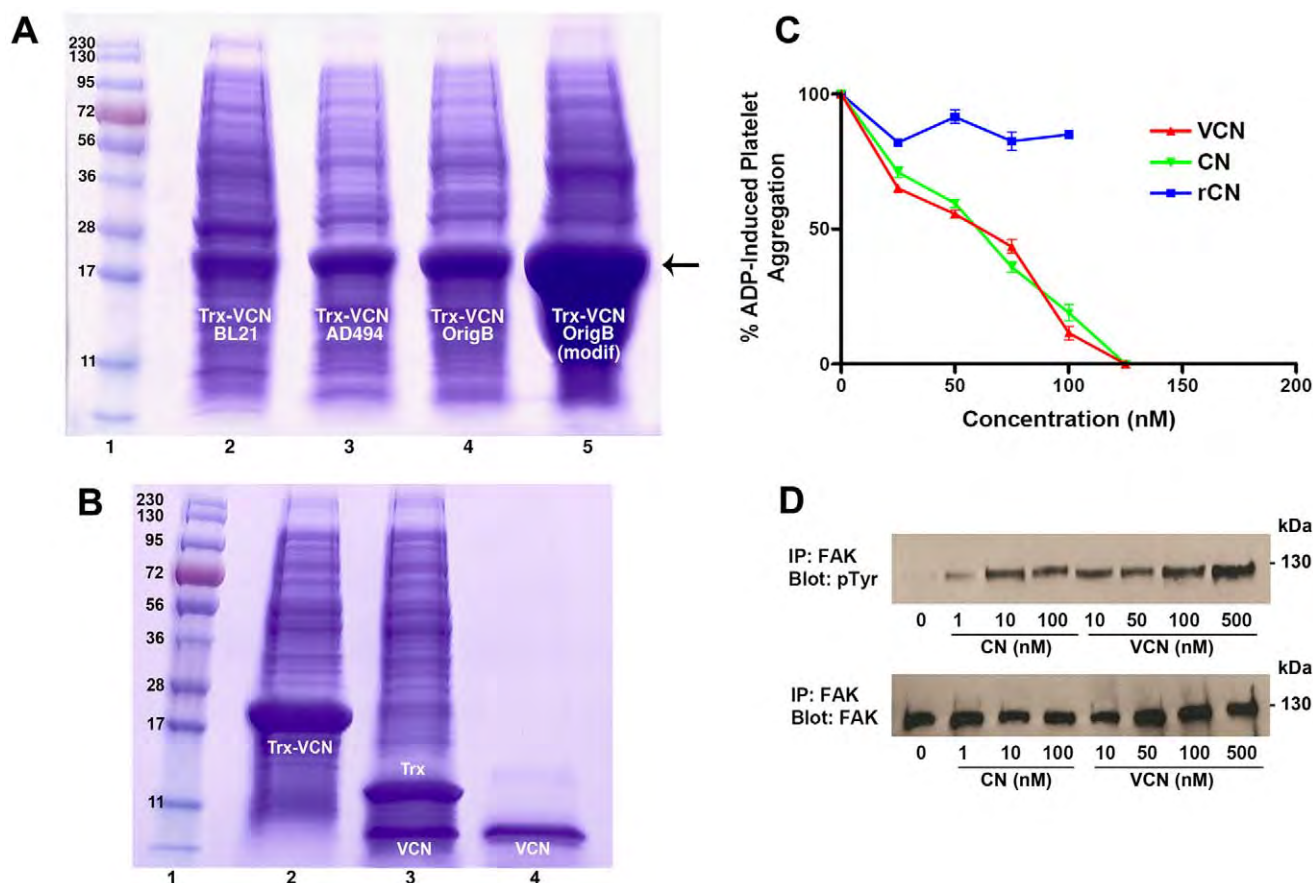
doi:10.1371/journal.pone.0010929.g001

Figure 2. The expression, purification and initial characterization of VCN as an active disintegrin. Panel A – The production of Trx-VCN was assessed in different *E. coli* strains that were transformed, grown, induced, and processed under identical conditions. The same amount (5 μl) of cell lysates from each induced strain was loaded on a precast gel and Coomassie stained. Unlike the BL21 (DE3) strain, the lysates from both AD494 (DE3) and Origami B (DE3) strains generate a unique and consistent Trx-VCN band (shown by the arrow). By employing a modified media recipe, the Origami B (DE3) Trx-VCN transformants achieve higher cell densities at the end of the induction time, generating up to 200 mg of soluble VCN per L of bacterial culture after purification. **Panel B –** Coomassie stained gel showing the migration of Trx-VCN before and after TEV proteolysis (lanes 2 and 3, respectively) versus C18 reverse phase-HPLC purified VCN (lane 4). **Panel C –** VCN and native CN exhibit an almost identical dose-dependent inhibitory effect against ADP-induced platelet aggregation when incubated with human platelet-rich plasma (with a calculated IC_{50} of ~60 nM). In contrast, the rCN construct, which is also expressed as a soluble polypeptide in Origami B (DE3), shows no inhibitory activity. **Panel D –** The agonistic activity of VCN (FAK activation) was assessed in serum-starved non-migratory MDA-MB-435 cells kept in suspension and exposed to increasing concentrations of disintegrins for 30 min. Similar to dimeric CN, VCN is also shown to engage integrins agonistically (outside-in signaling).
doi:10.1371/journal.pone.0010929.g002

Focal adhesion kinase (FAK) phosphorylation studies

Native CN was previously shown to bind to integrins agonistically [34,44], while acting as a potent soluble ECM-mimetic [35]. Interestingly, depending of the cellular context (adherent vs. suspended cells) CN was previously shown to alter the phosphorylation status of FAK (i.e., one of the earliest signaling events downstream of integrin engagement) by either activating (in serum-starved cancer cells kept in suspension in serum-free media and receiving no external input via integrins other than the disintegrin treatment) or deactivating (in adherent cells plated on various matrices) this non-receptor kinase [35]. In the present study we wanted to understand whether VCN: 1. retains the ability of native CN to signal via integrins agonistically in serum-starved non-migratory suspended cells receiving no external input other than disintegrins, and 2. has the same potency as CN by evoking this downstream signal in a dose-dependent manner. Our data suggest that indeed VCN also engages integrins agonistically (**Fig. 2D**), with a similar potency and in a dose-dependent manner comparable to native CN. These new data

imply that the previously described signaling effects of CN [44] observed downstream of integrins in suspended cells were not in fact owing to CN's dimeric structure (i.e., signaling via receptor crosslinking), but may have rather been the result of an intrinsic property of the disintegrin fold, common to all disintegrins regardless of their tertiary structure.

Cell surface binding analysis by flow cytometry

The ability of VCN to mimic the binding behavior of native CN against different cell lines, as well as in the presence of EDTA or specific competitors, was tested by flow cytometry (**Fig. 3**). Our results show that FITC-labeled VCN has a similar binding profile to CN against HUVEC, MDA-MB-231 and MDA-MB-435 cells. These cells were chosen because they all express varying amounts of the RGD-dependent integrins αvβ3, αvβ5 and α5β1, the targets of CN, VCN and other ligands used in the study. We tested these cells by flow cytometry for cell surface integrin expression and found that there was a little difference in the relative amounts of integrins αvβ5 and α5β1 expressed by these cells, but a significant
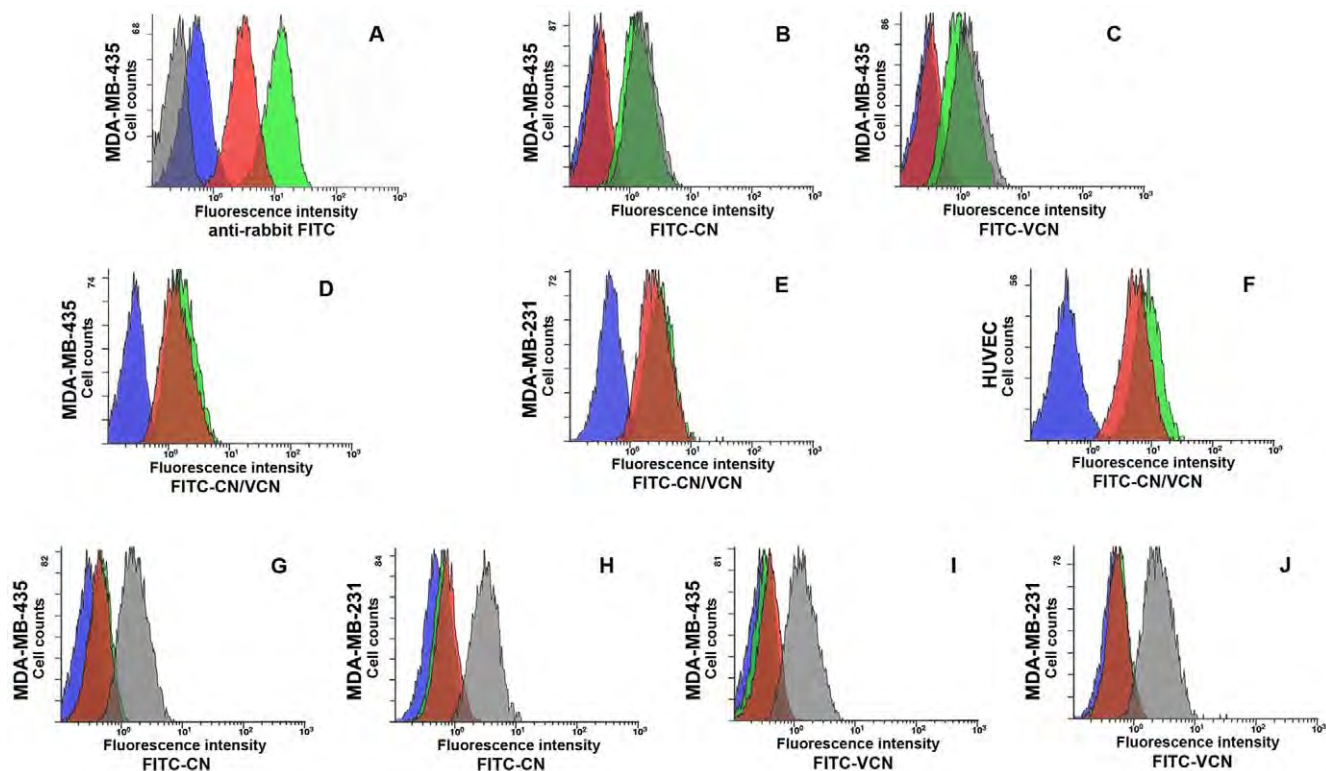
Figure 3. Binding analysis of FITC-labeled disintegrins by flow cytometry. Panel A – Both CN and VCN are detected at cell surface when probed with CN polyclonal antiserum. MDA-MB-435 cells were incubated with either VCN (red) or CN (green) followed by CN rabbit polyclonal antiserum and an anti-rabbit FITC-labeled secondary antibody. The controls included cells incubated with either anti-rabbit FITC-labeled secondary only (grey) or CN antiserum followed by the FITC-labeled secondary (blue). **Panels B, C –** FITC-CN (panel B) or FITC-VCN (panel C) fail to bind to cells prewashed in EDTA media, but once bound in regular media the subsequent addition of EDTA does not displace them from integrins. MDA-MB-435 cells were either incubated with FITC-labeled disintegrins only (grey) or with labeled disintegrins and then washed and resuspended in 3 mM EDTA media (green) or preincubated in 3 mM EDTA and then washed and exposed to labeled disintegrins (red) or just probed with an FITC-labeled irrelevant antibody control (blue). **Panels D, E and F –** Labeled disintegrins bind in a similar manner to cells with different integrin profiles. MDA-MB-435, MDA-MB-231 or HUVEC were either incubated with FITC-CN (green) or FITC-VCN (red) or probed with an FITC-labeled irrelevant antibody control (blue). **Panels G, H, I and J –** FITC-labeled disintegrins fail to bind to cells pretreated with either unlabeled disintegrins or an antibody competitor. MDA-MB-435 or MDA-MB-231 cells (panels G and H) were either incubated with FITC-CN only (grey) or an FITC-labeled irrelevant antibody control only (blue) or preincubated with unlabeled VCN (green) or 7E3 (red) and then probed with FITC-CN. Similarly, MDA-MB-435 or MDA-MB-231 cells (panels I and J) were either incubated with FITC-VCN only (grey) or an FITC-labeled irrelevant antibody control only (blue) or preincubated with unlabeled CN (green) or 7E3 (red) and then probed with FITC-VCN. The data are representative of four independent experiments.
doi:10.1371/journal.pone.0010929.g003

difference with respect to integrin $\alpha v\beta 3$ expression with MDA-MB-435 expressing much higher amounts of this integrin compared to the other two cell lines, and MDA-MB-231 expressing the least amount. We also found that cell surface-bound VCN is recognized by rabbit polyclonal CN antiserum and bound VCN has the ability to block the binding of FITC-labeled CN, while a specific competitor, the 7E3 antibody raised against $\beta 3$ integrin, is shown to block the binding of both FITC-labeled CN and VCN. Interestingly, regarding the latter observation, the converse appears to be also true for bound CN alone, Trx-VCN alone, or VCN plus polyclonal CN antiserum, since all these prevented the binding of 7E3 to the cell surface. However, VCN alone did not (data not shown), which led us to the conclusion that 7E3's binding site on $\beta 3$ integrin [45] must map very closely to the ligand-recognition region for both disintegrins. As reported by Artoni et al. [45] 7E3's binding site was mapped between the C177-C184 loop and W129 residue in human $\beta 3$ integrin subunit, in a region that is spatially close to the $\beta 3$ subunit MIDAS (metal-ion dependent binding site), where the Asp residue of the RGD motif is also known to bind. Similar flow cytometry results were observed when the cyclic RGD peptide, cyclo(Arg-Gly-Asp-DPhe-

Val) was used as a competitor instead of 7E3. When these cells were pre-incubated with micromolar concentrations of this cyclic RGD peptide before being exposed to fluorescently-labeled disintegrins, the cyclic RGD treatment also prevented the binding of both disintegrins. Unlike 7E3, the flow cytometry analysis showed that the $\alpha v\beta 3$-specific monoclonal antibody LM609 [46] does not compete for the same binding region with either CN or VCN (data not shown). Finally, since the engagement of integrins by disintegrins was previously shown to be a metal-ion depended process [41], we asked whether a metal chelator such as EDTA will affect the binding of both CN and VCN. As expected, both CN and VCN did not bind to cells that were washed in 3 mM EDTA before being exposed to either disintegrin. However, once CN or VCN bound to the cell surface, the subsequent addition of EDTA does not appear to displace either disintegrin from their receptors (**Fig. 3**).

Integrin binding kinetics by fluorescence polarization

To further determine the specific binding affinities of both native CN and VCN to purified ($\alpha v\beta 3$ and $\alpha v\beta 5$) or recombinant ($\alpha 5\beta 1$) functional integrins, we measured these interactions in

solution by fluorescence polarization. From this set of experiments, the dissociation constants for both native CN and VCN (**Table 1**) were deduced. These data showed that both disintegrins exhibit nearly identical affinities for αvβ3 and a similar affinity for αvβ5. The prediction that the sequence modification of VCN would alter its affinity for α5β1 compared to the native molecule was confirmed by this assay. The results demonstrated that there is at least an order of magnitude difference in these molecules' Kd values to α5β1 with VCN showing a higher binding affinity for this receptor (the average Kd values for integrin α5β1 were 15.2 nM for VCN, and 191.3 nM for native CN).

Cell viability studies with adherent cells

To understand how VCN affects cell viability, we tested a range of CN and VCN concentrations (1–1000 nM) on HUVEC, MDA-MB-231 and MDA-MB-435 cells seeded on top of Matrigel (see Materials and methods) and compared the results to either untreated cells or cells exposed to Staurosporine, a known apoptosis inducer. Neither disintegrin showed any significant impact on cell viability regardless of the length of the incubation time (up to 48 hr) these cells were exposed to disintegrins. The cell viability was monitored using a MTS-based colorimetric assay and further confirmed by TUNEL staining (**Fig. 4**). In this later assay, at the end of the incubation period, the cells from all conditions were fixed in 4% formaldehyde, permeabilized in 0.2% Triton X-100, FITC-TUNEL stained, and then counterstained with Hoechst 33342. The amount of cell death was plotted for each condition by counting the apoptosis events in random fields from multiple independent experiments using the formula 'number of apoptotic nuclei/total number of nuclei x 100'. Irrespective of the cells tested, neither CN nor VCN caused cell death under these conditions.

Inhibition of cell invasion through a reconstituted cell membrane

The anti-invasive properties of VCN were tested *in vitro* using a modified Boyden chamber assay where serum-starved HUVEC, MDA-MB-231 or MDA-MB-435 cells were preincubated with various concentrations of disintegrins (1–1000 nM) for 10 min before being seeded into Matrigel-coated (ECMatrix™, Millipore) porous inserts (pore size, 8 μm) and allowed to invade against a chemoattractant gradient (HT1080 human fibrosarcoma conditioned media) for up to 48 hr (depending on the cell line). At the end of the incubation time, the cells that invaded into the lower chamber were detached, lysed, stained with CyQuant and quantitated in a fluorescent plate reader. The fungal metabolite Cytochalasin D, a potent inhibitor of actin polymerization, was

Table 1. Disintegrin-integrin biding kinetics by fluorescence polarization.

Disintegrin	Integrin Kd (+/−SD)		
	αvβ3	α5β1	αvβ5
CN	6.6 nM (0.8)	191.3 nM (65.2)	19.5 nM (5.7)
VCN	7.4 nM (0.4)	15.2 nM (4.2)	41.2 nM (12.3)

The binding kinetics were calculated from the fluorescence anisotropy data generated by the steady state binding of FITC-labeled disintegrins to either purified (αvβ3 and αvβ5) or recombinant (α5β1) functional human integrins. The dissociation constants for interactions of either CN or VCN with soluble integrins were determined by Scatchard analysis using a non-linear curve fit.
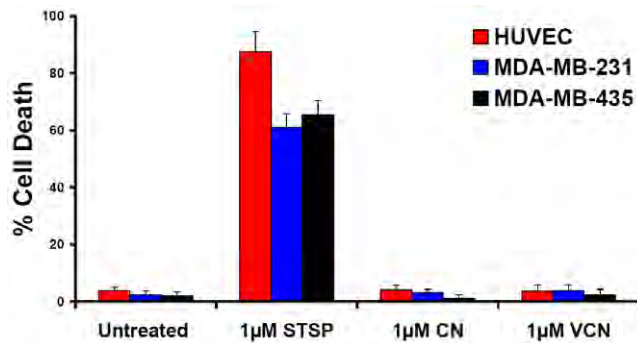doi:10.1371/journal.pone.0010929.t001

used as a positive control at a concentration of 200 nM. Similar to native CN, VCN is shown to significantly inhibit HUVEC, MDA-MB-231 or MDA-MB-435 cell invasion in a dose-dependent manner (**Fig. 5**).

Inhibition of HUVEC tube formation

The ability of VCN to inhibit HUVEC tubulogenesis was tested *in vitro* in an assay where HUVEC were plated on 'Endothelial Cell Tube Formation' plates (BD Biosciences) in the presence of various concentrations of either CN or VCN (1–1000 nM) and allowed to form tubes after incubation for 12–16 hr at 37°C in the presence of 5%CO$_2$. In this experimental setting, Suramin, a known tube formation inhibitor, was used as a positive control at two different concentrations (50 and 100 μM). At the end of incubation period, the cells were stained with Calcein AM and imaged by confocal microscopy. As previously reported with native CN [47], VCN was also shown to potently inhibit HUVEC tube formation in a dose-dependent manner (**Fig. 6i**). In this assay, the tubes in each field were measured by three individuals in a blinded experiment and the total tube length averaged and plotted for each data set (**Fig. 6ii**).

Disruption of HUVEC actin cytoskeleton organization

To assess the effect of VCN on cell morphology and actin cytoskeleton organization, HUVEC were allowed to adhere to complete Matrigel before being exposed to various treatments. Our results show that unlike other integrin ligands, including a small cyclic RGD peptide, and two integrin-binding antibodies (7E3 and LM609), VCN potently collapses the actin cytoskeleton of HUVEC in the low nanomolar range (**Fig. 7**). However, unlike VCN which exerts its maximal effects on the actin cytoskeleton of HUVEC in the low nanomolar range (10–100 nM), the cyclic RGD peptide used in the study appears to have some minor effects on the actin cytoskeleton of these cells (i.e., partial disassembly of stress fibers) only at a much higher concentration (10 μM). Moreover, the effect observed with VCN can be only partially prevented if the cells are preincubated with either the 7E3 antibody or the cyclic RGD peptide cRGDfV before being exposed to the recombinant disintegrin (data not shown). It is noteworthy that VCN does not detach HUVEC plated on Matrigel. Complete Matrigel is a tumorigenic matrix that was shown to be very similar in ECM composition to basement membranes (it is rich in collagen IV and laminins) and a number of collagen- and laminin-binding integrins (e.g., α1β1, α2β1, α3β1, α6β1, and α6β4) are employed by various cells to attach to Matrigel in a RGD-independent manner. On the other hand, VCN is an RGD-displaying polypeptide that was shown to bind to at least 4 RGD-recognizing integrins (i.e., αIIbβ3, αvβ3, αvβ5, and α5β1) but may, although not investigated yet, also bind to other RGD-dependent integrins. For instance, there are 8 human integrin members that have been described to recognize the RGD motif: all αv integrins (αvβ1, αvβ3, αvβ5, αvβ6, and αvβ8), αIIbβ3, α5β1, and α8β1. Because HUVEC do express collagen- and laminin-binding integrins that enable these cells to attach to Matrigel in a RGD-independent manner, it is not surprising that VCN does not detach HUVEC from Matrigel when these cells are exposed to the agent. However, the massive actin cytoskeleton reorganization induced by VCN in Matrigel-plated HUVEC raises the possibility that some of these effects might be relayed agonistically via one or a combination of integrins that VCN is know to bind to (i.e., transdominant integrin inhibition via either αvβ3, αvβ5, α5β1, or a combination of these receptors), integrins that are also expressed by these cells. Nonetheless, the observed signaling events induced by VCN in Matrigel-plated HUVEC

Figure 4. VCN does not affect the viability of cells plated on top of Matrigel. HUVEC, MDA-MB-231 or MDA-MB-435 cells were seeded in serum-free media in multiwell chamber slides on complete Matrigel and allowed to adhere for 1 hr. Once adherent, the cells were incubated for up to 48 hr with either CN or VCN up to a maximum concentration of 1 μM. Untreated cells or cells exposed to the apoptosis inducer Staurosporine (STSP) at a concentration of 1 μM were used as controls. The cells were fixed, TUNEL-stained and counterstained with Hoechst 33342. The amount of cell death was plotted for each condition by digitally counting the apoptosis events in random fields from images taken from multiple experiments for each condition.
doi:10.1371/journal.pone.0010929.g004

Induction of apoptosis in tubulogenic HUVEC embedded in Matrigel

As stated above, VCN does not affect HUVEC viability if adherent cells plated on top of Matrigel are exposed to this agent, but it has significant anti-proliferative and anti-migratory effects (inhibition of tube formation) on these cells. Interestingly, when HUVEC are sandwiched between two layers of complete Matrigel, a significant apoptotic effect is also observed in the presence of VCN, but not with other integrin ligands (**Fig. 8i**). Surprisingly, a similar effect was also seen with Avastin in this setting, though less pronounced than with VCN. It is noteworthy that the cells sandwiched between two Matrigel layers were observed to migrate and form tubes much faster than HUVEC plated on top of Matrigel. The faster migrating cells sandwiched in Matrigel may rely more on the integrity of their focal adhesions coupled with a more dynamic actin cytoskeleton not only for migration, but also for survival. Thus, the profound effect induced by VCN on the actin cytoskeleton of these cells may explain the discrepancy seen in cell survival between the two experimental settings. It is also important to note that, unlike the two integrin binding antibodies, the cRGDfV peptide did alter the morphology
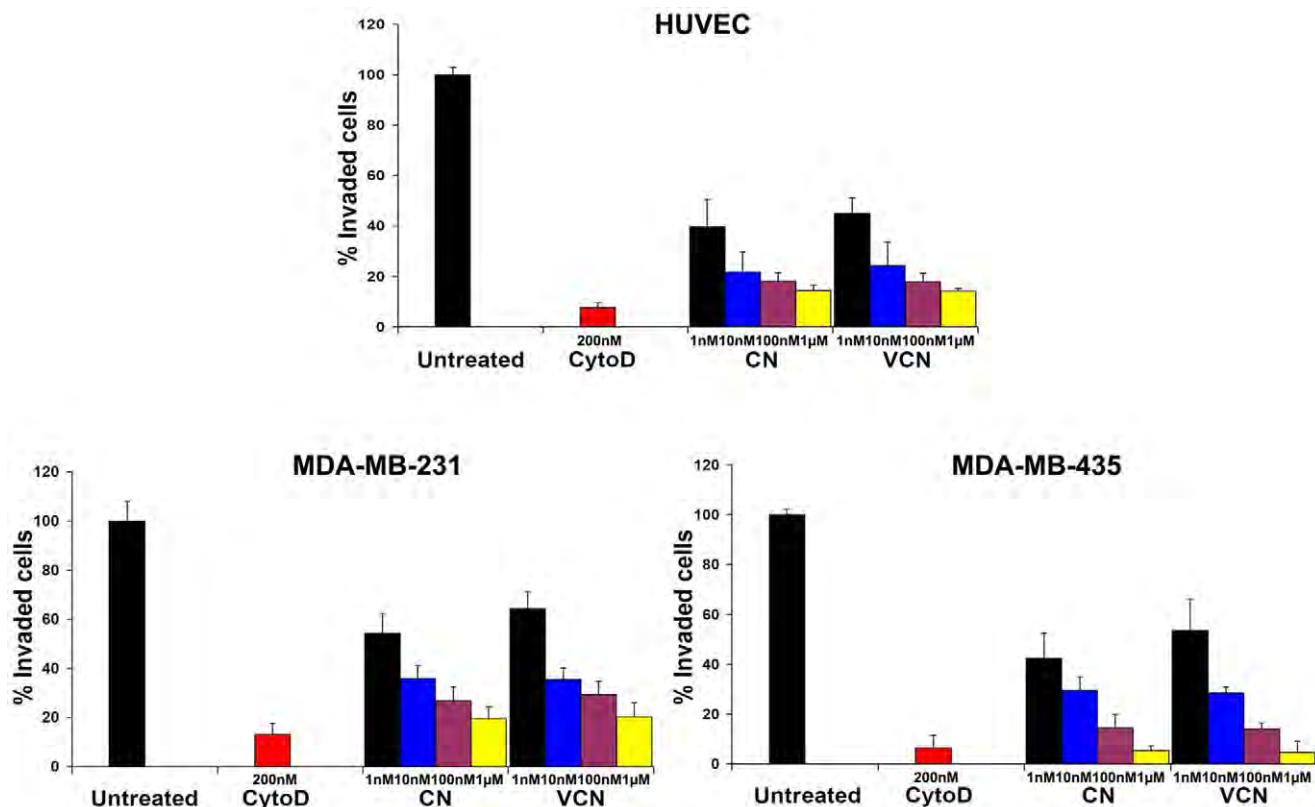

Figure 5. VCN inhibits cell invasion through a reconstituted basement membrane in a dose-dependent manner. The anti-invasive properties of VCN were tested in a modified Boyden chamber assay where serum-starved HUVEC, MDA-MB-231 or MDA-MB-435 cells were preincubated with various concentrations of disintegrins (1–1000 nM) for 10 min before being seeded into Matrigel-coated (ECMatrix™, Millipore) porous inserts (pore size, 8 μm) and allowed to invade against a chemoattractant gradient (HT1080 human fibrosarcoma conditioned media) for up to 48 hr. The fungal metabolite Cytochalasin D, a potent inhibitor of actin polymerization, was used as a positive control at a concentration of 200 nM. The above data were averaged from three independent experiments for each cell line tested.
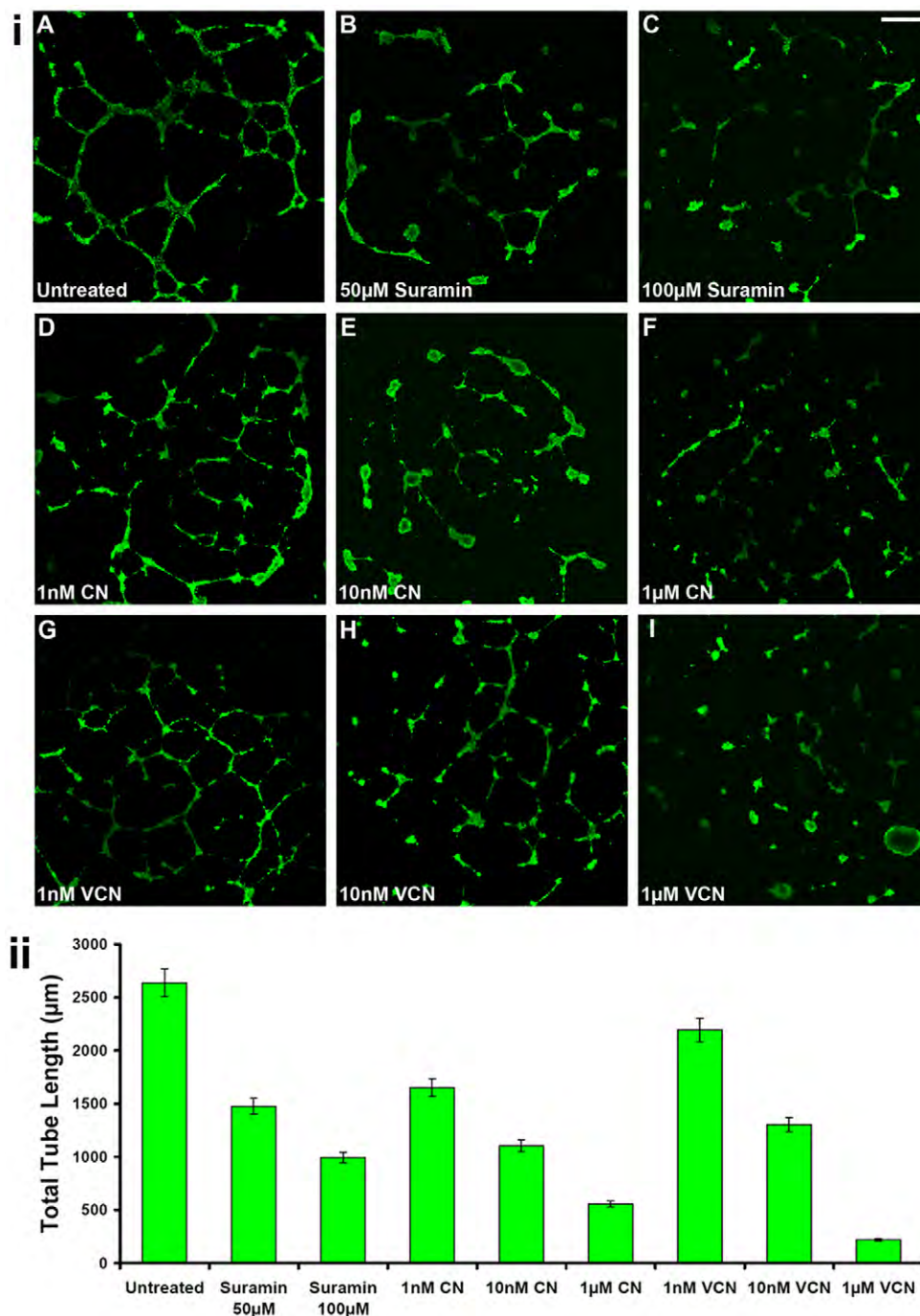doi:10.1371/journal.pone.0010929.g005

Figure 6. VCN inhibits HUVEC tube formation (tubulogenesis). (i) HUVEC were plated on 'Endothelial Cell Tube Formation' plates (BD Biosciences) in the presence of various concentrations of either CN or VCN (1–1000 nM) and allowed to form tubes after incubation for 12–16 hr at 37°C in the presence of 5%CO_2. Suramin, a known tube formation inhibitor, was used as a positive control at two different concentrations (50 and 100 µM). At the end of the incubation period, cells were stained with Calcein AM and imaged by confocal microscopy (magnification, ×25). Representative figures from three independent experiments are shown above (scale bar, 200 µm). **(ii)** The degree of tubulogenesis was assessed by capturing multiple photomicrographs for all conditions on which the total length of the tubes was measured and computed in multiple fields using the Zeiss LSM Image Browser (Carl Zeiss MicroImaging GmbH) and then averaged to form each data point. The data presented above was assembled from three independent experiments.
doi:10.1371/journal.pone.0010929.g006

of the tubes formed by HUVEC when sandwiched in Matrigel, although to a lesser extend than VCN and with no impact on cell viability. The amount of cell death was quantitated digitally (the 'SimplePCI' software) for each condition by counting the apoptosis events in multiple random fields from images taken from multiple experiments using the formula 'number of apoptotic nuclei/total number of nuclei x 100'. The quantitation data (**Fig. 8ii**) was generated from four independent experiments.
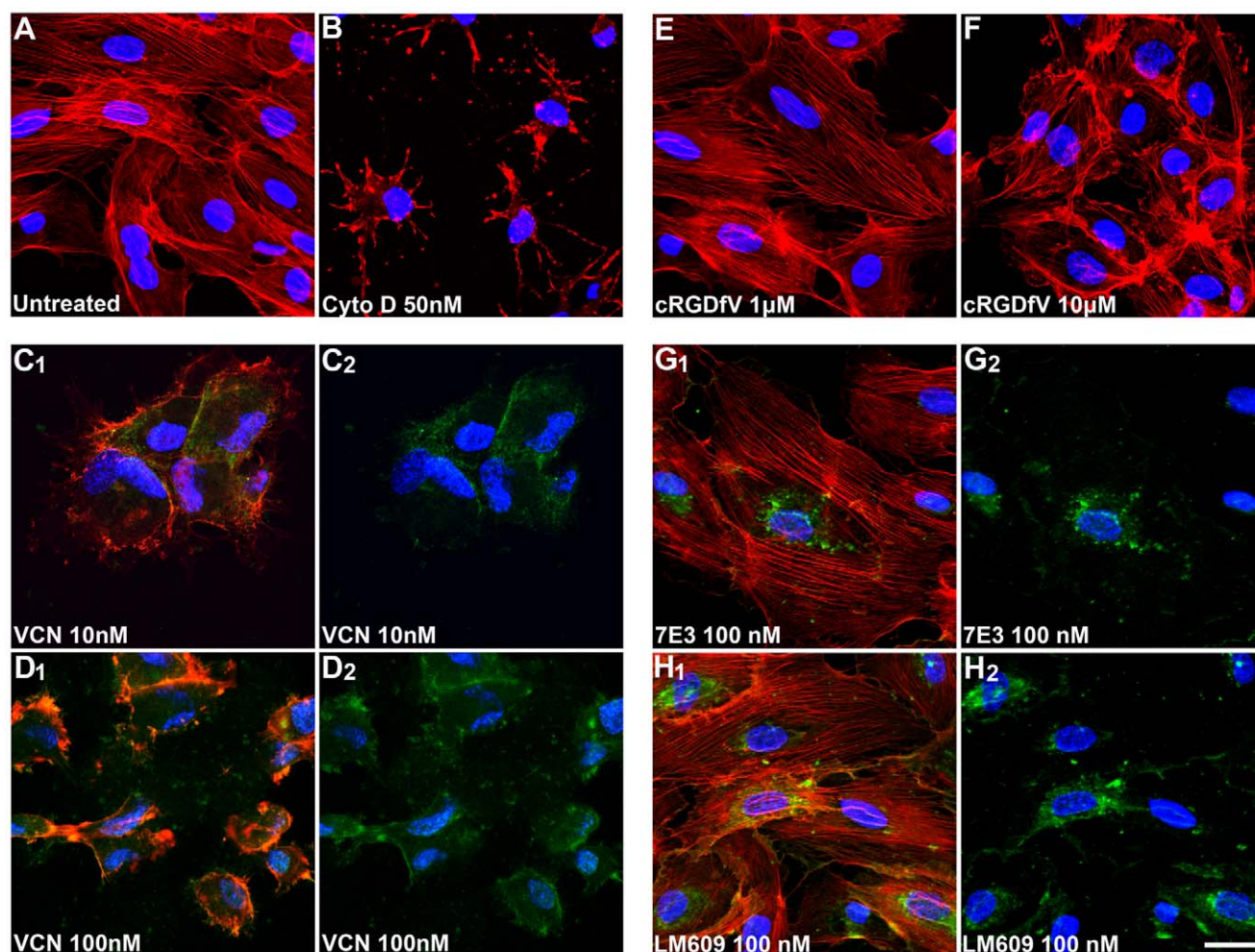
Figure 7. VCN induces massive actin cytoskeleton reorganization in HUVEC seeded on Matrigel. HUVEC were seeded in serum-free media in multiwell chamber slides on complete Matrigel, allowed to adhere, and then treated for 3 hr with various concentrations of cRGDfV peptide (1 and 10 µM) or FITC-VCN (10 and 100 nM) or the monoclonal antibodies 7E3 (100 nM) or LM609 (100 nM). When cells were incubated with integrin-binding antibodies (7E3 or LM609), a FITC-conjugated secondary antibody was used to track these treatments. The actin modifier Cytochalasin D was used as a positive control (50 nM). At the end of the incubation period, the cells from all conditions were fixed in 4% formaldehyde, permeabilized in 0.1% Triton X-100, stained with Rhodamine-Phalloidin and Hoechst 33342, and imaged by confocal microscopy. The cells exposed to FITC-labeled treatments (VCN or integrin-binding antibodies) are triple stained. The images shown above are Rhodamine-Hoechst only (panels A–B and E–F), FITC-Hoechst (panels C_2-D_2 and G_2-H_2) or overlayed three fluorophores (panels C_1-D_1 and G_1-H_1). Representative confocal images from multiple experiments taken at the same magnification ($\times 630$) are shown above (scale bar, 20 µm).
doi:10.1371/journal.pone.0010929.g007

Liposomal encapsulation of VCN

Some theoretical advantages associated with liposomal encapsulation include: (i) enhanced drug delivery by increased tumor entrapment (passive targeting), (ii) prolonged drug half-life and thus reduced dosing frequency, and (iii) fewer drug-related toxicities. Our previous study showed that liposomal CN has: no immunogenicity, extended circulatory half-life, and undetectable non-target effects [22]. In the present study, batches of LVCN were prepared by sonication (LVCN-S) or homogenization (LVCN-H) using different processing conditions. Due to some favorable structural attributes characteristic of the disintegrin class of polypeptides (i.e., hydrophilicity, excellent stability in solution, at low pHs, in organic solvents, and to a range of temperatures), we found that CN and VCN can be readily encapsulated in liposomes with high efficiencies while retaining full biological activity. The encapsulation efficiency for these batches was 70% or greater (the average size of homogenized LVCN was 83 nm).

In vivo efficacy studies with LVCN

The initial efficacy evaluation of LVCN formulations was done in the MDA-MB-435 animal model [48]. Although the breast origin of this human cell line is controversial and currently under scrutiny [49,50], these cancer cells are a high integrin $\alpha v\beta 3$ expressor and thus constitute a good model for screening pharmacological inhibitors directed at this receptor. In the MDA-MB-435 model, nude mice were inoculated orthotopically (mammary fat pads; 5×10^5 MDA-MB-435 cells in complete Matrigel per mouse) and tumors allowed to grow until they became palpable before the treatments were initiated. The animals (n = 5) were treated twice a week with liposomal formulations of VCN that were prepared either by sonication (LVCN-S) or homogenization (LVCN-H). Animals receiving saline or unencapsulated VCN (at the dose of 100 µg per injection administered twice weekly intravenously via tail vein) were used as controls. In this animal model both LVCN formulations showed good tumor
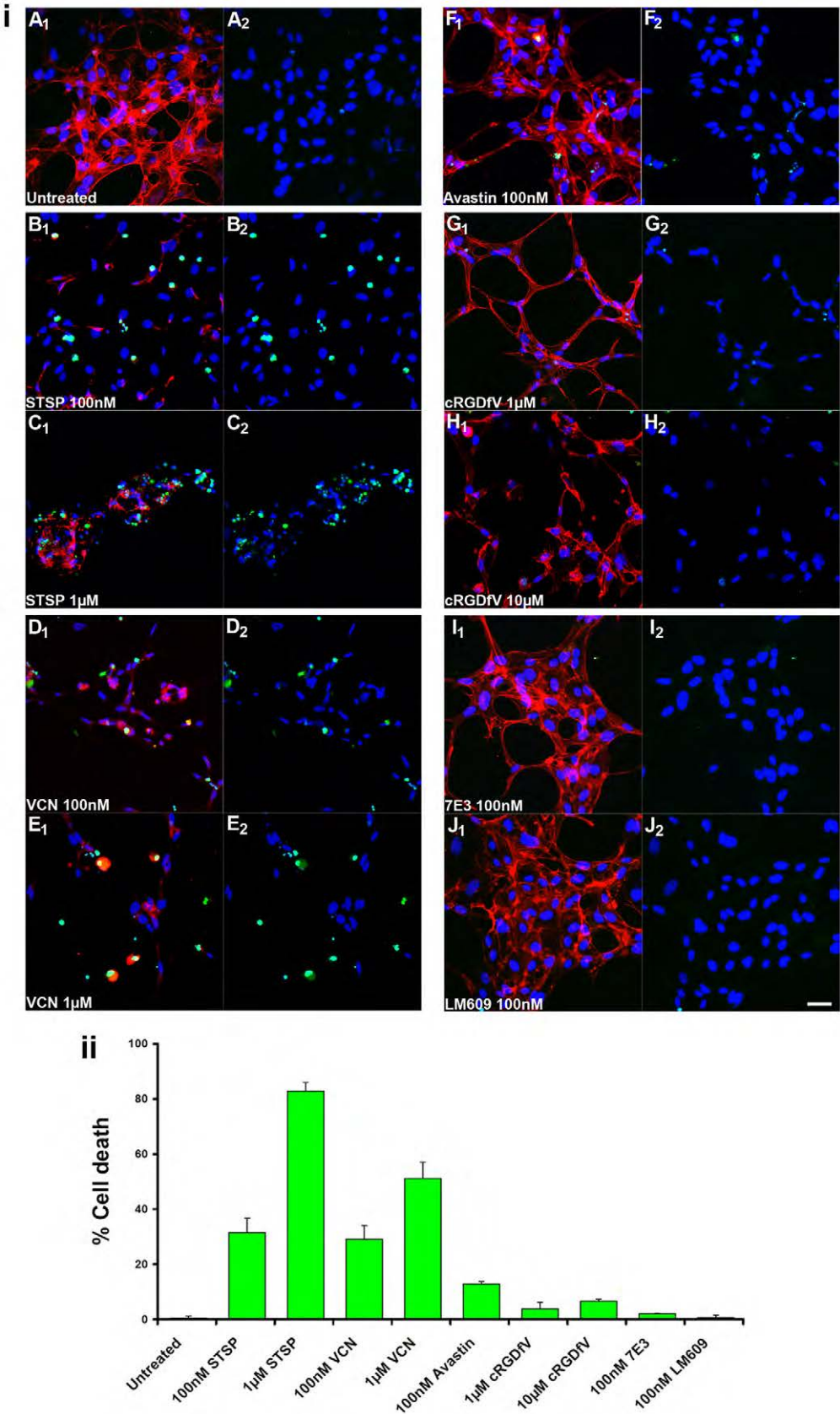
Figure 8. VCN induces apoptosis in tubulogenic HUVEC seeded between two Matrigel layers. HUVEC were seeded in serum-free media in multiwell chamber slides on complete Matrigel, allowed to adhere for 1 hr after which another layer of complete Matrigel was uniformly pipetted on top of the adherent cells. After another hour of incubation, different treatments were added to the media: either VCN (100 and 1000 nM), the cRGDfV

peptide (1 and 10 µM), Avastin (100 nM), the β3 integrin 7E3 antibody (100 nM) or the αvβ3 integrin antibody LM609 (100 nM). Staurosporine (STSP), a known HUVEC apoptosis inducer and actin modifier, was used as a positive control at two different concentrations (100 and 1000 nM). The cells were then incubated for 16 hr at 37°C in the presence of 5%CO_2. At the end of the incubation period, the cells from all conditions were fixed in 4% formaldehyde, permeabilized in 0.2% Triton X-100, FITC-TUNEL stained, and counterstained with Rhodamine-Phalloidin and Hoechst 33342. (**i**) Representative confocal images from multiple experiments taken at ×250 magnification are shown above (scale bar, 40 µm; panels A_1-J_1 –all fluorophores overlayed, panels A_2-J_2 - FITC-Hoechst). (**ii**) The amount of cell death was plotted for each condition by counting the apoptosis events from multiple random fields using the formula 'number of apoptotic nuclei/total number of nuclei x 100'. The data shown above was generated from four independent experiments.

doi:10.1371/journal.pone.0010929.g008

growth inhibition efficacy. The model was repeated three times and the overall effect on tumor growth inhibition quantitated (**Fig. 9**). LVCN was further tested in the MDA-MB-231 breast carcinoma model with similar results (**Fig. 10**). In the latter model, LVCN was compared to Avastin by looking at several parameters: tumor growth inhibition efficacy, animal survival and reduction in microvessel density. Avastin (bevacizumab), is a monoclonal antibody that interferes with neo-vessel formation in tumors by trapping an essential growth factor for angiogenesis, VEGF-A (vascular endothelial growth factor A), currently representing the gold standard for antiagiogenesis therapy, being approved by the FDA for the treatment of several types of solid cancers [51]. In the MDA-MB-231 model nude mice inoculated orthotopically (mammary fat pads; 2.5×10^6 MDA-MB-231 cells in complete Matrigel per mouse) were allowed to grow palpable tumors before treatment was initiated. The groups of animals (n = 10) were treated intravenously with either LVCN-H or LVCN-S (the dose-equivalent of 100 µg of VCN per injection) each administered twice a week, or Avastin (400 µg per injection; approx. 20 µg/gr) administered once a week. The control group received empty liposomes only. Another control group received unencapsulated VCN (at the dose of 100 µg per injection administered twice weekly intravenously via tail vein). When compared to the empty liposomes group, a significant delay in tumor growth was observed in all treatment groups. More importantly, in this model LVCN was found to significantly increase the survival of the animals similar to Avastin (all control animals in this model died by the end

of week 7). As mentioned, both animal models included a control group that received unencapsulated VCN. Interestingly, although the direct injection of unencapsulated VCN at the above dose appeared to be well tolerated by the animals for the duration of the study, in neither model was there a significant therapeutic response as compared to the LVCN group (data not shown).

In vivo evaluation of LVCN for anti-angiogenic activity

Tumor specimens from the MDA-MB-231 model were prepared for CD31 staining and microvessels quantitated as described in the 'Materials and methods' section. Tumor cryostat sections from all groups were fixed in acetone, stained with a polyclonal CD31 antibody (clone MEC13.3) and counterstained with hematoxylin. For microvessel quantitation, random CD31-positive areas in multiple fields on sections from multiple tumors were counted using a computer-assisted method (the 'SimplePCI' imaging software) and plotted as % of total stained area. Our data shows a dramatic reduction (>80%) in microvessel density in the LVCN group compared to the empty liposome control, and similar to the Avastin-treated group (**Fig 10**).

In vivo evaluation of LVCN for pro-apoptotic and anti-proliferative activities

The effect of LVCN on tumor cell death or proliferation was also evaluated in the MDA-MB-231 model. Unlike the efficacy study, in this study tumors were allowed to become more established (4 weeks from inoculation) before a short course of treatment (6 doses) with either LVCN or Avastin was initiated. Our results show that there was a large difference in the amount of cell death (TUNEL staining) between either LVCN- or Avastin-treated groups and the control. As mentioned above, the difference in tumor proliferation was assessed by Ki-67 staining, a commonly employed proliferation marker with prognostic value in various human malignancies including breast cancer [52,53]. Although there were statistically significant differences in the amount of Ki-67 staining between the groups, the LVCN group showing the least amount of staining, these differences were much smaller than the ones observed for cell death (**Fig. 11**). We chose to quantitate the effects of various treatments on tumor apoptosis and proliferation in more established tumors that received only a short course of therapy rather than in tumors harvested at the end of the efficacy study (after 7 weeks of treatment). The reason for this decision was because in the study shown in **Fig. 10**, despite the significant differences found in tumor size and animal survival between the treated groups and control, we did not see similar differences in tumor apoptosis nor in proliferation possibly due to the ability of both LVCN and Avastin to induce tumor stabilization/dormancy after repeated administration over a longer period of time (data not shown).

Discussion

Tumor angiogenesis involves a still poorly understood cross-talk between transformed epithelial cells and quiescent endothelial cells originating from preexisting vessels. In this process,
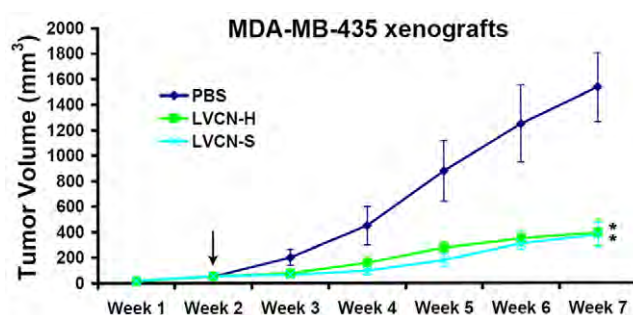

Figure 9. The initial evaluation of liposomal formulations of VCN in the MDA-MB-435 xenograft model. Nude mice were inoculated orthotopically (mammary fat pads; 5×10^5 MDA-MB-435 cells in complete Matrigel per mouse) and tumors allowed to grow until they became palpable before the treatments were initiated (indicated by the arrow). The animals (n = 5) were treated twice a week with liposomal formulations of VCN that were prepared either by sonication (LVCN-S) or homogenization (LVCN-H). The latter method of encapsulation is suitable for scale-up production and was done in a microfluidizer. All LVCN-treated animals received the dose-equivalent of 100 µg of VCN per injection and were compared to a control group that received saline only. All treatments were administered intravenously twice a week via tail vein. The statistical analysis was done using ANOVA with Dunnett's *post-hoc* multiple comparison tests (* signifies a P<0.001). The liposomal formulations tested showed comparable efficacies. This animal model was repeated three times.
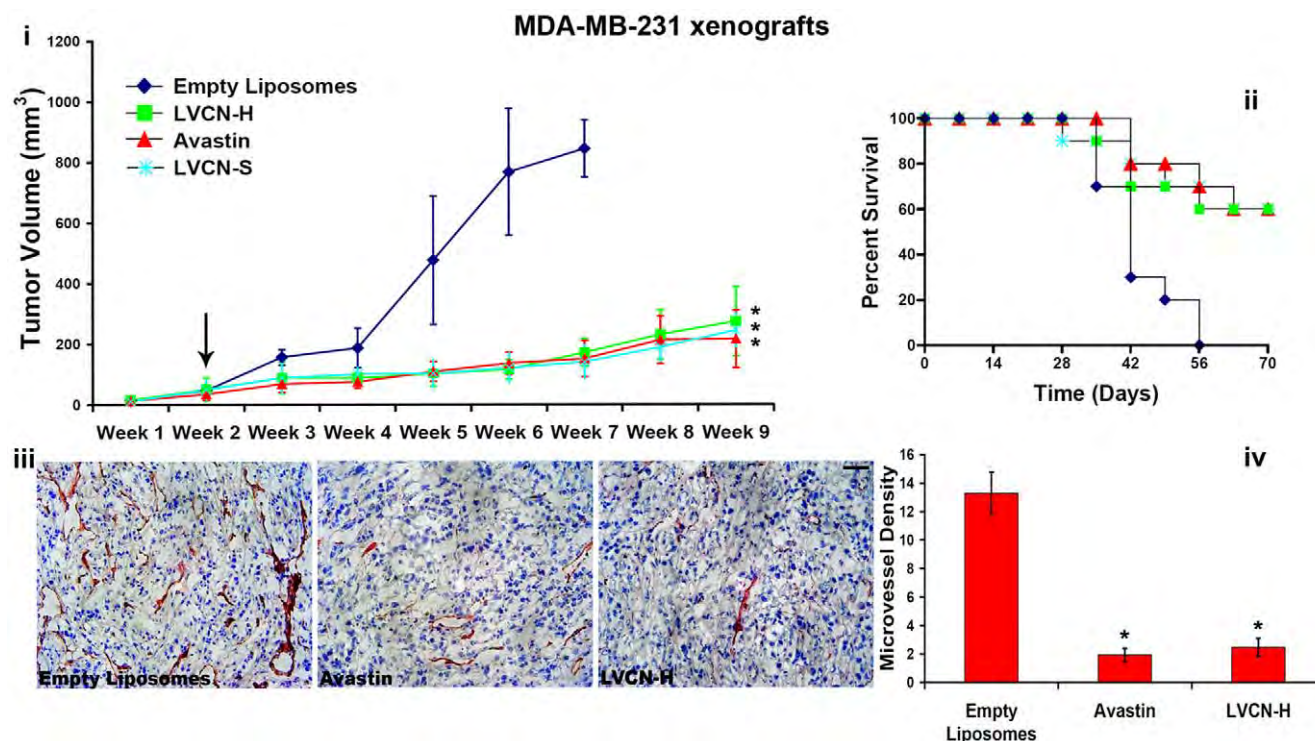doi:10.1371/journal.pone.0010929.g009

Figure 10. The efficacy and anti-angiogenic activity of LVCN in the breast MDA-MB-231 xenograft model. (i) Nude mice inoculated orthotopically (mammary fat pads; 2.5×10^6 MDA-MB-231 cells in complete Matrigel per mouse) were allowed to grow palpable tumors before treatment was commenced (indicated by the arrow). The groups of animals (n = 10) were treated intravenously with either LVCN-H or LVCN-S (the dose-equivalent of 100 µg of VCN per injection) each administered twice a week, or Avastin (400 µg per injection; approx. 20 µg/gr) administered once a week. The control group received empty liposomes only. When compared to the control group, a significant delay in tumor growth was observed in all treated groups. **(ii)** The animal data shows increased survival in all treated groups compared to the control group (all control animals died by the end of week 7) **(iii)** Tumor cryostat sections from all groups were fixed in acetone, stained with a polyclonal CD31 antibody (clone MEC13.3) and counterstained with hematoxylin. Representative CD31 photomicrographs are shown above (scale bar, 100 µm). **(iv)** For microvessel quantitation, random CD31-positive areas from multiple fields were counted using a computer-assisted method (the 'SimplePCI' imaging software) and plotted as % of total stained area. Similar to Avastin, our data indicates that VCN exhibits potent anti-angiogenic activity in this animal model. ANOVA was used for statistical analysis followed by Dunnett's multiple comparison tests (* signifies a P<0.001).
doi:10.1371/journal.pone.0010929.g010

events associated with a complex deposition of a new ECM in conjunction with multiple paracrine and autocrine loops are required to be precisely coordinated spatiotemporally for the successful execution of a specialized migratory program activated in quiescent endothelial cells [54]. As key regulators of cell migration, integrins function as centripetal signaling platforms or functional hubs [55] that bi-directionally integrate signaling circuitries downstream of different classes of cell surface receptors (e.g., the semaphorin/plexin/neuropilin, the growth factor/receptor tyrosine kinase and the cell surface protease systems) with the cellular locomotor apparatus [56]. In angiogenesis, integrins are known to regulate many cell decisions associated with this program by integrating the cellular viability pathways with various processes ranging from ECM deposition and degradation, directional endothelial cell migration and assembly into primitive cords, to lumen formation and vessel maturation [57,58]. The precise spatial distribution of integrin-binding motifs encoded in normal and oncogenic variants of ECM polymers [59] is likely to represent the most important organizing principle of the dynamics of focal adhesion complexes assembled across plasma membranes, which coordinate via integrins the motility in both angiogenic endothelial and metastatic cancer cells. The efficient disruption of various integrin-mediated interactions formed between tumorigenic ECMs and angiogenic EC in tumoral microenvi-

ronments seems to be critical from the therapeutic standpoint since, as recently reported [60], one important downside of pharmacologic VEGF/PDGF blockade is the persistence of basement membranes from involuted tumor vessels after both EC and pericytes undergo regression. This neo-vascular ECM that is left behind in the course of anti-angiogenesis therapy is suspected to provide a critical scaffold leading to a rapid repopulation of these ECM 'tracks' by new EC once the anti-VEGF/PDGF treatment is discontinued, in a process in which integrins probably play a major role.

The critical involvement of integrins in both angiogenesis [55,61] and tumor metastasis [6] provides the rationale for developing therapeutic antagonists aimed at disrupting these molecularly intertwined processes [14]. Nonetheless, the development of efficacious integrin-targeted anti-cancer agents is complicated by the fact that multiple members of the integrin family appear to be differentially involved in distinct phases of tumor angiogenesis [55] and possibly metastasis, and a clear understanding of what combination of integrins is optimally required to be simultaneously targeted in order to efficiently disrupt these processes is still lacking. For instance, most efforts in the past were channeled at developing pharmacological agents directed at the RGD-binding alphav integrin members, a subclass of integrins thought to play pivotal roles in the regulation of pathological angiogenesis. These efforts led to the development of small RGD-
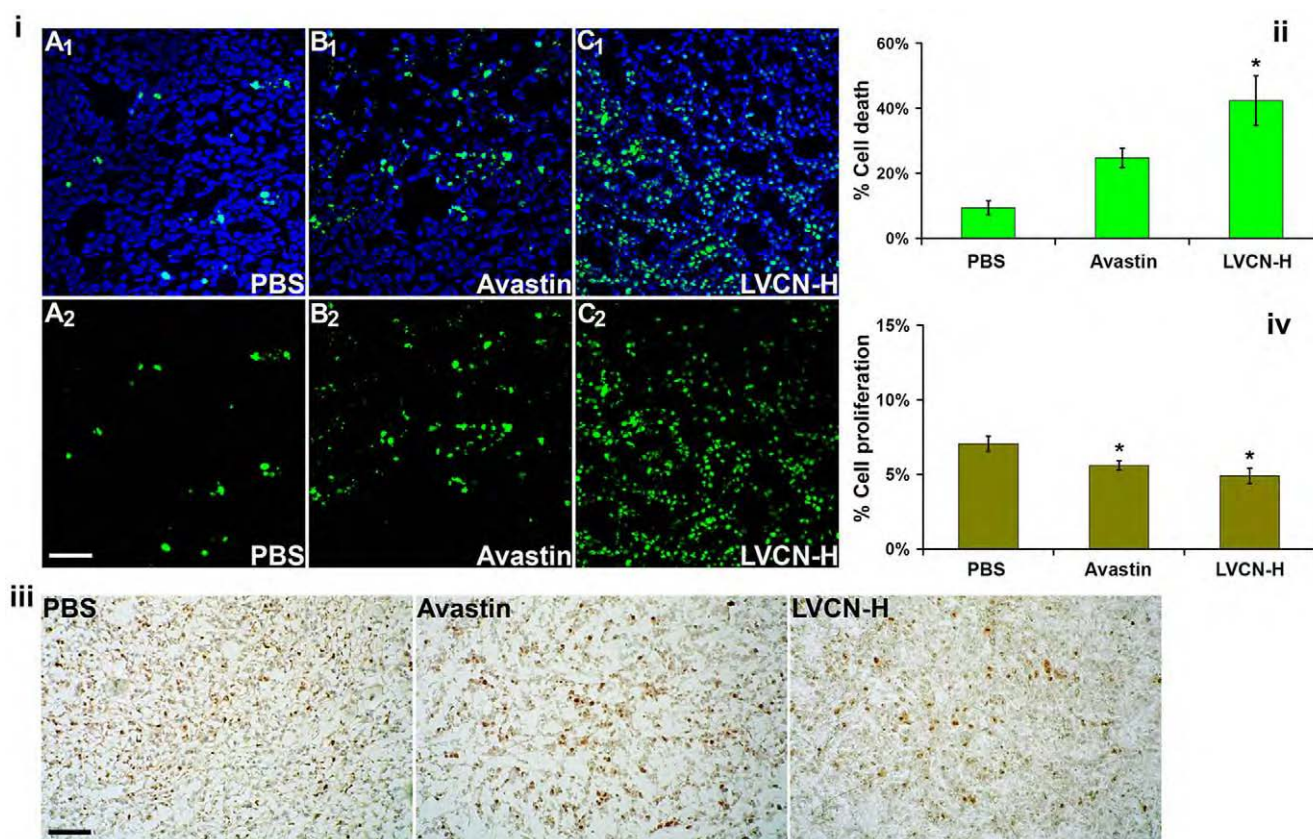
Figure 11. LVCN treatment shows enhanced tumor apoptosis in the breast MDA-MB-231 xenograft model. For this experiment, MDA-MB-231 xenografts were allowed to grow to a significantly larger volume (4 weeks after inoculation) before treatments were initiated. The animals received either liposomal VCN (at the dose-equivalent of 100 μg of VCN per injection) or Avastin (400 μg per injection) administered intravenously every other day and compared to a control group that received saline only. All animals were sacrificed after receiving 6 consecutive doses of each treatment. (**i**) To assess the impact of VCN on cell death, tumor cryostat sections from each group were stained with FITC-TUNEL, and counterstained with Hoechst 33342. Representative confocal images from multiple experiments taken at ×250 magnification are shown above (scale bar, 100 μm; panels A$_1$-C$_1$ - TUNEL-Hoechst, panels A$_2$-C$_2$ - TUNEL only). (**ii**) The amount of cell death was quantitated as 'number of TUNEL$^+$ nuclei/total number of nuclei x 100' by counting all nuclei in 'hotspot' areas from multiple fields using a computer-assisted approach (the 'SimplePCI' imaging software). The liposomal VCN group shows a significantly increased amount of cell death compared to either Avastin or control. (**iii**) The impact of VCN treatment on tumor proliferation was assessed by Ki-67 immunoperoxidase staining. Representative Ki-67 images are shown above (scale bar, 200 μm). (**iv**) Cell proliferation was quantitated using the same approach as for TUNEL staining. The differences in cell proliferation between the treatment groups were much smaller than those observed for cell death. The data was analyzed with ANOVA followed by *post-hoc* tests (* signifies a P<0.01).
doi:10.1371/journal.pone.0010929.g011

mimetics, cyclic RGD peptides, and integrin-targeting monoclonal antibodies [15,62]. The striking discrepancy that had been noticed to exist, however, between the genetic and pharmacologic models of alphav integrin ablation [10] prompted a reevaluation of these receptors as regulators of angiogenesis [63] and attempted to explain some of the disappointing results generated with alphav integrin targeting agents in clinical trials. The fact that mice deficient in either β3 or β5 or both β3 and β5 integrins not only develop normally, but paradoxically show an enhanced tumor angiogenic response [10] when challenged postpartum supports the idea that these two integrins might act in a more complex way than originally thought as regulators of pathological angiogenesis, and may be endowed with an unexpected tumor suppression function. Moreover, a tumor suppression function for alphav integrins appears to also exist in epithelial cells since the genetic ablation of alphav integrin gene in epithelial cells of murine skin leads to development of squamous cell carcinomas [64]. In order to reconcile these contradictory observations regarding the contextual role of alphav integrins alternative hypotheses must be explored. It is conceivable, for instance, that while the

overexpression of alphav integrins in angiogenic endothelial cells may be an important requirement in regulating the migration of these cells on solid ECM support (tethered migration) which leads to their assembly into neovessels (a net pro-angiogenic effect), in the presence of monovalent soluble ECM fragments a cascade of inappropriate signals might be initiated and relayed through the same alphav receptors (in the absence of tethering) which ultimately may lead to cessation of cell migration and a dramatic reorganization of actin cytoskeleton in cells exposed to such ligands (a net anti-angiogenic effect). Although in the course of pathological angiogenesis these two mechanisms might coexist, in the tumor microenvironment the abundance of pro-angiogenic circuitries, driven by a continuous deposition of new ECM polymers, appears to render the anti-angiogenic signals ineffectual thus favoring a perpetual state of angiogenesis. Even though other members in the integrin family have also been linked to different forms of angiogenesis (in development vs. adult life, physiological vs. pathological), we speculate that the alphav members may play critical roles in promoting and, possibly more importantly, terminating the cell migration events associated with angiogenesis

in adult life. This may help explain the inconsistency in outcomes between genetic and pharmacological models of alphav integrin ablation, providing a rationale for why animals devoid of β3 and β5 integrins display increased pathological angiogenesis postpartum. A number of endogenous ECM-derived fragments with anti-angiogenic activity have been characterized to date [17,65], and some of these promising molecules were found to bind to either one or multiple integrin receptors (i.e., endostatin, tumstatin, arresten, canstatin, PEX, endorepellin etc) [66]. It is noteworthy that the integrin ligation by some of these endogenous fragments (i.e., endostatin, endorepellin) was shown to lead to the collapse of actin cytoskeleton and focal adhesion disassembly in endothelial cells *in vitro* [32,33]. Interestingly, these cell motility deactivation effects observed in angiogenic endothelial cells with ECM fragments are reminiscent of those triggered by members [67,68] belonging to an unrelated class of signaling molecules (i.e., the semaphorins) which suggest that a high degree of integration may exist between the semaphorin-plexin-neuropilin and integrin systems in controlling the actin cytoskeleton dynamics during angiogenesis [57]. It could be argued that, if integrins physically connect the actin cytoskeleton with a plethora of complex molecules bound across plasma membrane, thus enabling the dynamic actin cytoskeleton in migratory cells to sense their extracellular microenvironment, then a pharmacological agent designed to efficiently disrupt integrins is also expected to induce a massive reorganization or collapse of actin cytoskeleton in these cells. Since some of the endogenous ECM-derived anti-angiogenic fragments have already been characterized as potent tumor suppressors in various animal models, the biggest stumbling block to their successful clinical translation remained the ability to produce them recombinantly in large scale. However, this proved to be more complicated than originally thought due to the fact that these ECM fragments are naturally derived through proteolytic cleavage from higher molecular weight matrix polymers which makes them dependent on their parental supermolecules for correct folding (i.e., intramolecular chaperoning). Because of this, these otherwise promising molecules proved to be refractory to correct folding when expressed in various recombinant systems, which led to altered or diminished biological activity for the recombinant versions when compared to the native ECM fragments, an issue that may have accounted for the disappointing performance seen with recombinant endostatin in clinical trials [66].

Interestingly, several classes of metalloproteases found in snake venoms also contain domains that share significant structural similarities with modules and domains buried in ECM proteins [69]. Among these, the disintegrin and disintegrin-like domains found in snake venoms display a variety of integrin-binding motifs with enormous pharmacological potential. Similar to the anti-angiogenic fragments derived from mammalian ECMs, disintegrin are also generated through proteolytic cleavage from larger multidomain metalloproteases [70].

In this study, we show that a chimeric disintegrin, vicrostatin (VCN), derived from a member of a well characterized family of naturally occurring broad-spectrum integrin inhibitors, could be successfully produced recombinantly in large scale in an engineered bacterial system. The recombinant production of VCN was a complex achievement complicated by the fact that disintegrins are small polypeptides with almost no secondary structure that depend for their proper folding and biological activity on the correct pairing of a large number of disulfide bridges (5 in VCN) relative to their molecular size. For this reason, and because disintegrins do not express well in mammalian cells or yeast, a bacterial system supportive of

disulfide bridge formation needed to be identified. We found that VCN can be expressed in such a system (e.g., Origami B) which prompted us to further optimize the expression method for this recombinant polypeptide in this system. Our optimization efforts led to consistent expression levels for this recombinant molecule in Origami B with minimal batch-to-batch variation and with yields around 200 mg of purified active VCN per liter of bacterial culture. Recombinant VCN is a synthetic construct that retains the RGD integrin-recognition motif displayed by the native disintegrin contortrostatin (CN) it was derived from, but was also engineered to exhibit some novel integrin biding characteristics. Therefore, in a number of *in vitro* functional assays, recombinant VCN was found to retain the binding properties of native CN, while showing an improved binding affinity compared to native CN for one important receptor in angiogenesis, integrin α5β1. The binding affinity of VCN for integrin α5β1 was measured by fluorescence polarization and found to be one order of magnitude higher than that of CN (Kd = 15.2 nM for VCN vs. 191.3 nM for native CN). The recombinant VCN behaves like a true disintegrin in that it inhibits platelet aggregation (by disrupting fibrinogen binding to integrin αIIbβ3) in a similar manner to native CN and with a almost identical IC_{50} (approx. 60 nM). Mass spectrometry analysis of VCN showed that this recombinant disintegrin is, unlike CN, a monomer which led us to speculate that VCN may have folded differently than CN in the N-terminal half of the molecule and this prevented its dimerization. Cell surface binding analyses by flow cytometry conducted with fluorescently-labeled disintegrins showed that VCN binds similarly to CN to different cell lines and, like CN, its cell surface binding is abolished in the presence of integrin ligands (either a cyclic RGD peptide or an antibody fragment) competing for the same binding sites. Since disintegrin binding is a metal-ion dependent process, we also showed that in the presence of metal chelators both CN and VCN cease to bind to cells. The ability of VCN to interfere with cell migration and invasion was further tested *in vitro* in two experimental settings: in a modified Boyden chamber using different cell lines (the transwell invasion assay) and against HUVEC in the tube formation assay. In all instances VCN was found to significantly inhibit cell migration and invasion in the nanomolar range and with a potency similar to that of native CN. Moreover, our previous studies indicated that disintegrins are not cytotoxic to cells cultured in normal conditions. In order to understand whether the anti-migratory/ anti-invasive effects observed with VCN were due to its ability to interfere with essential components of cellular locomotor apparatus (i.e., the dynamic actin cytoskeleton of migratory cells) and was not the result of a cytotoxic effect, we conducted cell viability studies with both CN and VCN using HUVEC and cancer cells. Our results showed that both CN and VCN were completely devoid of cytotoxicity at all concentrations tested (up to 1 μM). Surprisingly, however, when HUVEC were sand-wiched between two Matrigel layers, in an experimental setting that allows these cells to move faster and form tubes more rapidly, VCN did show a significant cytotoxic effect compared to other integrin-targeting ligands tested (a cyclic RGD peptide and two different antibodies). This effect was unexpected and suggests that rapidly migratory and/or invasive cells might be the most vulnerable to the effects of this agent. Our previous studies with native CN indicate that this disintegrin may behave like a soluble ECM-mimetic, potently altering the actin cytoskeleton dynamics by deactivating key molecular components of focal adhesions in both adherent HUVEC and glioma cells, the result of which is a net anti-migratory effect [35]. Like native CN and unlike other integrin-targeting ligands, we showed that VCN has a unique

integrin binding profile (simultaneously targeting integrins αvβ3, αvβ5, and α5β1) and is able to induce at nanomolar concentrations the disassembly of actin stress fibers and a massive actin cytoskeleton reorganization in HUVEC plated on Matrigel. The ability of disintegrins to elicit an inappropriate signaling and alter the tensional homeostasis in angiogenic and cancer cells alike may have profound therapeutic implications since the characteristic increase in tissue rigidity associated with cancers was shown to critically modulate the behavior of malignant cells by regulating the ability of these cells to form focal adhesions and efficiently signal through growth factor receptors [71]. Furthermore, the ability to manipulate pharmacologically the actin cytoskeleton and stress fiber assembly in transformed cells may represent a novel therapeutic goal towards achieving tumor dormancy [72,73]. Interestingly, the cytoskeletal effects observed with VCN in tubulogenic EC cultured in a rich tumorigenic matrix that is uniquely endowed to support both cell survival and migration are strikingly similar to those exerted by the endogenous ECM-derived fragments discussed above. As already mentioned, these effects distinguish VCN from the other integrin ligands that were tested in the same setting, including the small cyclic RGD peptide cyclo(Arg-Gly-Asp-DPhe-Val). It is noteworthy to emphasize that a methylated variant of the cyclic RGD peptide used in our experiments, the cyclo(Arg-Gly-Asp-DPhe-NMeVal) peptide or Cilengitide, which displays an improved specificity to integrins αvβ3 and αvβ5 [74,75], has been evaluated in a number of advanced solid tumors in several clinical trials and showed promise against glioblastoma multiforme [76,77]. Moreover, the two monoclonal antibodies that were included in our *in vitro* assays, the integrin αvβ3-targeting 7E3 and LM609, were also previously tested *in vivo* in a number of animal cancer models and reported to have good tumor growth inhibition efficacy [46,78]. By comparing different integrin ligands, our *in vitro* data seem to indicate that molecules that behave like soluble ECM-mimetics might have additional anti-angiogenic benefits compared to cyclic RGD peptides and integrin-targeting monoclonal antibodies. Furthermore, our results also suggest that, unlike cyclic RGD peptides, VCN may produce effective anti-angiogenic effects at much lower doses which may possibly translate into fewer side effects.

Although VCN retains native CN's ability to bind the activated αIIbβ3 platelet integrin, like CN [22] it does not interact with quiescent platelets, an *in vitro* observation further corroborated by our *in vivo* findings: no side effects were documented following direct intravenous administration of purified VCN in two different species: up to 1 mg per shot in mice or up to 5 mg per shot in rats. It is important to mention that there is an established link between activated platelets and metastasis [79,80] and from the therapeutic standpoint it may be advantageous to use a polypeptide like VCN that theoretically might also have the potential to address this metastasis strategy. As a small polypeptide, VCN is not expected to be immunogenic, and our preliminary animal studies showed that VCN indeed failed to elicit an antibody response following intravenous infusion. Despite these findings, for enhanced passive targeting of the drug to the tumor site, we opted for liposomal delivery. VCN can be efficiently encapsulated into unilamellar liposomes, unlike other proteins possibly due to its structural characteristics, and our findings indicate that the liposomal formulations of VCN have far superior efficacy compared to the naked polypeptide in two animal models of human cancer. In these models LVCN showed excellent tumor growth inhibition efficacy, increased animal survival and a significant reduction (>80% compared to control) in tumor microvessel density producing similar results compared to Avastin (bevacizumab).

Interestingly, in a separate study of the same breast cancer model (MDA-MB-231 xenografts) VCN showed superior tumor apoptosis effects compared to Avastin as indicated by the quantitation of the TUNEL-stained areas on tumor sections. As already mentioned, in all these models the liposomal delivery of VCN was far more efficacious compared to the intravenous administration of the naked polypeptide. We do not exclude, however, the therapeutic scenario in which the naked polypeptide administered at much higher doses than those used in this study might show improved therapeutic responses. On the other hand, the liposomal delivery has a number of other advantages showing good therapeutic responses at lower drug doses and less frequent administrations. To better understand how VCN is released from liposomes in the tumor microenvironment, we are currently conducting mechanistic studies aimed at elucidating the fate of LVCN in tumor-bearing animals. As a unique broad-spectrum anti-invasive drug, VCN may hold an advantage over other anti-tumor therapeutic modalities in that it may be better suited to address the cell survival loops operating in the avascular tissue in the early steps of angiogenesis and metastasis [81,82]. For instance, in an elegant animal study, Carbonell et al. [83] recently demonstrated the critical importance of interactions between the β1 integrin receptors on tumor cells and the vascular basement membrane in maintaining the viability of early metastatic seeds in the brain before the angiogenesis process is initiated. Moreover, recent studies have demonstrated that the use of various anti-VEGF/PDGF strategies is linked to an increased risk of early metastasis in animal cancer models [84,85]. Although the clinical relevance of these preclinical studies is not yet clear [86], these data support the idea that not only is there an imperative need to design novel anti-angiogenic drugs with better anti-invasive properties, but also to test the impact of established anti-angiogenics (such as Avastin) on metastasis and/or postoperative survival when administered in combination with anti-invasive modalities. In our previous studies conducted with native CN we showed that this agent was very effective at blocking metastasis in an animal model [87]. To better understand the ability of VCN to function as an anti-metastatic agent, we are currently testing this agent in several spontaneous models of breast cancer metastasis (i.e., the murine 4T1 and D2F2, and human MDA-MB-231). In summary, we believe that the novel agent described in this report holds a promising translational potential and has a design advantage over endogenous anti-angiogenic fragments in that it can be made recombinantly in large quantities, safely infused into animals, and efficiently encapsulated into liposomes for enhanced tumor delivery.

Acknowledgments

Author Contributions

References

1. Ferrara N, Hillan KJ, Novotny W (2005) Bevacizumab (Avastin), a humanized anti-VEGF monoclonal antibody for cancer therapy. Biochem Biophys Res Commun 333: 328–335.

2. Adams GP, Weiner LM (2005) Monoclonal antibody therapy of cancer. Nat Biotechnol 23: 1147–1157.

3. Petrelli A, Valabrega G (2009) Multitarget drugs: the present and the future of cancer therapy. Expert Opin Pharmacother 10: 589–600.

4. Imai K, Takaoka A (2006) Comparing antibody and small-molecule therapies for cancer. Nat Rev Cancer 6: 714–727.

5. Hanahan D, Weinberg RA (2000) The hallmarks of cancer. Cell 100: 57–70.

6. Hood JD, Cheresh DA (2002) Role of integrins in cell invasion and migration. Nat Rev Cancer 2: 91–100.

7. Bissell MJ, Rizki A, Mian IS (2003) Tissue architecture: the ultimate regulator of breast epithelial function. Curr Opin Cell Biol 15: 753–762.

8. Mizejewski GJ (1999) Role of integrins in cancer: survey of expression patterns. Proc Soc Exp Biol Med 222: 124–138.

9. Desgrosellier JS, Barnes LA, Shields DJ, Huang M, Lau SK, et al. (2009) An integrin alpha(v)beta(3)-c-Src oncogenic unit promotes anchorage-independence and tumor progression. Nat Med 15: 1163–1169.

10. Reynolds LE, Wyder L, Lively JC, Taverna D, Robinson SD, et al. (2002) Enhanced pathological angiogenesis in mice lacking beta3 integrin or beta3 and beta5 integrins. Nature Medicine 8: 27–34.

11. Hamano Y, Zeisberg M, Sugimoto H, Lively JC, Maeshima Y, et al. (2003) Physiological levels of tumstatin, a fragment of collagen IV alpha3 chain, are generated by MMP-9 proteolysis and suppress angiogenesis via alphavbeta3 integrin. Cancer Cell 3: 589–601.

12. Serini G, Valdembri D, Bussolino F (2006) Integrins and angiogenesis: a sticky business. Exp Cell Res 312: 651–658.

13. Mahabeleshwar GH, Chen J, Feng W, Somanath PR, Razorenova OV, et al. (2008) Integrin affinity modulation in angiogenesis. Cell Cycle 7: 335–347.

14. Folkman J (2007) Angiogenesis: an organizing principle for drug discovery? Nat Rev Drug Discov 6: 273–286.

15. Nemeth JA, Nakada MT, Trikha M, Lang Z, Gordon MS, et al. (2007) Alpha-v integrins as therapeutic targets in oncology. Cancer Invest 25: 632–646.

16. Silva R, D'Amico G, Hodivala-Dilke KM, Reynolds LE (2008) Integrins: the keys to unlocking angiogenesis. Arterioscler Thromb Vasc Biol 28: 1703–1713.

17. Bix G, Iozzo RV (2005) Matrix revolutions: "tails" of basement-membrane components with angiostatic functions. Trends Cell Biol 15: 52–60.

18. Sudhakar A, Sugimoto H, Yang C, Lively J, Zeisberg M, et al. (2003) Human tumstatin and human endostatin exhibit distinct antiangiogenic activities mediated by alphavbeta3 and alpha5beta1 integrins. Proc Natl Acad Sci U S A 100: 4766–4771.

19. Gould RJ, Polokoff MA, Friedman PA, Huang TF, Holt JC, et al. (1990) Disintegrins: a family of integrin inhibitory proteins from viper venoms. Proc Soc Exp Biol Med 195: 168–171.

20. McLane MA, Joerger T, Mahmoud A (2008) Disintegrins in health and disease. Front Biosci 13: 6617–6637.

21. Huang TF, Yeh CH, Wu WB (2001) Viper venom components affecting angiogenesis. Haemostasis 31: 192–206.

22. Swenson S, Costa F, Minea R, Sherwin RP, Ernst W, et al. (2004) Intravenous liposomal delivery of the snake venom disintegrin contortrostatin limits breast cancer progression. Mol Cancer Ther 3: 499–511.

23. Saudek V, Atkinson RA, Pelton JT (1991) Three-dimensional structure of echistatin, the smallest active RGD protein. Biochemistry 30: 7369–7372.

24. Moiseeva N, Bau R, Swenson SD, Markland FS, Jr., Choe JY, et al. (2008) Structure of acostatin, a dimeric disintegrin from Southern copperhead (Agkistrodon contortrix contortrix), at 1.7 A resolution. Acta Crystallogr D Biol Crystallogr 64: 466–470.

25. McLane MA, Marcinkiewicz C, Vijay-Kumar S, Wierzbicka-Patynowski I, Niewiarowski S (1998) Viper venom disintegrins and related molecules. Proc Soc Exp Biol Med 219: 109–119.

26. Trikha M, Rote WE, Manley PJ, Lucchesi BR, Markland FS (1994) Purification and characterization of platelet aggregation inhibitors from snake venoms. Thromb Res 73: 39–52.

27. Zhou Q, Nakada MT, Arnold C, Markland FS (1999) Contortrostatin, a dimeric disintegrin from Agkistrodon contortrix contortrix, inhibits angiogenesis. Angiogenesis 3: 259–269.

28. Trikha M, De Clerck YA, Markland FS (1994) Contortrostatin, a snake venom disintegrin, inhibits beta1 integrin-mediated human metastatic melanoma cell adhesion and blocks experimental metastasis. Cancer Res 54: 4993–4998.

29. Zhou Q, Nakada MT, Brooks PC, Swenson SD, Ritter MR, et al. (2000) Contortrostatin, a homodimeric disintegrin, binds to integrin alphavbeta5. Biochem Biophys Res Commun 267: 350–355.

30. Minea R, Swenson S, Costa F, Chen TC, Markland FS (2005) Development of a novel recombinant disintegrin, contortrostatin, as an effective anti-tumor and anti-angiogenic agent. Pathophysiol Haemost Thromb 34: 177–183.

31. Ribatti D (2009) Endogenous inhibitors of angiogenesis: a historical review. Leuk Res 33: 638–644.

32. Dixelius J, Cross M, Matsumoto T, Sasaki T, Timpl R, et al. (2002) Endostatin regulates endothelial cell adhesion and cytoskeletal organization. Cancer Res 62: 1944–1947.

33. Bix G, Fu J, Gonzalez EM, Macro L, Barker A, et al. (2004) Endorepellin causes endothelial cell disassembly of actin cytoskeleton and focal adhesions through alpha2beta1 integrin. J Cell Biol 166: 97–109.

34. Ritter MR, Zhou Q, Markland FS, Jr. (2000) Contortrostatin, a snake venom disintegrin, induces alphavbeta3- mediated tyrosine phosphorylation of CAS and FAK in tumor cells. J Cell Biochem 79: 28–37.

35. Schmitmeier S, Markland FS, Schonthal AH, Chen TC (2005) Potent mimicry of fibronectin-induced intracellular signaling in glioma cells by the homodimeric snake venom disintegrin contortrostatin. Neurosurgery 57: 141–153; discussion 141-153.

36. Park SH, Raines RT (2004) Fluorescence polarization assay to quantify protein-protein interactions. Methods Mol Biol 261: 161–166.

37. Osborne CK, Hobbs K, Clark GM (1985) Effect of Estrogens and Antiestrogens on Growth of Human Breast Cancer Cells in Athymic Nude Mice. Cancer Res 45: 584–590.

38. Protopapa E, Delides GS, Revesz L (1993) Vascular density and the response of breast carcinomas to mastectomy and adjuvant chemotherapy. Eur J Cancer 29A: 1391–1393.

39. Fox SB, Harris AL (2004) Histological quantitation of tumour angiogenesis. Apmis 112: 413–430.

40. LaVallie ER, DiBlasio EA, Kovacic S, Grant KL, Schendel PF, et al. (1993) A thioredoxin gene fusion expression system that circumvents inclusion body formation in the E. coli cytoplasm. Biotechnology (N Y) 11: 187–193.

41. Fujii Y, Okuda D, Fujimoto Z, Horii K, Morita T, et al. (2003) Crystal structure of trimestatin, a disintegrin containing a cell adhesion recognition motif RGD. J Mol Biol 332: 1115–1122.

42. Wierzbicka-Patynowski I, Niewiarowski S, Marcinkiewicz C, Calvete JJ, Marcinkiewicz MM, et al. (1999) Structural requirements of echistatin for the recognition of alpha(v)beta(3) and alpha(5)beta(1) integrins. J Biol Chem 274: 37809–37814.

43. Carrington JC, Dougherty WG (1988) A viral cleavage site cassette: identification of amino acid sequences required for tobacco etch virus polyprotein processing. Proc Natl Acad Sci U S A 85: 3391–3395.

44. Ritter MR, Markland FS, Jr. (2001) Differential regulation of tyrosine phosphorylation in tumor cells by contortrostatin, a homodimeric disintegrin, and monomeric disintegrins echistatin and flavoridin. Toxicon 39: 283–289.

45. Artoni A, Li J, Mitchell B, Ruan J, Takagi J, et al. (2004) Integrin beta3 regions controlling binding of murine mAb 7E3: implications for the mechanism of integrin alphaIIbbeta3 activation. Proc Natl Acad Sci U S A 101: 13114–13120.

46. Brooks PC, Stromblad S, Klemke R, Visscher D, Sarkar FH, et al. (1995) Antiintegrin alphavbeta3 blocks human breast cancer growth and angiogenesis in human skin. Journal of Clinical Investigation 96: 1815–1822.

47. Golubkov V, Hawes D, Markland FS (2003) Anti-angiogenic activity of contortrostatin, a disintegrin from Agkistrodon contortrix contortrix snake venom. Angiogenesis 6: 213–224.

48. Price JE, Polyzos A, Zhang RD, Daniels LM (1990) Tumorigenicity and Metastasis of Human Breast Carcinoma Cell Lines in Nude Mice. Cancer Res 50: 717–721.

49. Chambers AF (2009) MDA-MB-435 and M14 cell lines: identical but not M14 melanoma? Cancer Res 69: 5292–5293.

50. Rae JM, Creighton CJ, Meck JM, Haddad BR, Johnson MD (2007) MDA-MB-435 cells are derived from M14 melanoma cells–a loss for breast cancer, but a boon for melanoma research. Breast Cancer Res Treat 104: 13–19.

51. Shih T, Lindley C (2006) Bevacizumab: an angiogenesis inhibitor for the treatment of solid malignancies. Clin Ther 28: 1779–1802.

52. Brown DC, Gatter KC (2002) Ki67 protein: the immaculate deception? Histopathology 40: 2–11.

53. Wiesner FG, Magener A, Fasching PA, Wesse J, Bani MR, et al. (2009) Ki-67 as a prognostic molecular marker in routine clinical use in breast cancer patients. Breast 18: 135–141.

54. Folkman J (2006) Angiogenesis. Annu Rev Med 57: 1–18.

55. Contois L, Akalu A, Brooks PC (2009) Integrins as "functional hubs" in the regulation of pathological angiogenesis. Semin Cancer Biol 19: 318–328.

56. Ivaska J, Heino J (2009) Interplay between cell adhesion and growth factor receptors: from the plasma membrane to the endosomes. Cell Tissue Res 339: 111–120.

57. Serini G, Napione L, Bussolino F (2008) Integrins team up with tyrosine kinase receptors and plexins to control angiogenesis. Curr Opin Hematol 15: 235–242.

58. Napione L, Cascone I, Mitola S, Serini G, Bussolino F (2007) Integrins: a flexible platform for endothelial vascular tyrosine kinase receptors. Autoimmun Rev 7: 18–22.

59. Geiger B, Spatz JP, Bershadsky AD (2009) Environmental sensing through focal adhesions. Nat Rev Mol Cell Biol 10: 21–33.

60. Baluk P, Hashizume H, McDonald DM (2005) Cellular abnormalities of blood vessels as targets in cancer. Curr Opin Genet Dev 15: 102–111.

61. Mahabeleshwar GH, Feng W, Phillips DR, Byzova TV (2006) Integrin signaling is critical for pathological angiogenesis. J Exp Med 203: 2495–2507.

62. Tucker GC (2006) Integrins: molecular targets in cancer therapy. Curr Oncol Rep 8: 96–103.

63. Hynes RO (2002) A reevaluation of integrins as regulators of angiogenesis. Nature Medicine 8: 918–921.

64. McCarty JH, Barry M, Crowley D, Bronson RT, Lacy-Hulbert A, et al. (2008) Genetic ablation of alphav integrins in epithelial cells of the eyelid skin and conjunctiva leads to squamous cell carcinoma. Am J Pathol 172: 1740–1747.

65. Sund M, Hamano Y, Sugimoto H, Sudhakar A, Soubasakos M, et al. (2005) Function of endogenous inhibitors of angiogenesis as endothelium-specific tumor suppressors. Proc Natl Acad Sci U S A 102: 2934–2939.

66. Clamp AR, Jayson GC (2005) The clinical potential of antiangiogenic fragments of extracellular matrix proteins. Br J Cancer 93: 967–972.

67. Varshavsky A, Kessler O, Abramovitch S, Kigel B, Zaffryar S, et al. (2008) Semaphorin-3B is an angiogenesis inhibitor that is inactivated by furin-like pro-protein convertases. Cancer Res 68: 6922–6931.

68. Serini G, Maione F, Giraudo E, Bussolino F (2009) Semaphorins and tumor angiogenesis. Angiogenesis 12: 187–193.

69. Eble JA (2010) Matrix biology meets toxinology. Matrix Biol 29: 239–247.

70. Juarez P, Comas I, Gonzalez-Candelas F, Calvete JJ (2008) Evolution of snake venom disintegrins by positive Darwinian selection. Mol Biol Evol 25: 2391–2407.

71. Paszek MJ, Zahir N, Johnson KR, Lakins JN, Rozenberg GI, et al. (2005) Tensional homeostasis and the malignant phenotype. Cancer Cell 8: 241–254.

72. Barkan D, Green JE, Chambers AF (2010) Extracellular matrix: A gatekeeper in the transition from dormancy to metastatic growth. Eur J Cancer 46: 1181–1188.

73. Barkan D, Kleinman H, Simmons JL, Asmussen H, Kamaraju AK, et al. (2008) Inhibition of metastatic outgrowth from single dormant tumor cells by targeting the cytoskeleton. Cancer Res 68: 6241–6250.

74. Dechantsreiter MA, Planker E, Matha B, Lohof E, Holzemann G, et al. (1999) N-Methylated cyclic RGD peptides as highly active and selective alpha(v)beta(3) integrin antagonists. J Med Chem 42: 3033–3040.

75. Goodman SL, Holzemann G, Sulyok GA, Kessler H (2002) Nanomolar small molecule inhibitors for alphavbeta6, alphavbeta5, and alphavbeta3 integrins. J Med Chem 45: 1045–1051.

76. Hariharan S, Gustafson D, Holden S, McConkey D, Davis D, et al. (2007) Assessment of the biological and pharmacological effects of the alphavbeta3 and alphavbeta5 integrin receptor antagonist, cilengitide (EMD 121974), in patients with advanced solid tumors. Ann Oncol 18: 1400–1407.

77. Reardon DA, Nabors LB, Stupp R, Mikkelsen T (2008) Cilengitide: an integrin-targeting arginine-glycine-aspartic acid peptide with promising activity for glioblastoma multiforme. Expert Opin Investig Drugs 17: 1225–1235.

78. Varner JA, Nakada MT, Jordan RE, Coller BS (1999) Inhibition of angiogenesis and tumor growth by murine 7E3, the parent antibody of c7E3 Fab (abciximab; ReoPro). Angiogenesis 3: 53–60.

79. Nash GF, Turner LF, Scully MF, Kakkar AK (2002) Platelets and cancer. Lancet Oncol 3: 425–430.

80. Jurasz P, Alonso-Escolano D, Radomski MW (2004) Platelet–cancer interactions: mechanisms and pharmacology of tumour cell-induced platelet aggregation. Br J Pharmacol 143: 819–826.

81. Kim S, Harris M, Varner JA (2000) Regulation of integrin alphavbeta3-mediated endothelial cell migration and angiogenesis by integrin alpha5beta1 and protein kinase A. J Biol Chem 275: 33920–33928.

82. Kim S, Bell K, Mousa SA, Varner JA (2000) Regulation of angiogenesis in vivo by ligation of integrin alpha5beta1 with the central cell-binding domain of fibronectin. Am J Pathol 156: 1345–1362.

83. Carbonell WS, Ansorge O, Sibson N, Muschel R (2009) The vascular basement membrane as "soil" in brain metastasis. PLoS One 4: e5857.

84. Ebos JM, Lee CR, Cruz-Munoz W, Bjarnason GA, Christensen JG, et al. (2009) Accelerated metastasis after short-term treatment with a potent inhibitor of tumor angiogenesis. Cancer Cell 15: 232–239.

85. Paez-Ribes M, Allen E, Hudock J, Takeda T, Okuyama H, et al. (2009) Antiangiogenic therapy elicits malignant progression of tumors to increased local invasion and distant metastasis. Cancer Cell 15: 220–231.

86. Ellis LM, Reardon DA (2009) Cancer: The nuances of therapy. Nature 458: 290–292.

87. Zhou Q, Sherwin RP, Parrish C, Richters V, Groshen SG, et al. (2000) Contortrostatin, a dimeric disintegrin from Agkistrodon contortrix contortrix, inhibits breast cancer progression. Breast Cancer Res Treat 61: 249–260.

The use of pepsin in receptor internalization assays

Corey M. Helchowski, Radu O. Minea, Stephen D. Swenson, Francis S. Markland Jr. *

Department of Biochemistry and Molecular Biology and Norris Comprehensive Cancer Center, University of Southern California, Keck School of Medicine, Los Angeles, CA, USA

ARTICLE INFO

ABSTRACT

For internalization experiments that use fluorescent antibody (Ab) staining to distinguish between inside versus outside cellular localization of various receptor targeting ligands, it is critical that there be efficient removal of all residual surface-bound fluorescent Ab. To achieve this, a fluorescent Ab removal technique is commonly employed in receptor internalization assays that utilizes low pH glycine-based buffers to wash off the residual non-internalized fluorescent Ab retained on cell surfaces. In this study, we highlight the shortcomings of this technique and propose an alternative *in situ* proteolytic approach that we found to be non-deleterious to the cells and significantly more effective in removing the residual fluorescence resulting from non-internalized surface-bound Ab.

Introduction

Receptor internalization assays are important for understanding how a particular ligand or receptor is involved in endocytosis. What is being measured by these assays is the rate the ligand/receptor pair is internalized into the cytoplasm of the cell. This information can be used for mechanistic studies in multiple areas of research such as receptor-mediated endocytosis and drug uptake.

One common way to explore the rate of cellular uptake for a particular ligand is to label the ligand with a fluorescent tag and estimate the amount of fluorescence that becomes internalized over time by either flow cytometry (FCM) [1] or confocal microscopy [2]. During these ligand/receptor internalization experiments, the ability to distinguish between the amount of ligand that remains on the cell surface and the amount that becomes internalized during the course of the experiment is a significant challenge. With either technique, in order to obtain an accurate estimate of the amount of fluorescence inside the cell that is derived from internalized ligands, it is critical to be able to efficiently wash off 100% of the residual fluorescence (i.e., the fluorescent ligands that were not internalized during the time course of the experiment). If the fluorescent signal remaining on the surface is not close to zero after washing at the end of the internalization experiment, what is measured as the intracellular signal is rendered unreliable [1]. When the ligand analyzed is a targeting antibody (Ab) that has been labeled with a fluorescent tag, removal of the non-internalized Ab from the cell surface can be achieved, but depends on the strength of the washing buffer. When the analyzed

ligand is not an Ab but a protein that forms a stable complex with its receptor, removal of residual cell surface fluorescence (i.e., the non-internalized ligands) becomes quite difficult. Nonetheless, when analyzing internalization of a non-antibody ligand that interacts tightly with its receptor, one solution to the residual fluorescence problem would be to label the ligand with a specific fluorescent Ab. The interaction between the fluorescent Ab and the ligand is expected to be weaker than that between the ligand and its cell surface receptor. Therefore, by using buffers that dissociate the Ab from the bound ligand, one should be able to efficiently remove residual fluorescence associated with the ligand. The solution to the residual fluorescence problem in internalization experiments is to find a method that efficiently removes fluorescent Ab from the cell surface.

The classical approach for stripping Ab from cell surfaces requires washing cells at the end of the experiment in a simple acidic buffer containing either 50 mM glycine [1,3,4] or 100 mM Na Acetate [5]. However, after repeatedly testing this approach in our laboratory, we concluded that these buffers are very inefficient at displacing surface-bound Ab. To address this problem, we decided to use a different approach and explore the efficacy of removing surface-bound Ab by employing a proteolytic enzyme known to cleave specific regions of the Ab.

The proteolytic enzyme pepsin, which is crucial for digestive processes in the stomach, is synthesized from pepsinogen and secreted by the gastric chief cells [6]. Pepsin cleaves preferentially at the C-terminal end of aromatic amino acids such as phenylalanine and tyrosine [7]. Pepsin worked most efficiently at removing surface-bound Ab without any detrimental effects on the assay. When incubated with an immunoglobulin G (IgG), pepsin is known to proteolytically separate the Ab into two fragments, the bivalent F(ab′)2 (fragment, antigen-binding) region and the Fc (fragment, crystallizable) region, by specifically cleaving the Ab between these

* Corresponding author. Address: Department of Biochemistry and Molecular Biology, University of Southern California, Keck School of Medicine, 1303 N Mission Road, CRL-106B, Los Angeles, CA 90033, USA. Fax: +1 323 224 7679.
E-mail address: marklan@usc.edu (F.S. Markland Jr.).

two regions [8] (Fig. 1A). We theorized that this proteolytic action of pepsin could also be employed *in situ* to strip away fluorescently labeled Ab from cell surfaces. In our experiments, we used either an anti-integrin or transferrin primary antibody and an Fc-specific Alexa-488 (Invitrogen, Carlsbad, CA) conjugated secondary antibody (Fc A488 secondary Ab) in combination with pepsin digestion to demonstrate, by both FCM and confocal microscopy, that *in situ* proteolysis could effectively remove labeled secondary Ab.

Because pepsin specifically cleaves the Ab at the junction between the F(ab′)2 fragment and the Fc fragment [8], we can take advantage of this cleavage specificity by using an A488 secondary Ab that is Fc-specific. Proteolysis by pepsin will cleave both the primary and the secondary Ab bound on the cell surface. When this happens the F(ab′)2 fragment of the primary antibody will be left in place, but the Fc fragment of the primary Ab along with the bound F(ab′)2 fragments from the secondary Ab will be cleaved off the cellular surface (Fig. 1B). This results in a very efficient removal of any surface fluorescence. If we were to use a secondary Ab that was not Fc-specific, the remaining F(ab′)2 fragment from the primary Ab would still have fluorescent F(ab′)2 fragments from the Fc A488 secondary Ab bound to the cell surface, resulting in persistent signal even after proteolysis.

Materials and methods

Evaluating the efficiency of different stripping buffers on removing cell surface fluorescence. MDA-MB-435 human cancer cells [9,10] were grown in tissue culture flasks and collected by brief trypsinization with 10% trypsin stock (0.05% trypsin–0.02% EDTA) in phosphate buffered saline (PBS) for 5-min. The trypsin was quenched by complete media and the cells were resuspended as needed. We incubated the MDA-MB-435 cells (10^6), in suspension, with a monoclonal Ab against the beta1 integrin subunit (1:500, clone P5D2, Santa Cruz Biotechnology, Santa Cruz, CA) for 30 min. We then washed the cells three times with PBS and incubated the cells with an anti-mouse Fc A488 secondary Ab (1:1000, Jackson ImmunoResearch, West Grove, PA) for 30 min (the secondary Ab was conjugated to Alexa-488 dye following Invitrogen's protocol). During the labeling process the cells were kept at 4 °C to ensure that there was no membrane traffic and that Fc A488 secondary Ab was not internalized by the MDA-MB-435 cells. These conditions allowed for maximum surface fluorescence to be retained on the plasma membrane (i.e., no membrane traffic) and for the evaluation of the efficiency of different buffers in removing membrane-bound Fc A488 secondary Ab. Three different stripping buffers were analyzed; two were traditional buffers containing either 50 mM glycine, 150 mM NaCl, pH 2.5 (glycine/HCl buffer), or 100 mM Na Acetate, 50 mM NaCl, pH 5.5 (acetate/HCl buffer). For the above buffers the cells were washed for 30 min at 4 °C with gentle agitation. The third buffer was one of the traditional buffers (glycine/HCl buffer) further supplemented with 0.01 mg/ml pepsin (pepsin/HCl buffer). In buffer supplemented with pepsin, cells were washed for 15-min at 4 °C with gentle agitation. After the stripping step, the cells were then either fixed in 3.7% formaldehyde and mounted onto coverslips with fluorescent mounting media (KPL, Gaithersburg Maryland) for confocal microscopy analysis or washed and resuspended in PBS, pH 7.4, for fluorescence-activated cell sorting (FACS) analysis.

Internalization rates of beta1 integrin and transferrin receptors. MDA-MB-435 cells were grown and collected as previously described. Cells (10^6) were labeled with either the beta1-integrin Ab (1:500) or the transferrin receptor (TFR) Ab (1:500, clone 9F81C11, Santa Cruz Biotechnology, Santa Cruz CA), washed and further stained with an anti-mouse Fc A488 secondary Ab (1:1000). Cells were washed three times and incubated with Ab for 30 min at 4 °C. In evaluating beta1 integrin receptor internalization cells were transferred to a 37 °C incubator and internalization of the integrin-bound Ab was allowed to proceed for 5-min, 1-h, or 3-h. Cells with TFR-bound Ab were resuspended in complete media, supplemented with 200 nM transferrin [11], then left to internalize at 37 °C for 5-min, 20-min, or 60-min. At the end of each time point, cells were either washed in glycine/HCl stripping buffer for 30 min, pepsin/HCl-stripping buffer for 15-min, or PBS for 15-min. Washings were done at 4 °C with gentle agitation and the cells were then fixed in 3.7% formaldehyde and mounted onto coverslips with fluorescent mounting media for confocal microscopy.

The confocal images were quantified using the software program Simple PCI (Hamamatsu, Sewickley, PA). Each representative image was scanned, with this software, and every fluorescent pixel was counted that was between the minimum and maximum signal strength which yielded the highest quality image. These same boundaries were applied to all slides. Any pixel above or below the boundary was excluded. The same images were then used to calculate the area of the measured cells. From these two numbers, we obtained the amount of pixels per unit area for each image. This represents the rate that the beta1 integrins or TFRs are internalized per unit area of cell surface.
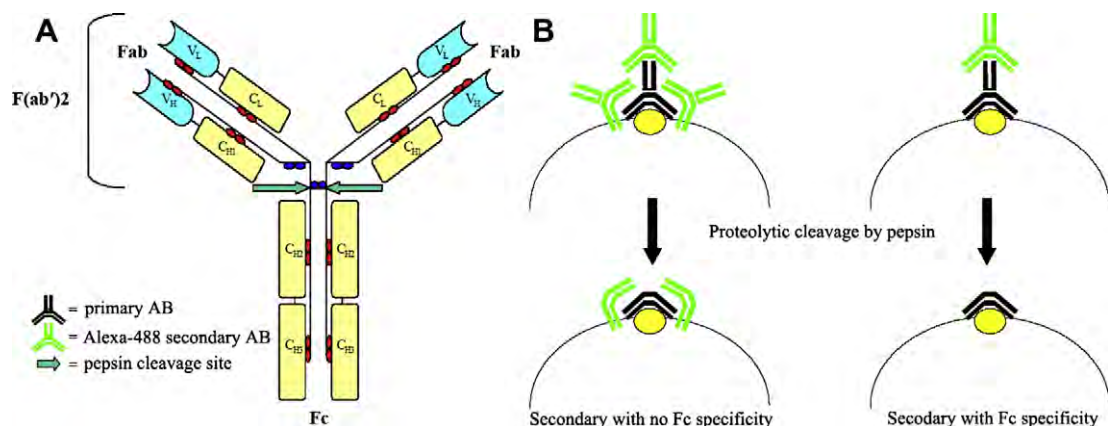

Fig. 1. Fc-specific secondary antibody requirement for pepsin removal of the residual fluorescent signal. (A) Pepsin cleaves antibodies at the junction between the bivalent F(ab′)2 fragment and the Fc fragment. (B) Diagram illustrating the need for an Fc-specific secondary Ab in order for the pepsin cleavage to eliminate the Alexa-488 signal from the cell surface. After proteolytic cleavage, cells that were treated with a non-Fc-specific Ab still have the Alexa-488 F(ab′)2 attached to the primary F(ab′)2, while cells that were treated with the Fc-specific Ab no longer have any portion of the Fc A488 secondary Ab attached to the primary F(ab′)2.

Trypan blue viability. MDA-MB-435 cells were grown and collected as previously described. Cells (10^6) were either left untreated, exposed to UV light for 15-min, treated with actinomycin D (0.05 μg/ml) for 18 h, or washed in pepsin/HCl-stripping buffer for 15-min at 4 °C with gentle agitation. When each treatment concluded, cells were stained with 4% Trypan Blue (EMD Biosciences, San Diego California) in PBS for 5-min and evaluated for cell viability by counting stained cells on a hemocytometer at 10× magnification. Four separate counts were taken and averaged, and the experiment was repeated three times.

Results

When evaluated at maximum surface fluorescence, meaning that no fluorescent Ab was internalized, our results clearly demonstrate the advantage of using pepsin to remove surface-bound Ab. Cells were visualized by confocal microscopy, which showed that the acidic washes done with traditional buffers were so ineffective that the retained fluorescent signal nearly matched the control (i.e., cells washed in PBS), indicating very little secondary Ab removal. By contrast, the pepsin-supplemented acid wash completely abolished the Alexa-488 signal from the surface of the MDA-MB 435 cells (Fig. 2). These results were similar to those observed using FACS analysis, where the glycine/HCl wash showed only a minimal shift in the fluorescent signal as compared to that observed in the control (i.e., cells washed in PBS); while the acetate wash showed no shift at all. In contrast, the pepsin/HCl wash brought the FACS signal down to 1.8% of control (Fig. 2).

To demonstrate how our technique can be employed to effectively and efficiently measure the internalization rates of different receptors, we conducted two experiments to measure internalization of the beta1 integrin receptor and the TFR on MDA-MB-435 cells. We chose these two systems because of their different rates of internalization. Beta1 integrin is internalized constitutively over time in a non-ligand induced manor, which leads to a slower rate of internalization. Conversely, the TFR was internalized after binding its natural ligand, transferrin, and is internalized via receptor-mediated endocytosis, resulting in a faster rate of internalization. The time course chosen for each experiment was determined by observations made in our laboratory using MDA-MB 435 cells, as well as internalization experiments conducted by other laboratories [4,11,12]. We chose 5-min, 1-h, and 3-h for the beta1 integrin and 5-min, 20-min, and 60-min for the TFR, in order to allow the maximum amount of internalized receptors before recycling became the predominant event in the suspended MDA-MB 435 cells. Representative images from the beta1 integrin internalization experiment are shown (Fig. 3A). The fluorescent signal coming from the MDA-MB 435 cells after 5-min of internalization at 37 °C followed by a PBS wash was considered the negative control with no removal of residual fluorescence (Fig. 3A, Row 1). By comparison, MDA-MB-435 cells washed in pepsin/HCl buffer after 5-min of incubation at 37 °C completely lose the cell surface fluorescent signal (Fig. 3A, Row 3). Cells washed in glycine/HCl buffer after 5-min of incubation still maintained a high amount of surface fluorescence (Fig. 3A, Row 2). At the later time points the signal disparity still persisted on the cell membrane with a strong signal coming from cells washed in either PBS or glycine/HCl and considerably less signal from cells washed in pepsin/HCl (Fig. 3A, Rows 4–9). Thus, the residual surface signal coming from non-internalized Ab in cells washed in PBS or glycine/HCl represents a confounding variable in interpreting receptor internalization data. We believe that unlike other washing techniques previously employed in receptor internalization studies, the combination of Fc-specific Ab and pepsin could be employed to remove surface fluorescence and thereby gener-

ate a much more interpretable signal coming from the internalized receptor–ligand complexes.

Quantitation of beta1 integrin internalization illustrates the efficiency of our pepsin-based stripping buffer. After 5-min of incubation, the PBS control group had a pixel per cell area count of 33.6, the glycine/HCl group had a count of 20.2, while the pepsin/HCl treatment resulted in a count of 0.008 (Fig. 3B). Clearly, the most effective stripping buffer was the pepsin/HCl wash, since after an incubation time of only 5-min, a very small amount of integrin should be internalized by the cells. The signal disparity that was seen after a brief incubation was the result of the inability of buffers, which do not contain pepsin, to efficiently remove the non-internalized Fc A488 secondary Ab from the cell surface. At the 1-h time point, quantitation for the PBS group had a pixel per cell area count of 39.2, glycine/HCl was 17.0, and pepsin/HCl 4.16. At the 3-h time point, the same trend was observed with the PBS pixel per cell area count of 57.5, glycine/HCl of 24.9, and pepsin/HCl 11.6 (Fig. 3B). The only internalization rate that demonstrated consistent progression throughout the three time points was from the pepsin/HCl treatment group.

Quantitation of the TFR data yielded similar results to the beta1 integrin experiment. After 5-min of incubation, the PBS control group had a pixel per cell area count of 13.4, the glycine/HCl group had a count of 12.7, while the pepsin/HCl treatment resulted in a count of 0.9. When compared to the 5-min time point for the beta1 integrin, the only logical data set was from the pepsin/HCl treatment group; TFR is expected to be internalized at a greater rate and we found 0.9 pixels per cell area for TFR and only 0.008 pixels per cell area with beta1 integrin, while the other two treatment groups had lower pixels per cell area counts for the TFR (Fig. 3B and C) when compared to the beta1 integrin pixels per cell area counts. At the 20-min time point, quantitation for the PBS group had a pixel per cell area count of 26.3, glycine/HCl was 16.1, and pepsin/HCl 4.00. At the 60-min time point, the same trend was observed with the PBS pixel per cell area count of 27.3, glycine/HCl of 21.0, and pepsin/HCl 14.2 (Fig. 3C). Again, the only treatment group that established a consistent trend for all three time points was from the pepsin/HCl wash.

Trypan Blue staining confirmed that the pepsin-supplemented acid wash has no impact on the stability of the cellular membrane of MDA-MB-435 cells exposed to the pepsin/HCl-stripping buffer. Results of pepsin treatment were compared to two agents known to initiate membrane instability and cell death, UV light and Actinomycin D treatment, which left the majority of the MDA-MB-435 cells non-viable. The untreated cells showed that only 6.3% of the cells were non-viable, while the positive controls of UV light and Actinomycin D demonstrated 69.1% and 52.7% to be non-viable. Exposure of these cells to pepsin treatment resulted in very low cell death of 6.5%, similar to results seen in the untreated control group (Fig. 4).

Discussion

The method described in this paper is a simple but efficient technique for removing residual surface bound fluorescence in receptor internalization assays. The utility of this procedure becomes evident when it is compared to the classical acid buffer wash recommended by most standard protocols (Fig. 2). Without including pepsin in the wash, the fluorescent signal generated with classical acidic buffer washes almost exactly matches the PBS treated controls, indicating that stripping Ab off the cellular surface with traditional buffers is very ineffective. Furthermore, the traditional Ab stripping buffers have demonstrated poor results in other types of assays. For example, one group found that in a surface plasmon resonance experiment the glycine/HCl acid wash was
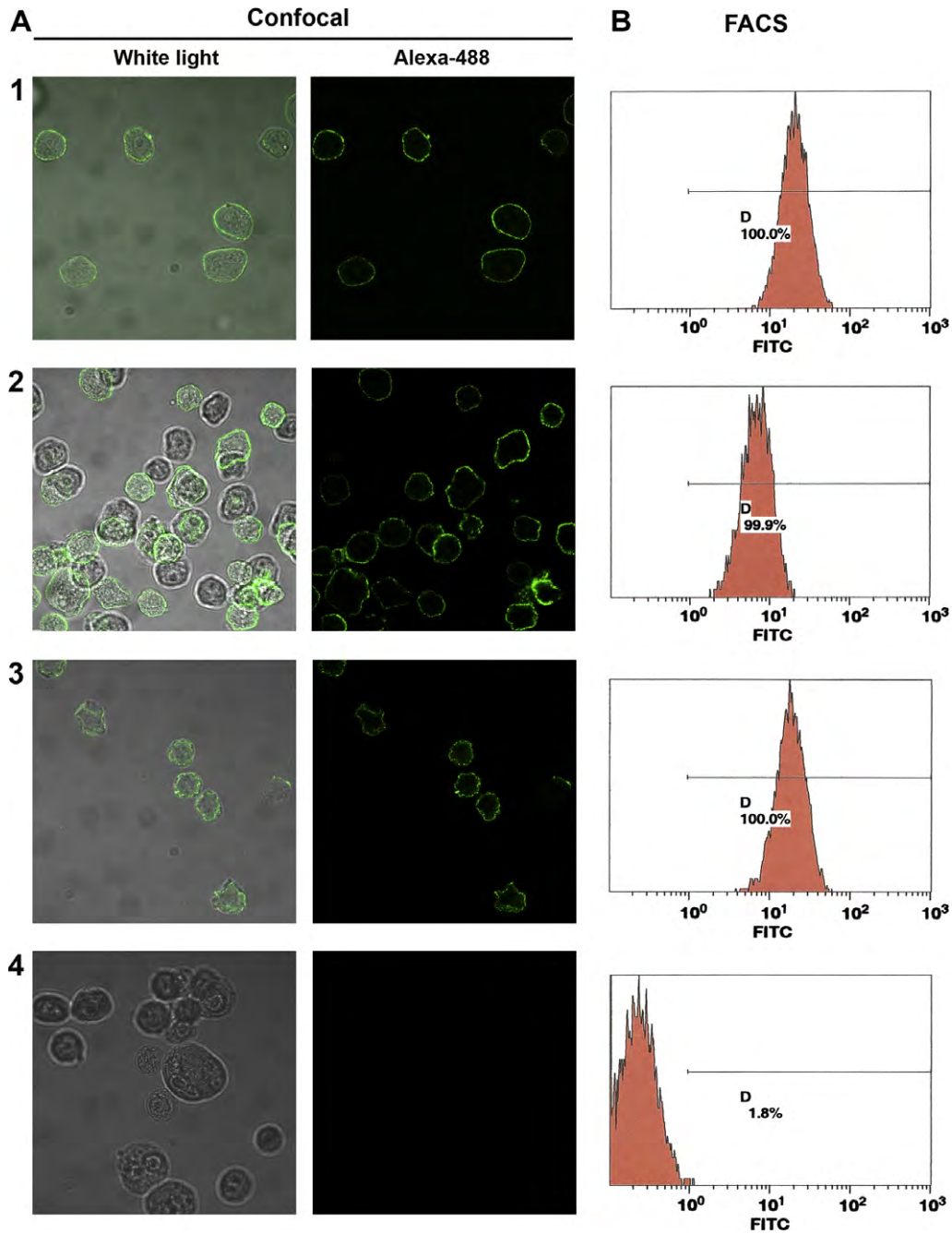
Fig. 2. Effect of pepsin on labeled antibody removal at maximum residual fluorescence. MDA-MB-435 cells were incubated at 4 °C with a mouse monoclonal Ab against the cell surface beta 1 integrin (30-min), washed with PBS, and then further incubated with an A488 secondary Ab that is specific for the Fc portion of mouse IgG (30-min). The cells were then immediately washed with 3 different Ab stripping buffers or PBS at 4 °C with gentle agitation. Row 1: PBS; Row 2: 50 mM glycine, 150 mM NaCl, pH 2.5; Row 3: 100 mM Na Acetate, 50 mM NaCl, pH 5.5; Row 4: 0.1 mg/ml pepsin, 50 mM glycine, 150 mM NaCl, pH 2.5. The cells were then either (A) fixed in 3.7% formaldehyde and mounted onto coverslips with fluorescent mounting media (KPL, Gaithersburg Maryland) for confocal microscopy under either white light (left panels) or light at a wavelength of 488 nm to visualize the Alexa-488 dye conjugated to the Fc-specific secondary Ab (right panels), or (B) washed and resuspended in PBS, pH 7.4, for FACS analysis.

totally ineffective at disrupting an Ab–receptor complex [13]. The only limiting factor of the method presented herein is that, compared to the traditional methods, our method calls for the usage of an Fc-specific secondary Ab, but these are common and fairly inexpensive reagents.

While evaluating our technique with two internalization systems, one slow (beta1 integrin) and one fast (TFR), a true advantage for our technique emerged. Although all three treatment groups demonstrated increasing internalization rates when comparing beta1 integrin to TFR, the PBS and glycine/HCl groups were

inconsistent and unreliable. The reason for this was due to strong cell-membrane signals (non-internalized complexes) that were not present in the pepsin/HCl treatment groups. This produced a key difference between the data sets. Given the conditions for each experiment, from the 1-h to the 3-h time point in the beta1 integrin experiment, and from the 20-min to the 60-min time point in the TFR experiment, we would expect the amount of internalized receptor to triple in an almost linear process. The pepsin/HCl group demonstrated a consistent rate that confirmed our expectation, while the PBS and glycine/HCl groups did not
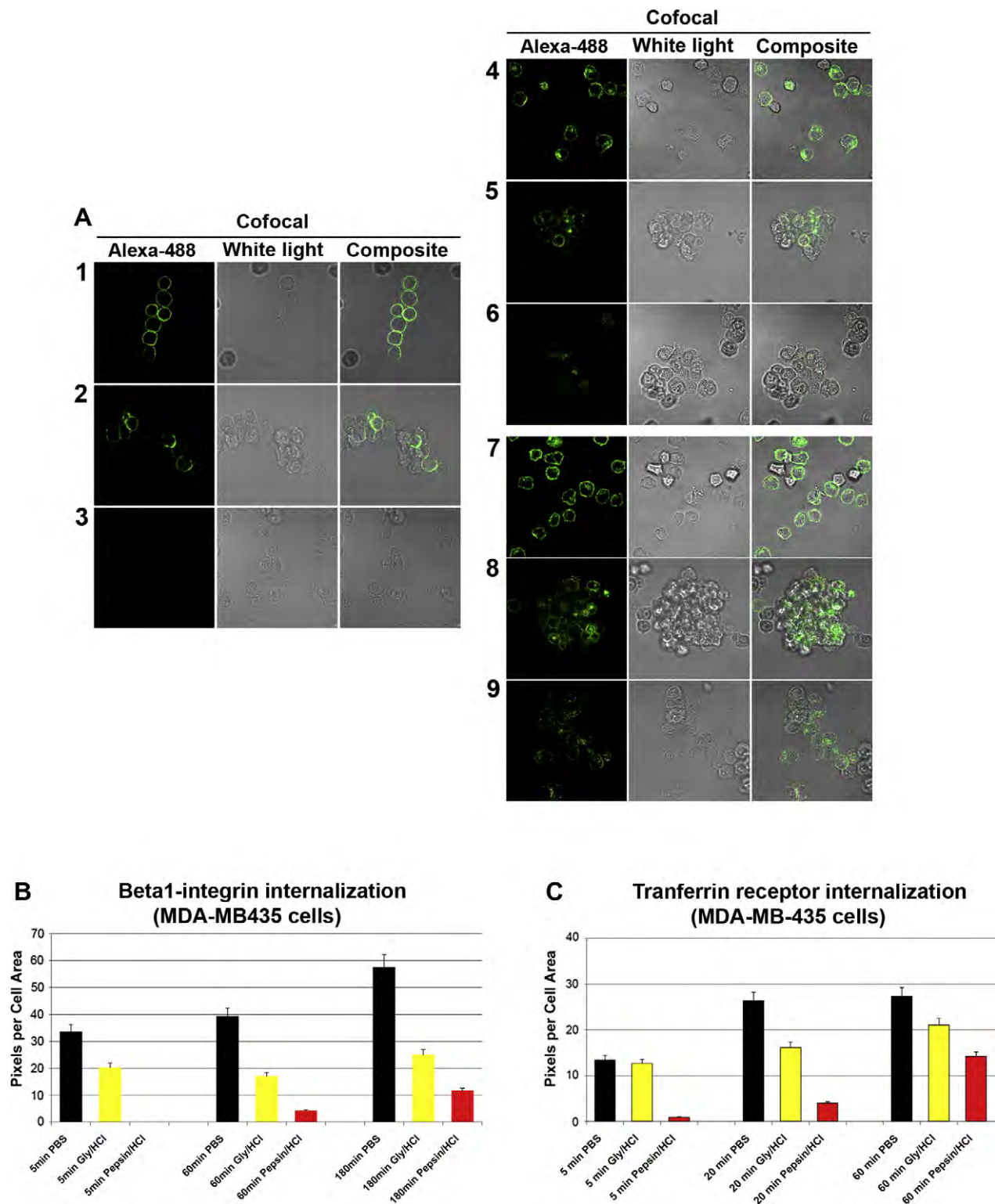
Fig. 3. The advantages of using the pepsin/HCl-stripping buffer to accurately measure the internalization rates of receptors in two systems. (A) MDA-MB-435 human cancer cells were labeled at 4 °C with a beta1-integrin Ab or a TFR Ab, washed, and further stained with an anti-mouse Fc A488 secondary Ab. The cells treated with the beta1-integrin Ab and secondary Ab were then transferred to 37 °C and allowed to internalize the integrin-bound antibody for three separate time intervals (5-min, 1-h, and 3-h), while cells treated with the TFR Ab were resuspended in complete media supplemented with 200 nM transferrin and transferred to 37 °C and allowed to internalize the TFR-bound antibody for three different time intervals (5-min, 20-min, and 60-min). At the end of each time point, the cells were either washed in glycine/HCl, pepsin/HCl or PBS, after which they were fixed in 3.7% formaldehyde and mounted onto coverslips with Fluorescent Mounting Media and analyzed by confocal microscopy. Representative images only from the beta1 integrin internalization study are shown (A). Alexa-488 column: images shown at a wavelength of 488 nm; White light column: images shown under white light; Composite column: super imposed images showing views under both 488 nm wavelength and white light. Row 1: 5-min, PBS; Row 2: 5-min, glycine/HCl; Row 3: 5-min, pepsin/HCl; Row 4: 1-h, PBS; Row 5: 1-h, glycine/HCl; Row 6: 1-h, pepsin/HCl; Row 7: 3-h, PBS; Row 8: 3-h, glycine/HCl; Row 9: 3-h, pepsin/HCl. Images from the beta1 integrin internalization experiment (B) and the TFR internalization experiment (C) were subjected to quantification by the Simple PCI software. Fluorescent pixels were counted and divided by the total area for the counted cells to obtain the amount of pixels per unit area for each image.
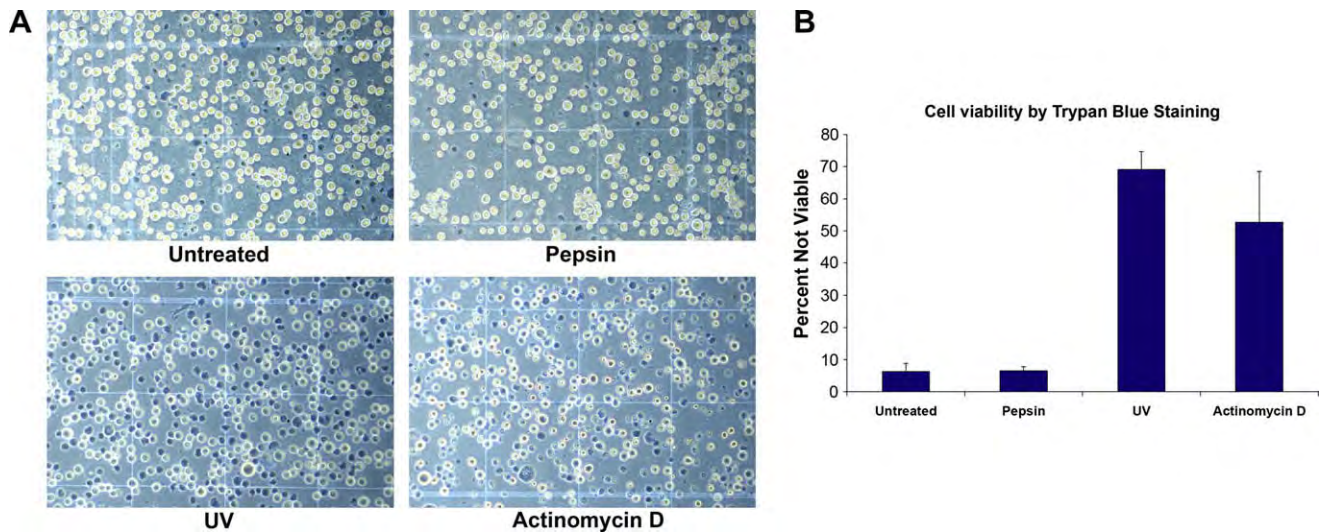
Fig. 4. Cell viability assessed by trypan blue staining. (A) Composite of MDA-MB-435 cells after no treatment, exposed to UV light for 15-min, treated with actinomycin D for 18 h, or washed in pepsin/HCl-stripping buffer for 15-min. When each treatment concluded, cells were stained with 4% Trypan Blue for 5-min. This figure contains representative images from multiple experiments. (B) Bar graph showing the percent of non-viable cells for each treatment group.

(Fig. 3B and C). The false data points with these washing conditions also lead to other inaccuracies. From the 5-min to 1-h time points in the beta1 integrin experiment, the glycine/HCl group actually showed a negative internalization rate going from 20.2 to 17.0 pixels per cell area. This result would not be possible in a properly conducted internalization experiment, but because of the false signal coming from the non-internalized receptors, this type of result was obtained.

Other interesting observations can be made when examining the confocal images generated from the beta1 integrin internalization experiment (Fig. 3A). The PBS and glycine/HCl images clearly showed a pronounced fluorescent signal (a fluorescent corona) coming from the plasma membrane of the MDA-MB-435 cells at all time points. This residual signal, which was generated by the Fc A488 secondary Ab that was not washed off the cell surface, was very pronounced as compared to the pepsin/HCl treatment group. We overcame the residual surface fluorescence problem in our internalization experiments by successfully cleaving off the Fc fragment of our Fc A488 secondary Ab with pepsin. Another solution to this problem would be to use computer software to only count the internal area of the cell, excluding the fluorescent corona, rendering the stripping of the non-internalized signal unnecessary. However, this would not be appropriate for several reasons. First, artificially eliminating the residual corona would not be possible when conducting studies such as flow cytometry. Second, one would not be able to distinguish an internal from an external membrane, meaning that newly released vesicles would not be counted. Third, a closer look at the 3-h pepsin/HCl treatment images (Fig. 3A, Row 9) shows that in distinct pockets at the cell surface a faint corona starts forming again, even after very efficient stripping of all fluorescence on the cellular surface. This phenomenon could represent the beginning of recycling vesicles carrying the beta1 integrin receptor still bound to the Ab ligand back to the plasma membrane, but before the vesicle fused to the plasma membrane. This new level of complexity should be investigated as a separate event. The use of traditional buffers would make the recycling phenomenon impossible to quantitate because these methods never fully eliminate the fluorescence coming from the cell surface.

The recycling aspect of receptors demonstrates another possible application for this technique – analysis of the rate of recycling of receptors after internalization. A method to investigate

recycling of receptors requires a reliable procedure for removing the initial surface signal, similar to internalization studies [11,14]. One way to utilize the pepsin/HCl buffer would be to bring the cells, after initial Ab stripping, back to 37 °C, a temperature that would allow the internalization process to resume. After a predetermined time interval, in which recycling of the receptor being studied was shown to occur, the surface of the cells would be stripped again with the pepsin/HCl buffer. Then comparisons could be made, using flow cytometry, between the signals generated from cells that were stripped once to cells stripped a second time. The difference in the two measurements should provide an indication of the amount of receptor recycled to the cell surface. However, this would only be possible if you were able to completely remove all residual fluorescence from the cell surface.

In summary, the method we describe herein can be effectively used to completely remove residual cell surface fluorescent signal in receptor internalization assays. By doing an even more detailed internalization time course, the pepsin/HCl wash would be expected to generate a clearer, but more complex image of receptor internalization. This would allow for better understanding of the internalization rates for specific receptors.

References

[1] J. Bernhagen, R. Krohn, H. Lue, J.L. Gregory, A. Zernecke, R.R. Koenen, M. Dewor, I. Georgiev, A. Schober, L. Leng, T. Kooistra, G. Fingerle-Rowson, P. Ghezzi, R. Kleemann, S.R. McColl, R. Bucala, M.J. Hickey, C. Weber, MIF is a noncognate ligand of CXC chemokine receptors in inflammatory and atherogenic cell recruitment, Nat. Med. 13 (2007) 587–596.

[2] M. Casartelli, G. Cermenati, S. Rodighiero, F. Pennacchio, B. Giordana, A megalin-like receptor is involved in protein endocytosis in the midgut of an insect (Bombyx mori, Lepidoptera), Am. J. Physiol. Regul. Integr. Comp. Physiol. 295 (2008) R1290–R1300.

[3] G. Altankov, F. Grinnell, Fibronectin receptor internalization and AP-2 complex reorganization in potassium-depleted fibroblasts, Exp. Cell. Res. 216 (1995) 299–309.

[4] G. Baochong, T.M. Curtis, F.A. Blumenstock, F.L. Minnear, T.M. Saba, Increased recycling of $\alpha 5 \beta 1$ integrins by lung endothelial cells in response to tumor necrosis factor, J. Cell Sci. 113 (2000) 247–257.

[5] R.C. Carroll, E.C. Beattie, H. Xia, C. Lüscher, Y. Altschuler, R.A. Nicoll, R.C. Malenka, M.V. Zastrow, Dynamin-dependent endocytosis of ionotropic glutamate receptors, Proc. Natl. Acad. Sci. USA 96 (1999) 14112–14117.

[6] I. Gritti, G. Banfi, G.S. Roi, Pepsinogens: physiology, pharmacology pathophysiology and exercise, Pharmacol. Res. 41 (2000) 265–281.

[7] T. Kageyama, Pepsinogens, progastricsins, and prochymosins: structure, function, evolution, and development, Cell. Mol. Life Sci. 59 (2002) 288–306.

[8] S.M. Andrew, J.A. Titus, Fragmentation of immunoglobulin G, Curr. Protoc. Cell Biol. 16 (4) (2000) 1–10.

[9] M. Lacroix, MDA-MB-435 cells are from melanoma, not from breast cancer, Cancer Chemother. Pharmacol. 63 (2008) 567.

[10] A.F. Chambers, MDA-MB-435 and M14 cell lines: identical but not M14 melanoma?, Cancer Res. 69 (2009) 5292–5293.

[11] J. Barroso-González, J.D. Machado, L. García-Expósito, A. Valenzuela-Fernández, Moesin regulates the trafficking of nascent clathrin-coated vesicles, J. Biol. Chem. 284 (2009) 2419–2434.

[12] S. Severa, H. Damkea, S.L. Schmida, Dynamin: GTP controls the formation of constricted coated pits, the rate limiting step in clathrin-mediated endocytosis, J. Cell Biol. 150 (2000) 1137–1148.

[13] M. Brigham-Burke, D.J. O'Shannessy, A micro-scale method employing surface plasmon resonance detection for the determination of conditions for immunoaffinity chromatography of proteins, Chromatographia 35 (1992) 45–49.

[14] A. Pagano, P. Crottet, C. Prescianotto-Baschong, M. Spiess, In vitro formation of recycling vesicles from endosomes requires adaptor Protein-1/clathrin and is regulated by Rab4 and the connector Rabaptin-5, Mol. Biol. Cell 15 (11) (2004) 4990–5000.